NASA Technical Paper 3437

The NASA Langley 8-Foot Transonic Pressure Tunnel Calibration

Cuyler W. Brooks, Jr., Charles D. Harris, and Patricia G. Reagon

August 1994

NASA Technical Paper 3437

The NASA Langley 8-Foot Transonic Pressure Tunnel Calibration

Cuyler W. Brooks, Jr., Charles D. Harris, and Patricia G. Reagon
Langley Research Center • Hampton, Virginia

National Aeronautics and Space Administration
Langley Research Center • Hampton, Virginia 23681-0001

August 1994

Summary

The NASA Langley 8-Foot Transonic Pressure Tunnel (8-Foot TPT) is a continuous-flow, variable-pressure wind tunnel with control capability to independently vary Mach number, stagnation pressure, stagnation temperature, and humidity. The test section is square with corner fillets and a cross-sectional area approximately equivalent to that of an 8-ft-diameter circle. The top and bottom walls of the test section are axially slotted to permit a continuous variation of the test section Mach number from 0.2 to 1.2; the slot-width contour provides a gradient-free test section 50 in. long. The stagnation pressure may be varied from 0.25 to 2 atm.

The tunnel has been recalibrated to determine the relationship between the free-stream Mach number and the test chamber reference Mach number. The hardware was the same as that of the previous calibration in 1972 but the pressure measurement instrumentation available for the recalibration was about an order of magnitude more precise. Detailed tunnel contraction and test section geometries are presented in the appendix.

The principal result of the recalibration was a slightly different schedule of reentry flap settings for Mach numbers from 0.80 to 1.05 than that determined during the 1972 calibration. An analysis of a longer test section suitable for Mach numbers from 0.2 to 1.0 is included. Limited test section sidewall boundary layer data are presented.

Introduction

The NASA Langley 8-Foot Transonic Pressure Tunnel (8-Foot TPT) is a continuous-flow, variable-pressure wind tunnel with control capability to independently vary Mach number, stagnation pressure, stagnation temperature, and humidity. The test section is square with corner fillets and a cross-sectional area approximately equivalent to that of an 8-ft-diameter circle. The top and bottom walls of the test section are axially slotted to permit a continuous variation of the test section Mach number from 0.2 to 1.2; the slot-width contour provides a gradient-free test section 50 in. long for Mach numbers equal to or greater than 1, and 100 in. long for Mach numbers less than 1. The stagnation pressure may be varied from 0.25 to 2 atm.

Calibration in this report refers specifically to the determination of an empirical relationship between the calculated free-stream Mach number and the nominal Mach number based on the pressure in the essentially motionless air in the plenum outside the slots. The most significant parameter affecting this relationship is the position of the diffuser entrance flaps (referred to hereafter as *reentry flaps*) at the downstream end of the test section. (See fig. 1.) Other parameters varied during the calibration tests were stagnation pressure, diffuser spoiler position (fig. 1(a)), and plenum suction.

Since the last test section calibration in 1972, an antiturbulence system consisting of a honeycomb and five screens has been installed in the settling chamber upstream of the test section (fig. 1(b)) in conjunction with the NASA Langley laminar flow control (LFC) experiment (refs. 1 and 2); the precision of the pressure measurement instrumentation available for the recalibration has improved by an order of magnitude. In addition, the test section walls were no longer as smooth as in 1972 because of both normal tunnel use and substantial repairs of the liner anchor points and large access holes cut in the test section for the LFC experiment. Also, the schedule of reentry flap position with Mach number as determined from the 1972 calibration was not optimum near Mach 0.9. Because of all of these factors, a complete recalibration was advisable after the tunnel was restored to normal transonic operation following completion of the LFC experiment in 1988.

The objective of this paper is to present the following:

1. An appropriate selection of the local test section Mach number distributions on the centerline probe
2. Variation of test section Mach number correction and gradient with reentry flap position
3. Analysis leading to the table of optimal reentry flap position and the corresponding value of Mach number correction as a function of Mach number
4. Diffuser spoiler and boundary layer suction system effects
5. A limited set of data on the test section sidewall boundary layer
6. A detailed description of the geometry of the tunnel contraction, the test section walls, and the slots

Symbols

D_f	diagonal depth of corner fillet at 45°, in.
f_R	flap setting, counts
H	boundary layer stability parameter, $\frac{\delta^*}{\theta}$
M	Mach number

M_{set} — Mach number equivalent to reference Mach number with slots closed

p — pressure, psf

r — radius, in.

R/l — Reynolds number per foot

S — change in local Mach number over streamwise extent of test section, $(x_d - x_u)\dfrac{dM}{dx}$

T — temperature, °R

x — distance downstream from slot origin, parallel to tunnel centerline, in.

X — distance downstream from origin of tunnel contraction, ft

y — lateral dimension, in.

y_s — slot width, in.

Y — lateral dimension from tunnel centerline, ft

z — vertical dimension, in.

$\alpha_{f,R}$ — reentry flap angle (positive when flap surface is divergent from tunnel centerline), deg

δ — diffuser spoiler angle (positive into flow), deg

δ^* — boundary layer displacement thickness, in.

Δ — difference operator

ΔM — $M_{\text{avg}} - M_{\text{tc}}$

γ — ratio of specific heats (1.4 for air)

θ — boundary layer momentum thickness, in.

Subscripts:

avg — average for range x_u to x_d

d — downstream limit

e — boundary layer edge, $\dfrac{p_t}{p_{t,\infty}} \geq 0.99$

f — corner fillet

local — value at surface pressure measurement orifice

R — reentry

s — slot

t — stagnation condition

tc — test chamber (plenum)

u — upstream limit

wall — tunnel sidewalls or top and bottom walls

∞ — free stream

Abbreviations:

BL — boundary layer

LFC — laminar flow control

rpm — revolutions per minute

TPT — Transonic Pressure Tunnel

Facility Description

The NASA Langley 8-Foot Transonic Pressure Tunnel (8-Foot TPT) is a continuous-flow, variable-pressure wind tunnel with control capability to independently vary Mach number, stagnation pressure, stagnation temperature, and humidity. The test section is square with corner fillets and a cross-sectional area approximately equivalent to that of an 8-ft-diameter circle. The top and bottom walls of the test section are axially slotted to permit a continuous variation of the test section Mach number from 0.2 to 1.2; the slot-width contour provides a gradient-free region of the test section 50 in. long at Mach numbers up to 1.2. The stagnation pressure may be varied from 0.25 to 2 atm; because of power and screen load limitations, the higher Mach numbers can only be obtained at pressures below 1.5 atm. The geometric shape of the contraction and test section is specified in the appendix.

Stagnation pressure in the 8-Foot TPT can be varied from about 0.25 atm at all test Mach numbers to about 1.2 atm at a Mach number of 1.2, to about 1.5 atm at high subsonic Mach numbers, and to about 2.0 atm at Mach numbers of 0.4 or less. The tunnel is capable of achieving Mach numbers up to about 1.3 but most testing is limited to a maximum Mach number of 1.2 because the calibrated region of the test section for the higher Mach number is located farther downstream and requires that a model be located farther aft in the test section.

Temperature is measured only for the minimal effect of the Sutherland viscosity parameter on Reynolds number. Small changes in Reynolds number caused by temperature effects can be counterbalanced by small pressure changes. The calibration was conducted at the standard operating temperature of 120°F. Depending on the time of year, limitations of the cooling system generally result in an operating temperature of 100°F or more at Mach numbers above about 0.6; window and expansion joint safety considerations restrict operation to temperatures below 140°F. Figure 2 shows a typical thermocouple array and distribution of stagnation temperatures superimposed on a sketch of the honeycomb structure in the settling chamber.

Test Section Geometry

The test section within the plenum is cantilevered from the tunnel shell at the upstream end and supported in the middle by six vertical columns. Detailed coordinate tables are given in the appendix. The six columns are pinned at both top and bottom to allow for any movement of the test section due to thermal expansion and contraction. The contour of the tunnel contraction region of the test section is fixed and the test section is joined to the contraction region and diffuser with bolted flanges. The flange joints are reasonably smooth and airtight and do not create harmful airflow disturbances. At the downstream end of the test section, a region of transition from a square to a circular cross section is followed by a region of a constant-area circular cross section; at the entrance to the conical (included angle of 6°) diffuser, a sliding expansion joint accommodates differences in thermal expansion between the test section and the outer shell of the plenum. The expansion joint is essentially an air gap sealed with a plate which is welded to the interior tunnel wall on the upstream side of the gap and free to slide over the downstream edge of the tunnel wall.

Because of wall boundary layer development, the aerodynamic throat of the test section occurs about 30 in. downstream of the geometrical throat. At the aerodynamic throat, which corresponds to the slot origin ($x = 0$ in., $X = 50$ ft), the test section is an 85.51-in. square. After allowing for 8.55-in-radius fillets in the corners, the cross-sectional area is 50.3 ft^2—equivalent to the area of a circle with a diameter of 8.01 ft. Although the slot origin is at the 50-ft station ($X = 50$ ft) of the tunnel circuit dimensional system, dimensions in the test section are normally referenced for convenience to the slot origin as the 0-in. station ($x = 0$).

Sidewall curvature in the contraction region decreases gradually downstream until the curvature of the walls at the aerodynamic throat (0-in. station, the slot origin) becomes zero and all four wall surfaces diverge at an angle of $5'$ with respect to the tunnel centerline. Downstream of the slot origin, the divergence of the solid sidewalls of the test section remains constant at $5'$. On the top and bottom slotted surfaces, the wall divergence gradually increases to $13'$ at the 60-in. station and remains constant thereafter for both the remaining 96 in. of the slotted test section and the diffuser entrance section.

Slots. The top and bottom test section walls (floor and ceiling) each contain four equally spaced rectangular cutouts approximately 7.5 in. wide in which steel inserts are bolted to form the contours of the slots. (See figs. 1(c) and 1(d).) The slot contours are based on experience gained during the development of the slotted-wall concept in the 8-Foot Transonic Tunnel (the predecessor to the 8-Foot TPT) and experimentation with different slot configurations in the 8-Foot TPT. (See fig. A2.)

Because the slot openness varies along the test section, the value assigned for the average openness ratio is somewhat arbitrary and depends on which segment of the test section is the basis for the calculated average. The average open ratio from the slot origin to the leading edge of the diffuser entrance flaps is about 8.5 percent. If the average were weighted more toward the narrow slot region in the middle of the test section where a model would be located (between approximately the 70-in. and 120-in. stations), a more meaningful average open ratio would be about 6.9 percent.

The tunnel can be operated as a closed subsonic tunnel by covering the slots with thin plates bolted to the windward side of the slot edges. No significant pressure load is created on these plates because the test section is vented to the plenum at the trailing edge of the slot covers.

Reentry flaps. The 8-ft-long diffuser entrance section between the 156-in. and the 252-in. stations contains the 98.5-in-long diffuser entrance flaps, which are located outside the slots in the top and bottom walls with the leading edge at the 147.5-in. station. (See figs. 1(a) and 1(d).) The diffuser entrance flaps are more commonly referred to as the reentry flaps because the air exits the test section over the upstream end of the slots and reenters over the downstream end, which permits continuous operation through transonic speeds. These flaps can be rotated about a hinge line at the 250.4-in. station. The reentry flaps are fully closed (leading edge positioned at the underside of the slot lips) for subsonic Mach numbers up to 0.80 in the current calibration (0.95 in the 1972 calibration). Above a Mach number of 0.80, the flaps are progressively opened with increasing Mach number in order to flatten the test section Mach number distribution. Calibration of the test section includes optimization of the reentry flap position for each Mach number.

Diffuser spoilers. Just downstream of the reentry flap hinge (upstream of the diffuser transition section), spoilers are mounted on the tunnel top and bottom walls (figs. 1(a) and 1(d)) with their hinge line located at the 255-in. station. The spoilers are simply flat plates that completely span the width of the tunnel. They have a chord of 24 in. and are referred to as diffuser spoilers. They can be remotely adjusted through an angle range of about $-3°$ to $27°$ relative to the tunnel horizontal centerline (positive as the spoiler trailing edge approaches the tunnel centerline) or $0°$ to $30°$ relative to the local wall. The spoilers are combined with a semiautomatic servosystem to provide rapid Mach number control, which compensates for test section blockage as models are rotated through the range of angle of attack. In order to use the spoilers as a Mach number trim device, fan rpm is set high enough to achieve the desired Mach number with the model positioned at maximum blockage (usually maximum angle of attack) and the spoilers against the wall. As the angle of attack (thus model blockage) varies, the diffuser spoilers are moved in and out of the flow to hold the test section Mach number constant. Generally, only $2°$ to $3°$ of movement are needed to trim the Mach number with conventional size models. Care must be taken to avoid large spoiler deflections which would affect the model base pressures. Previous experiments have indicated that for deflections less than $10°$, the diffuser spoilers have no discernible effect on model base pressure or afterbody drag.

Tunnel Wall Boundary Layer Suction

Boundary layer (BL) suction is available to compensate for model blockage, which permits the testing of larger models at the top end of the Mach number range. The exact wall boundary layer displacement thickness removed by this technique is not known, but from measurement data, the solid sidewall boundary layer displacement thickness is estimated to be about 0.25 in. If 0.25 in. of displacement is removed from the 85-in.-wide top and bottom walls, the blockage area recovered amounts to about 43 in^2 or 0.3 ft^2, comparable to a reasonable fraction of the blockage of a typical model.

Boundary layer suction is only applicable for Mach numbers of 1.15 and above; at lower Mach numbers, the Mach number distribution develops streamwise gradients which render it unusable. The use of the boundary layer suction system also requires an entirely different reentry flap schedule.

The system used for boundary layer suction consists of two large compressors, precoolers, aftercoolers, and piping arranged to return the boundary layer air removed from the plenum through the slots to the circuit so that stagnation pressure is unchanged. The return passage is through the trailing edge of the hollow turning vanes at the downstream end of the diffuser and upstream of the fan. (See fig. 1(b).)

Each compressor has a rating of 96 000-cfma-inlet volume when operating at a pressure ratio of 4:1 and is referred to as the 100 000-cfma compressor. Each three-stage centrifugal type compressor is coupled directly to a 3600 rpm synchronous motor. Each motor is rated at 4000 hp for continuous operation and may be operated at a 5000-hp overload condition for a 30-min period. The acceptance tests of these motors indicated that the motors may be continuously operated above their rated horsepower (possibly as high as 6000 hp) without overheating the motor windings.

Effects of Laminar Flow Control Modifications on the Facility

In 1981, a honeycomb and five screens were permanently installed in the settling chamber upstream of the test section (fig. 1(b)) to improve the flow quality of the facility in support of the LFC experiment. General characteristics of the honeycomb and screens are presented in reference 1. In conjunction with the LFC experiment, a temporary 54-ft contoured test section liner was installed in the tunnel in 1981 to simulate unbounded flow about a swept airfoil model with infinite span. This liner was removed at the conclusion of the experiment in 1988.

Two possible effects of the LFC experiment alterations on recalibration of the facility were considered. First, additional power would be required to compensate for airflow friction losses in the screens and honeycomb; initial recalibration tests indicated that no such losses existed. Second, the test section wall smoothness could have been degraded by the welding and grinding of attachment points for the laminar flow control liner, the removing and reinstalling of the corner fillets, and the burning and rewelding of about 3 ft^2 of access holes in the top and bottom walls just upstream of the slot origin. No effects were found to be directly attributable to these alterations; however, the new calibration takes into account possible residual effects of the restoration of the tunnel to transonic testing.

Theory of Calibration

The term *calibration* is defined as the empirical relationship between the reference Mach number (M_{tc}), which is based on the free-stream total pressure and the static steady-state pressure in the plenum surrounding the test section, and the undisturbed free-stream Mach number (M_∞) (defined as an average of local centerline Mach numbers in the region chosen as the calibrated test section). Such a calibration is essential to the operation of the wind tunnel; even though M_{tc} can be computed whether a model is installed or not, the local Mach numbers along the centerline on which M_∞ is based can only be obtained with the calibration fixture. Note the assumption that a model near the centerline in the calibrated region of the test section will be subjected to the Mach numbers observed on a calibration probe in the same region.

The data from previous calibrations show that many variables including reentry flap position, boundary layer suction, and diffuser spoiler position may affect the relationship by which M_∞ is obtained from M_{tc}. Of the variables, the reentry flap position has the greatest effect.

From a practical standpoint, the calibration includes the determination of the reentry flap position that yields the best centerline Mach number distribution over the selected region of the test section. These Mach number data can then be used to compute the new relationship between M_∞ and M_{tc}. For operation of the facility, the reentry flap settings f_R are specified for each Mach number on the instruction sheet used by the tunnel operators (table I(a), the 1972 calibration, and table I(b), the 1989 calibration); the facility computer is programmed with the analytical relationship by which M_∞ is obtained from M_{tc}. Table I(c) is the operational instruction sheet for the closed-slot calibration performed in 1978.

The Mach numbers computed from the static pressure data along the centerline tube show that the Mach number is constant over a considerably longer region of the test section than is actually utilized. Discussion of the calibration of the extended test section length (table I(d)) follows.

The basis for the original selection of the test section between the 70- and the 120-in. station is not known other than the requirement that the Mach number be constant throughout the test section. The design procedure for the contours of the walls and slots no longer exists in any useful detail. Between the 70-in. and 120-in. stations, the empty tunnel Mach number is essentially constant for each test Mach number up to 1.2 even though the slot width varies with the station. Between the 50-in. and 150-in. stations, the empty tunnel Mach number is invariant for each subsonic Mach number; when using this extended calibration, the assumption is again made that this invariance persists in the presence of a model. However, note that the slot width variation of the 50- to 150-in. station range is entirely different than that of the 70- to 120-in. station range.

The procedure for calibrating the tunnel consists of the following steps. A cylindrical probe (figs. 1(c) and 1(d)) is installed on the longitudinal axis of the test section; the probe extends from upstream of the contraction region to the beginning of the diffuser. Data from densely spaced (about every 0.5 in.) pressure taps are obtained for suitable ranges of Mach number, stagnation pressure, and reentry flap position; the reentry flap positions are optimized by real-time observation of Mach number profiles. These data are summarized in a table that specifies the Mach number, the reentry flap position, and the correlation between the free-stream Mach number and the nominal Mach number, which is based on the stagnation pressure and the static pressure in the plenum chamber surrounding the test section. At the same time, wall surface pressure data are acquired at 2-in. intervals along three rows of orifices in the test section: the center of the top wall, the position at 45° in the top east corner fillet, and 1 ft above the centerline of the east wall. The wall pressure data are used to compute local surface Mach numbers, which are plotted along with the centerline probe data as a check on flow uniformity. The data are retained at the facility but are not presented in this report.

The guidelines for the selection of the optimal reentry flap positions are as follows:

1. The Mach number distribution on the centerline calibration probe should be as invariant as possible in the streamwise direction, especially in the test section with the slot edge-shape design between the 70-in. and 120-in. stations provided for the transonic model. The reentry flaps are positioned for the smallest possible value of the linear regression slope of the local probe Mach number as a function of axial distance over the calibrated region.

2. The Mach number distribution should be invariant with streamwise distance as far beyond the downstream end of the calibrated region as possible.

Although the pressure measurement instrumentation that was used in this calibration is superior to that which was available in 1972, the same centerline probe was installed with the same guideline that it should deviate no more than 1° from level. The calibration was performed (as in 1972) at the nominal operating temperature of 120°F. Data were obtained for the effect on Mach number distribution of the diffuser spoilers, which are used to balance model blockage, and for the effect of the boundary layer suction system, which is used to compensate for model blockage at the high end of the Mach number range.

Experimental Apparatus

Photographs of the test section with the centerline probe installed are shown in figure 1. The stainless steel probe is 27 ft long by 3 in. in diameter with a polished outer surface. The probe was installed along the longitudinal axis of the test section by suspending the upstream end, which extends into the contraction section, from four 0.125-in.-diameter wall-mounted cables swept about 45° to the flow; the downstream end was mounted on a stub sting that was attached to the angle-of-attack arc sector. By adjusting the upstream cable tension to about 400 lb and the stub sting to a slight positive angle, the gravity-induced sag in the centerline probe was minimized; the probe took on a single-cycle wave shape (with the low peak upstream and the high peak downstream) which resulted in less than 1° of slope at any point. The test section is level to within 0.08°.

The orifices on the centerline probe are located at 2-in. intervals on the top up to the 62-in. station. From the 62-in. station to the 170-in. station, the orifices are located on the top, bottom, and both sides of the cylindrical probe in a spiral pattern that has an overall X-direction spacing of 0.5 in. Downstream of the 170-in. station, the 2-in. interval pattern resumes. Thus, the primary calibration region between the 70-in. and 120-in. stations has about 200 orifices on the centerline probe, with about 50 each distributed on the top, bottom, and either side.

In addition, the east wall (the right-hand wall as one faces upstream), the top east corner fillet, and the top wall contain surface static pressure taps which have an inside diameter of 0.020 in. The east wall orifice row is about 1 ft above the centerline and the top wall orifice row is on the centerline except where it deviates about 3 in. to the east around the four small view windows.

The pressure measurement instrumentation that was used during the calibration consisted of two absolute mercury manometers that are the primary tunnel standards for the free-stream stagnation and plenum pressures and an electroscanning pressure data acquisition system, which recorded all the other pressure data. The pressure standards are maintained to a precision of ±0.2 psf, which provides an accuracy in the calculated reference Mach number

$$M_{\text{tc}} = \sqrt{5\left[\left(\frac{p_{t,\infty}}{p_{\text{tc}}}\right)^{2/7} - 1\right]}$$

of about ±0.0005 for most Mach numbers and pressures. This value is based upon the worst-case condition that both the free-stream stagnation pressure $p_{t,\infty}$ and plenum pressure $p_{t,c}$ manometers have the maximum error of 0.2 psf simultaneously and of opposite sign. (See fig. 3(a).) The electroscanning data acquisition system is calibrated daily and/or whenever it deviates more than 1 psf from zero on a check port. It scans up to 512 ports at about 10 000 ports per second.

Figure 3(b) shows the variation of the error in the Mach number

$$M_{\text{local}} = \sqrt{5\left[\left(\frac{p_{t,\infty}}{p_{\text{local}}}\right)^{2/7} - 1\right]}$$

computed from a local static pressure orifice for various Mach numbers and pressures for the worst-case condition of the $p_{t,\infty}$ manometer having a 0.2-psf error and the p_{local} pressure data sensor having the 1-psf error simultaneously.

The calibration obtained is independent of the type of pressure instrumentation used; however, the precision of the results depends on the precision of the instrumentation. In the years between the 1972 calibration and the present calibration (the data was acquired in 1989), the two primary pressure standards had been replaced. Those in use in 1972 were absolute mercury manometers with the column height determined by an electromechanical follower, which resulted in data precision of ±1 psf; in 1989, data were acquired using a similar manometer in which the mercury column height is determined by an electronically monitored sound wave, which resulted in data precision of ±0.2 psf.

Between 1972 and 1989 improved instrumentation was installed to acquire pressure data from the large number of surface orifices. In 1972, data were acquired using 48-port electromechanical stepping valves attached to electronically monitored diaphragm pressure gages. About 45 sec were needed to acquire a data set (during which time the tunnel conditions might alter slightly) and the precision was no less than about ±5 psf. The electroscanning pressure data acquisition system of 1989 acquires a data set in less than 0.01 sec, with a precision of about ±1 psf.

Discussion of Analytical Methods

Figure 4 presents plots of M versus x, one for each reference Mach number. The data are presented only for a 1-atm pressure because the pressure effect is not discernible in this type of plot. For each reference

Mach number, the Mach number distribution with the optimal reentry flap position is shown in its entirety; for comparison, other profiles of interest are shown in the region downstream of the test section for variations of reentry flap position, diffuser spoiler position, or boundary layer suction. Mach number profile comparisons of this type were used during the calibration tests to aid in the selection of optimal reentry flap settings. Figure 4 data are presented with coded lines rather than symbols for clarity in the comparisons; no fairing technique was applied. Figure 5 presents the profiles as symbol-coded data selected as the final calibration.

The vertical scale on the calibration plots is somewhat coarse when compared with the resolution of the data system. The symbol size in figures 5(a) and 5(b) corresponds to about ± 0.005 uncertainty in Mach number; whereas figure 3 shows that, because of the estimated precision of the pressure measurement instrumentation, most of the local Mach number data in figure 4 have a precision of better than ± 0.002. However, the vertical scale is acceptable because the data clearly have small random variations larger than the ± 0.002 attributable to the pressure instrument precision. These variations are clearly visible with the vertical scale of $M_\infty = 0.1$ per division and are believed to be caused by imperfections in the smoothness of the probe or wall surface at the orifice.

The top wall and bottom wall reentry flaps are mechanically constrained to move in symmetry. (See fig. 1.) The position of the reentry flaps f_R is given in terms of arbitrary counter numbers, which range from 2000 (flap leading edge farthest away from the test section, maximum flap angle) to 8400 (flap leading edge flush with the outer bevel of the slot edge, minimum flap angle). Flap leading edge position or flap angle could have been substituted but either value would have had to be reconverted to the counter reading that is used to operate the tunnel. Neither the flap leading edge position nor the flap angle have any real physical significance outside of the context of a slotted-wall tunnel design.

For the range of Mach numbers from 0.2 to 0.8 (fig. 5(b)), the design position of the reentry flaps is the closed position, which is represented by the counter reading of 8400. Thus, the new calibration only provides a slightly more accurate correction from the reference Mach number to the calibrated test section free-stream Mach number ($M_\infty = M_{\text{avg}}$). For Mach numbers greater than 0.8 but less than 1.05 (figs. 4(b)–4(l)), the more open reentry flap settings (lower counter readings) of this calibration provide a Mach number profile that is flatter in the $x = 140$-in. to 150-in. region than the 1972 calibration. These profiles were continuously updated in real-time displays during the calibration runs, which made selection of correct flap settings easier. For Mach numbers of 1.05 and greater, the new calibration was in close agreement with the 1972 calibration.

In order to obtain the correct reentry flap setting for each Mach number, as well as the corresponding relationship between M_{tc} and the calibrated test section M_∞, two factors were taken into account beyond inspection of the Mach number profiles shown in figure 4. First, the Mach number gradient as represented by the linear least-square regression slope dM/dx should be as close to zero as possible for the centerline probe profile from x_u to x_d. Figure 6 presents the Mach number gradient effect over the calibrated region as

$$S = (x_d - x_u)\frac{dM}{dx}$$

plotted versus M_{tc} or the reentry flap setting f_R. Second, the variation of reentry flap setting with Mach number should be monotonic, smooth, and independent of stagnation pressure.

For Mach numbers of 0.2 to 0.8 (fig. 6(a)), S is plotted versus Mach number because the reentry flap setting is constant ($f_R = 8400$). For Mach numbers between 0.8 and 1.05 (figs. 6(b)–6(l)), S is plotted versus f_R for each Mach number. For Mach numbers greater than 1.05 (fig. 6(m)), S is plotted versus Mach number and the value of f_R noted. Also presented in figure 6 are the values of $\Delta M = M_{\text{avg}} - M_{\text{tc}}$. This is a parameter which permits a simple comparison of the current calibration with the 1972 calibration; $M_{\text{avg}} - M_{\text{tc}}$ is comparable to $M_\infty - M_{\text{tc}}$ of table I(a). During the 1989 calibration test, the 1972 reentry flap setting was always tried first; this data point and the optimal data point of the 1989 calibration are both noted on figure 6 with an arrow and date.

Note that both f_R and ΔM (and thus the function $M_\infty = f(M_{\text{tc}})$) could be varied with stagnation pressure as well as with M_{tc} in order to correct for the small but consistent effect of total pressure on S and ΔM shown in figure 6. However, a comparison of ΔM of figure 6 with the Mach number errors presented in figure 3 indicates that the slight gain in optimization of the Mach number profiles by considering stagnation pressure would not be worth the additional effort. Also, the available data are inadequate because calibration data were only recorded at the three stagnation pressure levels of 0.5, 1.0, and 1.5 atm. Figure 7 presents the tunnel operating range as curves of constant dynamic pressure q_∞ and constant unit Reynolds number R/l for the variation of stagnation pressure versus Mach number.

Figure 8(a) presents the variation of optimal f_R, versus $M_{\rm tc}$; figure 8(b) presents the same data in terms of the geometric angle $\alpha_{f,R}$ of the reentry flap to the tunnel centerline versus the reference Mach number. The curve fairing (fig. 8(b)) in the range of $M = 0.8$ to 1.05 is marked 7th-2d-order fit because the reentry flap angle is a 2d-order function of the counter number (fig. 8(a)) which is, itself, a 7th-order polynomial function of the Mach number in this region. Although not used in the operation of the tunnel, the angle would be useful in theoretical studies of the slot and reentry flap system. Figure 9 compares the smoothed curves of f_R and ΔM from the current calibration with the same variables from the 1972 calibration. This figure also presents curves of the fan rpm from these two calibrations. The fan rpm is a measure of the energy required to sustain test section Mach number at a given stagnation pressure. The new calibration indicates that the tunnel will be operated with slightly greater efficiency than with the 1972 calibration (fig. 9(b)) because the fan rpm required for a given Mach number is slightly lower for the new calibration, particularly for the Mach numbers between 0.9 and 1.05 where the greatest variation of reentry flap position was noted.

The free-stream Mach number is computed as a single empirical function of the form

$$M_\infty = f(M_{\rm tc})$$

for each of the various modes of operation. Figure 10(a) shows this function for the complete Mach number range of the facility in the following four operational modes: open slots without boundary layer suction (condition most frequently used), open slots with boundary layer suction, the extended subsonic test section (50-in. to 150-in. station), and the closed-slot calibration from sidewall orifice data obtained in 1978 ($f_R = 8400$). The calibration curve endpoint is extrapolated to $M = 0.1$ to avoid computational problems when the Mach number varies slightly at $M = 0.2$. Note that for the closed-slot mode, the reference Mach number is computed from the primary manometer normally used for $p_{\rm tc}$ but with the manometer connected by a manifold to the east wall pressure orifices at $x = -15$, -5, and 5 in. Thus to the operator, the $M_{\rm set}$ of table I(c) is equivalent to $M_{\rm tc}$ even though it is not, in this case, based on test chamber pressure. The closed-slot calibration was not based on the test chamber pressure because this pressure can respond to the venturi pressure drop of the flow only through the vents at the reentry flap leading edge, which would be useless for calibration purposes if the flow reached sonic conditions upstream of the point at which this vent intersects the test section wall. The closed-slot calibration is included only for reference purposes and will not be used in any test subsequent to the 1989 restoration of the tunnel to transonic testing; new hardware is available for closing the slots and a new calibration will be performed after the hardware is installed.

Similar curves for Mach numbers greater than 1 are presented in figure 10(b) for a better comparison with and without boundary layer suction. These curves show the effect of the complex interaction at the slots between the free-stream flow and the essentially motionless plenum air. The fact that the curves with and without boundary layer suction match so closely indicates that the benefit of suction has been obtained without significantly disturbing the manner in which the slot edge shape provides a flat Mach number distribution.

Figure 11 presents the effect of diffuser spoiler angle δ on the Mach number correction ΔM and tunnel fan rpm for three representative Mach numbers. These effects are not included in the calibration curve of $M_\infty = f(M_{\rm tc})$ because the effect on ΔM is small and irregular. However, the effect on tunnel fan rpm is quite regular and consistent with what would be expected; as the spoilers are deflected into the flow, more power (as represented by fan rpm) is required to maintain the same Mach number at a given stagnation pressure because of the energy lost in the separated flow downstream of the spoilers.

Figure 11 also shows that a greater fan rpm is required for a given Mach number as the stagnation pressure is reduced. For this comparison, fan rpm cannot be used as a direct measure of power because the power required is also directly proportional to the density of the moving air; thus, at a constant fan rpm, the motor current will increase with stagnation pressure. The consistent increase of about 10 rpm required to maintain the same Mach number at the lower stagnation pressure of 0.5 atm is probably related to a loss of fan blade efficiency at lower Reynolds numbers.

Effect of Boundary Layer Suction for $M > 1.1$

A comparison of table I(b) from the 1989 calibration with table I(a) from the 1972 calibration shows an extension of the useful Mach number region down to $M_\infty = 1.1$ with boundary layer suction. This part of table I(b) is based on the two test data points of $M_\infty = 1.1$ and $M_\infty = 1.15$; the intermediate values were obtained by interpolation. The footnote to table I(b) provides a warning that at $M_\infty = 1.1$, the data were obtained with the compressors throttled to less than approximately 50 percent as measured by the power level in megawatts and that at $M_\infty = 1.15$ with full boundary layer suction, a severe Mach number gradient occurred at $x = 130$ in. This range of Mach numbers must be used with caution because if more suction than necessary is applied (fig. 12), then the downstream Mach number gradient intrudes into the test section ($x_u < x < x_d$) and affects the probe Mach number data, which are averaged for M_∞. The flow situation with any given model at these Mach numbers is not predictable; however, the position of the severe downstream Mach number gradient can be detected by analyzing the data from the sidewall pressure taps, which are located at 2-in. intervals in the test section.

Alternative Extended Test Section

Figure 5(a) shows that the Mach number distribution is flat for a considerable distance beyond the chosen calibration region of $x_u = 70$ in. to $x_d = 120$ in. In order to have a test section capability for longer models, the available Mach number distribution data has been re-averaged and the variations of S and ΔM with Mach number are shown in figure 13 both for the 70-in. to 120-in. test section and for several other test sections. The alternative test sections were chosen by inspection of the data of figure 5(a) with the criterion that the Mach number distributions should have no gradients larger than those in the baseline 70-in. to 120-in. test section.

For the condition without boundary layer suction, figure 13(a) shows that for Mach numbers less than 1.0, the gradient S is no worse overall for the chosen 50-in. to 150-in. test section than for the baseline 70-in. to 120-in. test section; the values of ΔM are almost unchanged by the increase in range. For Mach numbers greater than 1.0, figure 5(a) shows that the test section cannot be extended to $x_d = 150$ in. For the extended test section of 50 to 140 in. and $M_\infty = 1.0$ to 1.1, the gradient S becomes erratic with Mach number; the value of ΔM still seems unaffected. For $M_\infty = 1.15$, no significant loss in performance results by choosing a test section of 60 to 120 in. instead of the baseline test section of 70 to 120 in.; for $M_\infty = 1.2$ to 1.22, no significant loss in performance results by choosing a test section of 70 to 130 in. instead of the baseline range of 70 to 120 in. However, note that depending on model tunnel blockage, Mach numbers above 1.15 may not be attainable without boundary layer suction.

With boundary layer suction, figure 13(b) shows that at $M_\infty = 1.10$, the Mach number distribution is so erratic that both the 70-in. to 120-in. and the 50-in. to 150-in. test section resulted in similar performance. As noted above, this test condition is marginal and requires setting the boundary layer suction to less than 50 percent. For $M_\infty = 1.15$, the test section can be extended to 60 to 120 in. with no significant effect. For $M_\infty = 1.2$, the test section can be extended to 70 to 130 in.; beyond $x = 133$ in. a sharp gradient appears. (See fig. 5(a).) For $M_\infty = 1.25$, the test section can be extended to $x = 160$ in., although as shown in figure 5(b), the distribution is quite irregular for any useful range of x.

From the standpoint of facility operation, the selection of test sections tailored to changes in Mach numbers is not practical. Most models are run through a Mach number range at one location. However, the 50-in. to 150-in. test section calibration has potential use as an option for Mach numbers less than 1.0. Table I(d) presents the values of M_{tc} and corresponding pressure ratios for the 50-in. to 150-in. test section calibration parallel to that of table I(b). Note that the correlation between M_∞ and reentry flap setting is the same for both the 50-in. to 150-in. and the 70-in. to 120-in. test section.

Wall Boundary Layer

There is a limited amount of data on the sidewall boundary layer in the test section. In 1991, a 6-in. boundary layer rake with 0.060-in. total-pressure tubes mounted at 0.25-in. intervals was installed near the centerline of the west wall at the 52-in. station through a slot in an aluminum plate mounted in place of the glass window at that location. The boundary layer profile data were plotted and have the shape expected for a turbulent boundary layer. Table II is a summary of the data obtained by using this rake and includes values of the displacement and momentum thicknesses.

Concluding Remarks

The 8-Foot Transonic Pressure Tunnel has been recalibrated for the relationship between the free-stream Mach number and the test chamber reference Mach number. The calibration hardware was the same as that of the previous calibration in 1972, but the pressure measurement instrumentation used was about an order of magnitude more precise than that used in 1972.

The recalibration resulted in a slightly different schedule of reentry flap settings for use with Mach numbers from 0.80 to 1.05. Care must also be taken to limit the use of the boundary layer suction option for Mach numbers below 1.15.

An alternative longer test section was calibrated for possible use with models too long for the standard test section. Limited test section sidewall boundary layer data are presented.

NASA Langley Research Center
Hampton, VA 23681-0001
May 23, 1994

Appendix

Contraction and Test Section Geometry

The purpose of this appendix is to specify the geometry of the 8-Foot Transonic Pressure Tunnel contraction region, test section walls, and slot edges. These geometries as well as the flow parameters such as pressure and temperature determine the nature of the calibrated flow.

The data given in the tables for this appendix are taken from the engineering drawings used in the construction of the wind tunnel. The streamwise coordinate is given as a station in feet measured from the origin in the stagnation chamber at the beginning of the contraction. With the assumption of symmetry about the streamwise centerline (which is within 0.08° of horizontal), the dimensions of the walls are given as either radius or total width in the horizontal or vertical direction.

The original contraction began at the stagnation chamber with a diameter of 36 ft. When the five flow-quality screens were added (ref. 1), a cylindrical false wall with a diameter of 33.83 ft was installed to cover the screen edge hardware and intersects the curve of the original contraction at station 11.34 ft. Table AI gives the coordinates of the axially symmetric section of the original contraction wall from station 0 ft to station 28 ft.

Table AII gives the coordinates of the circular-to-square transition section (with corner fillets) from station 28 ft to station 36 ft. In this transition section, the wall contours between the fillets are straight lines in the direction perpendicular to the flow and have a faired curvature in the free-stream X direction.

Table AIII gives the coordinates of the section from station 36 ft to station 50 ft (the slot origin). This section is square with corner fillets.

Upstream of station 50 ft, the walls are steel plate approximately 1 in. thick. Although the locating coordinate density is as low as one per foot in places, all plates were contoured and welds were ground smooth in the construction process. From station 50 ft to station 71 ft (table AIV), the coordinates were generally given to within 0.001 in. every 2 in. The wall surfaces are stainless steel and were polished to a smoothness specified as 120 microinches during construction in 1952. During the recalibration of 1989 discussed in this report, the stainless steel walls were less smooth because of abrasion from test articles and numerous mounting holes filled with epoxy and sanded smooth after use. Also, steps of about 0.01 in. often occur between the glass windows and the steel frames because the windows are mounted against a rubber shim.

Table AIV gives the coordinates of both the wall and the slot edges from station 50 ft to station 71 ft. This set of slot edges was the only set ever made in steel and was designated 2f in the design process. Several experimental and special-purpose sets of slot edges made of mahogany exist but were not used in the recalibration procedure. Table AIV also shows the origin of the reentry flaps, which are hinged at station 71 ft, and gives the coordinates for the windward surface of the reentry flaps in the closed position. Reentry flap surface coordinates for any other setting can be computed from table AV data, which relates the reentry flap surface angle to the arbitrary counter reading f_R used in operation of the tunnel. The shapes of the slot edges and leading edge of the reentry flap are specified in figure A1. These edges are the outermost parts of the windward flow surfaces and are shaped for aerodynamic smoothness. Figure A2(a) shows the width of one of the eight identical slots as a function of x for the entire length; for greater detail, figure A2(b) shows the shape of the curved portion of the slot for the upstream 10 ft. The corners in figure A2(b) reflect the values from table AIV, which were taken from the construction drawing of the slot edges. No such corners are actually perceptible on the slot edge. The calibrated streamwise test sections are marked on figure A2(a) for reference.

The open ratio of the slots, which is based on twice the width of the test section (only the top and bottom walls are slotted), increases rapidly from 0 percent at the tunnel 0-in. station (the slot origin) to 10 percent at the 42-in. station. It then decreases less rapidly to an open ratio of about 4 percent at the 82-in. station and remains constant to about the 88-in. station. The rate of opening provides for a rapid expansion of the flow and the closing counteracts this effect to prevent overexpansion, which establishes the uniformity of the axial flow distributions. Downstream of the 88-in. station, the slots again expand to an open ratio of 10 percent at the 108-in. station and remain a constant width to the 132-in. station. A very rapid expansion occurs to give an open ratio of 20 percent at the 136-in. station. From the 136-in. station to the nose of the diffuser entrance flaps at the 147.5-in. station, the open ratio remains constant at 20 percent. Downstream of the nose of the diffuser entrance flaps, the open ratio remains constant at 20 percent to the 167-in. station. From the 167-in. station, the slots diverge at 6°15′ until adjacent slots come together at a point at the 246-in. station. A top view of the slot layout is presented in figure A2(c).

Note that the 50-ft station in table AIV corresponds to the 0-in. station used as the reference of the Mach number distribution plots in this report. Thus, as marked on table AIV and figure A2(a), the standard 70-in. to 120-in. test region where most models are installed corresponds to stations 55.833 to 60.000 ft in the construction coordinate system.

Table AI. Tunnel Circuit Coordinates for Station 0 ft to Station 28 ft

X, ft	r, in.
0.0	216.00
2.0	215.63
7.0	211.75
10.0	206.63
11.34[a]	203.00
12.0	201.20
13.0	197.95
14.0	194.25
15.0	189.80
16.0	184.60
17.0	178.55
18.0	171.70
19.0	164.05
20.0	155.70
24.0	120.70
25.0	112.55
26.0	104.80
27.0	97.55
28.0	90.80

[a]Cylindrical false floor intersects curved wall.

Table AII. Tunnel Circuit Coordinates for Station 28 ft to Station 36 ft

X, ft	y_{wall} or z_{wall}, in.	r, in.
28.0	181.6	90.80
29.0	166.0	76.16
30.0	150.8	61.75
31.0	138.0	49.63
32.0	127.4	38.88
33.0	118.0	28.91
34.0	110.2	19.84
35.0	103.8	12.53
36.0	99.2	8.55

Table AIII. Tunnel Circuit Coordinates
for Station 36 ft to Station 50 ft

X, ft	y_{wall} or z_{wall}, in.	r, in.
36.0000	99.200	8.55
37.0000	95.590	
38.0000	92.820	
39.0000	91.110	
40.0000	89.420	
41.0000	88.070	
42.0000	87.020	
43.0000	86.307	
43.2500	86.160	
43.5000	86.046	
43.7500	85.952	
44.0000	85.870	
44.2083	85.806	
44.4166	85.748	
44.6250	85.696	
44.8333	85.648	
45.0000	85.616	
45.1667	85.588	
45.3333	85.563	
45.5000	85.541	
45.6667	85.522	
45.8333	85.505	
46.0000	85.491	
46.1667	85.480	
46.3333	85.470	
46.5000	85.462	
46.6667	85.456	
46.8333	85.452	
47.0000	85.449	
47.1667	85.447	
47.3333	85.447[a]	
47.5000	85.447	
47.6667	85.448	
47.8333	85.450	
48.0000	85.453	
48.1667	85.456	
48.3333	85.460	
48.5000	85.464	
48.6667	85.469	
48.8333	85.474	
49.0000	85.479	
49.1667	85.484	
49.3333	85.489	
49.5000	85.494	
49.6667	85.499	
49.8333	85.505	
50.0000	85.510	↓

[a]Geometric minimum.

Table AIV. Tunnel Circuit Coordinates for Station 50 ft to Station 71 ft

X, ft	y_{wall}, in.	y_s, in.	z_{wall}, in.	z_R, in.	D_f, in.	r_f, in.
50.000	85.510[a]	0.000	85.510		3.55	8.55
50.167		.200				
50.333		.310				
50.500	85.527	.420	85.529			
50.667		.540				
50.833		.640				
51.000	85.545	.750	85.552			
51.167		.860				
51.333		.974				
51.500	85.562	1.082	85.578			
51.667		1.200				
51.833		1.306				
52.000	85.579	1.420	85.606			
52.167		1.530				
52.333		1.640				
52.500	85.597	1.750	85.636			
52.667		1.860				
52.833		1.960				
53.000	85.614	2.036	85.669			
53.167		2.100				
53.333		2.134				
53.500	85.631	2.140	85.704			
53.667		2.136				
53.833		2.110				
54.000	85.649	2.080	85.742			
54.167		2.020				
54.333		1.970				
54.500	85.666	1.900	85.782			
54.667		1.820				
54.833		1.740				
55.000	85.683	1.660	85.824[b]			
55.167		1.580				
55.333		1.500				
55.500	85.701	1.420	85.869			
55.667		1.340				
55.833		1.260				
56.000	85.718	1.184	85.916			
56.167		1.104				
56.333		1.024				
56.500		.956				
56.667		.890				
56.833		.860				
57.000		.860				

[a]5′ wall divergence through station 71 ft.

[b]13′ wall divergence through station 71 ft.

Table AIV. Concluded

X, ft	y_{wall}, in.	y_s, in.	z_{wall}, in.	z_R, in.	D_f, in.	r_f, in.
57.000		0.860			3.55	
57.167		.860				
57.333		.860				
57.500		.960				
57.667		1.100				
57.833		1.260				
58.000		1.420				
58.167		1.580				
58.333		1.740				
58.500		1.900				
58.667		2.060				
58.833		2.100				
59.000		2.138				
61.000		2.138				
61.167		3.200				
61.333		4.276				
62.250				L.E.[c]		
63.000	85.962		86.548	89.14	3.55[d]	8.55
63.917		4.276[e]		89.14	3.55[d]	
64.750		6.440		Linear runout	Linear runout	
70.500		21.378		Linear runout	Linear runout	
70.830					.37	8.55
71.000	86.242		87.274	95.10		

[c]Closed RF = 8400 at 1.955° divergent through station 71 ft, offset = 1.30 in. at station 63 ft.

[d]Linear runout of fillet offset through station 70.83 ft.

[e]Slot edge radius runout from 0.15 in. forward (135° to 45° outside bevel) to 0.50 in. aft (180° half round) through station 64.75 ft.

Table AV. Lower Reentry Flap Angle (From Horizontal) Versus Counter Setting

f_R, counts	$\alpha_{f,R}{}^{a}$, deg
8400	1.95500
8380	1.94600
8345	1.93000
8299	1.90900
8248	1.88500
8197	1.86100
8149	1.83800
8105	1.81600
8068	1.79800
8035	1.78200
8006	1.76700
7978	1.75300
7948	1.73700
7914	1.72000
7873	1.69800
7824	1.67200
7766	1.64100
7699	1.60500
7627	1.56500
7552	1.52200
7477	1.47900
7408	1.43800
7346	1.40100
7293	1.36900
7247	1.34100
7200	1.31200
6700	.98270
6330	.71576
6200	.61720
6000	.46100
5750	.25753
5275	−.15394
4800	−.59800
3970	−1.45200

[a]These coordinates represent the 2d-order fit referred to in figure 8(b).

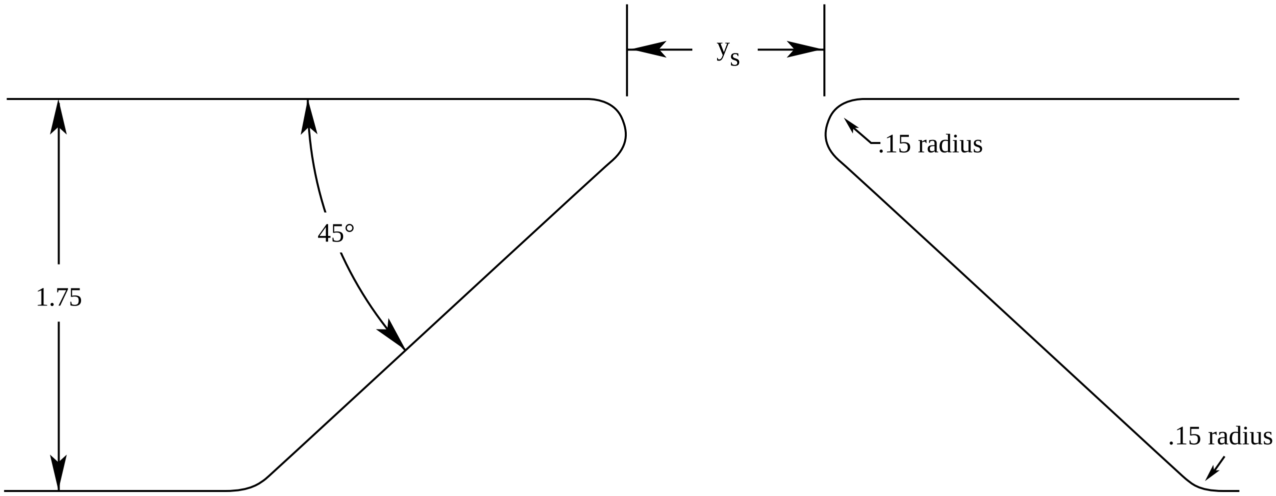

(a) Bottom slot edge cross section perpendicular to tunnel centerline. All linear dimensions in inches.

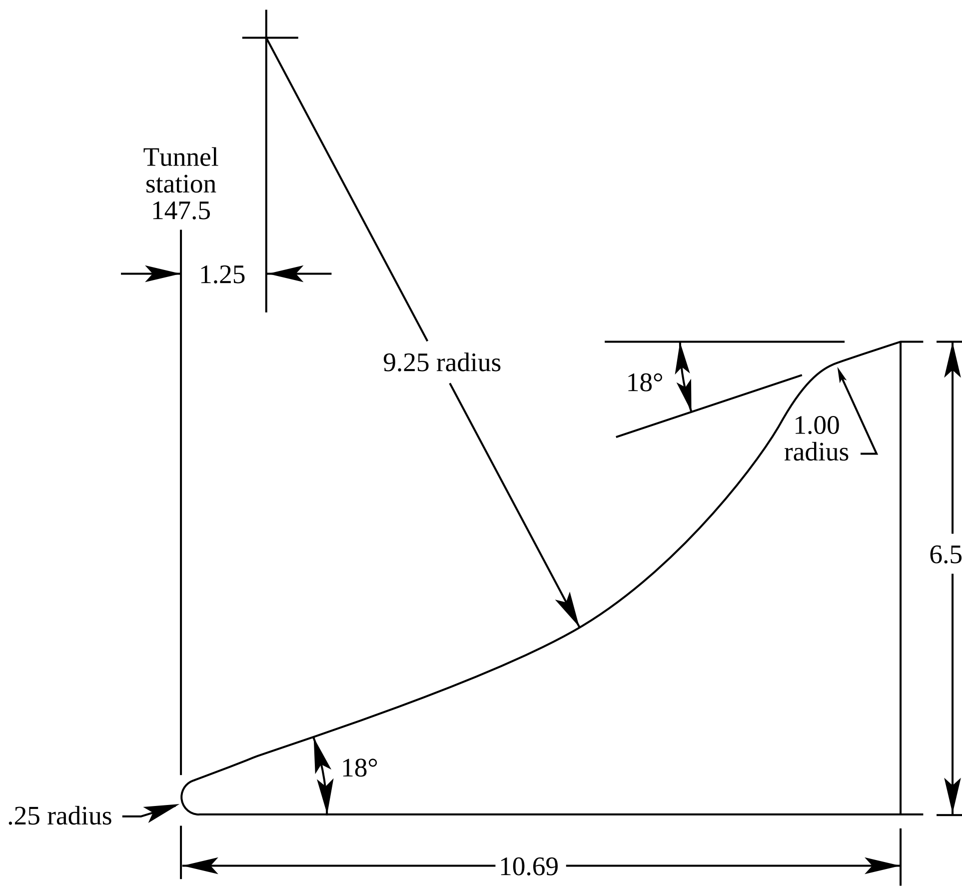

(b) Top reentry flap leading edge profile. All linear dimensions in inches.

Figure A1. Tunnel components.

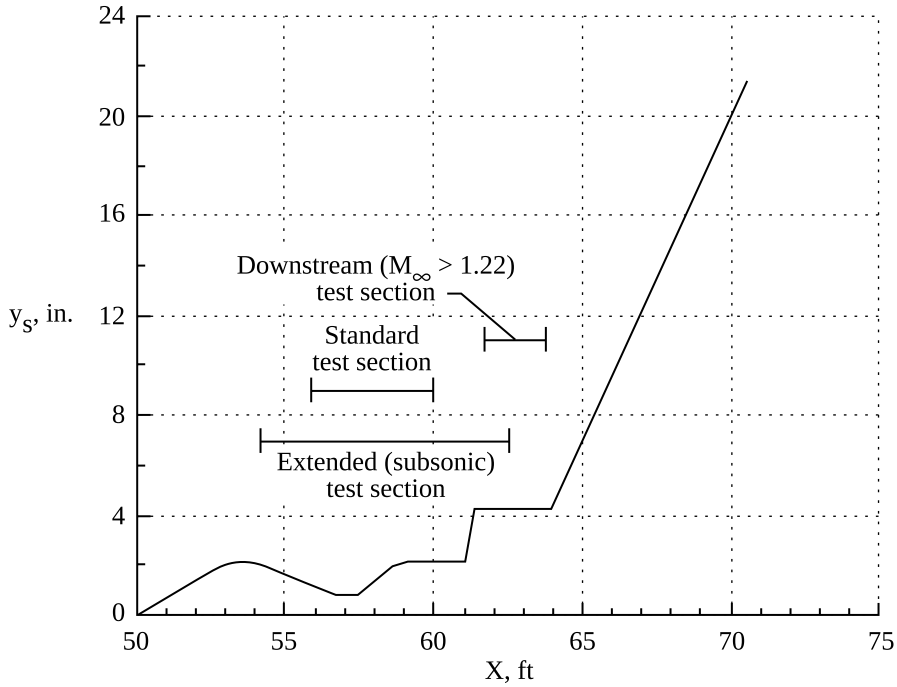

(a) Full length.

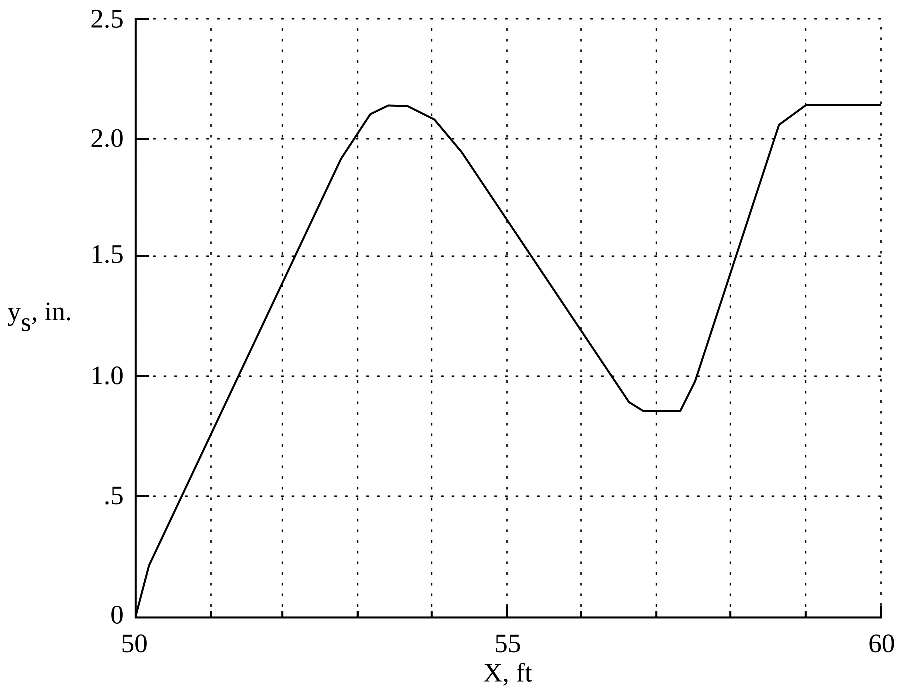

(b) Partial length (enlarged).

Figure A2. Slot details.

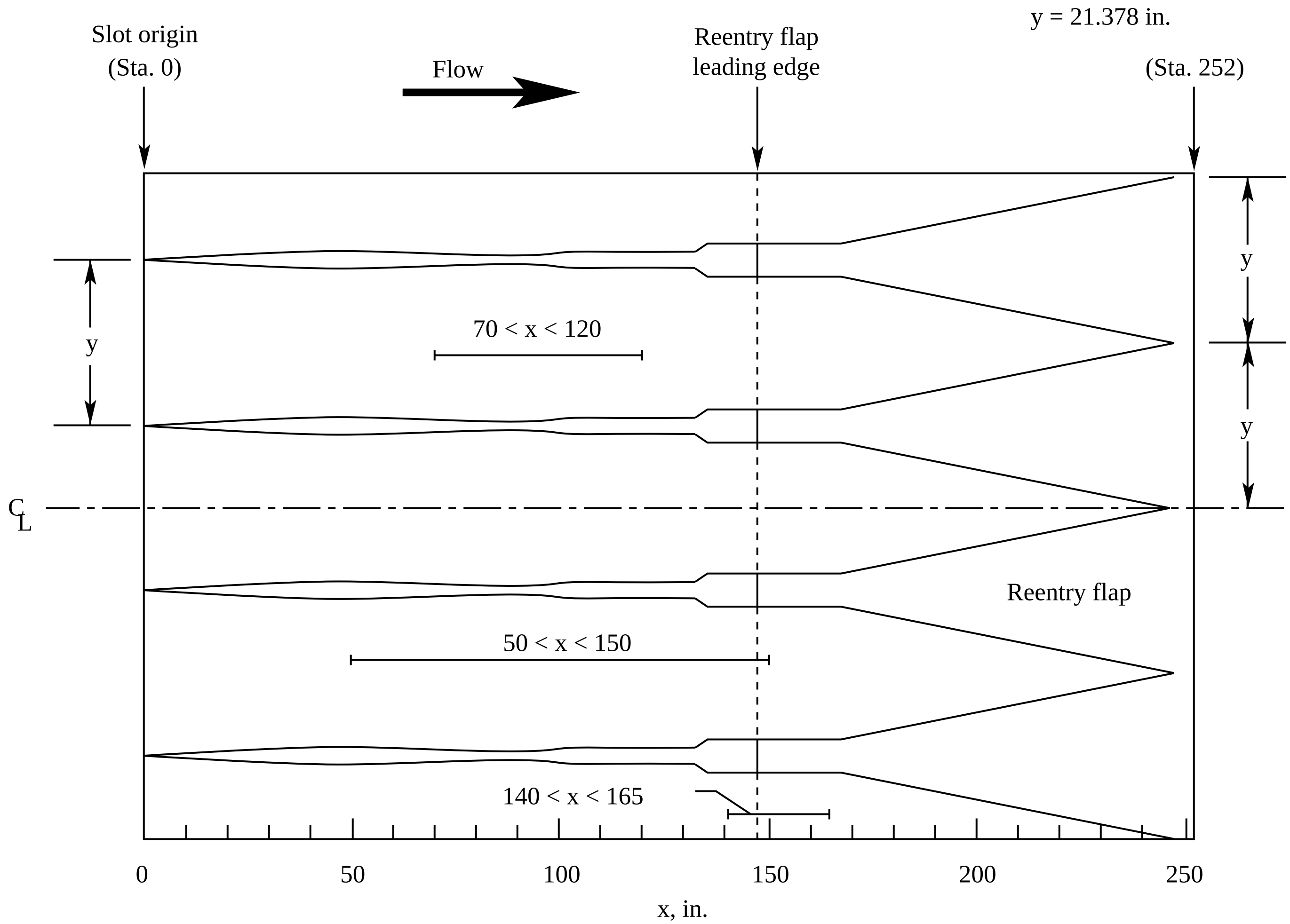

(c) Plan view of slot spacing. Width aspect exaggerated by factor of 2 for clarity.

Figure A2. Concluded.

References

1. Harris, Charles D.; Harvey, William D.; and Brooks, Cuyler W., Jr.: *The NASA Langley Laminar-Flow-Control Experiment on a Swept, Supercritical Airfoil—Design Overview.* NASA TP-2809, 1988.

2. Harris, Charles D.; and Brooks, Cuyler, W., Jr.: *Modifications to the Langley 8-Foot Transonic Pressure Tunnel for the Laminar Flow Control Experiment.* NASA TM-4032, 1988.

Table I. Tunnel Operational Parameters

(a) Calibration of 1972

M_∞	M_{tc}	$\frac{p_{\mathrm{tc}}}{p_{t,\infty}}$	$1 - \frac{p_{\mathrm{tc}}}{p_{t,\infty}}$	Optimal reentry flap	Test section, in.	M_∞	M_{tc}	$\frac{p_{\mathrm{tc}}}{p_{t,\infty}}$	$1 - \frac{p_{\mathrm{tc}}}{p_{t,\infty}}$	Optimal reentry flap	Test section, in.
0.10	0.1000	0.9930	0.0070	8400	70–120	0.90	0.9026	0.5896	0.4104	8400	70–120
.15	.1500	.9844	.0156	8400	70–120	.91	.9125	.5833	.4167	8400	70–120
.20	.2000	.9725	.0275	8400	70–120	.92	.9224	.5769	.4231	8400	70–120
.25	.2507	.9572	.0428	8400	70–120	.93	.9322	.5707	.4293	8400	70–120
.30	.3010	.9391	.0609	8400	70–120	.94	.9421	.5644	.4356	8400	70–120
.35	.3509	.9184	.0816	8400	70–120	.95	.9521	.5581	.4419	8400	70–120
.40	.4013	.8950	.1050	8400	70–120	.96	.9623	.5517	.4483	8400	70–120
.45	.4526	.8689	.1311	8400	70–120	.97	.9728	.5452	.4548	8400	70–120
.50	.5040	.8408	.1592	8400	70–120	.98	.9840	.5382	.4618	8400	70–120
.55	.5542	.8117	.1883	8400	70–120	.99	.9950	.5314	.4686	8400	70–120
.60	.6035	.7819	.2181	8400	70–120	1.00	1.0030	.5264	.4736	7700	70–120
.61	.6134	.7757	.2243	8400	70–120	1.01	1.0118	.5210	.4790	7700	70–120
.62	.6232	.7696	.2304	8400	70–120	1.02	1.0222	.5147	.4853	7650	70–120
.63	.6330	.7635	.2365	8400	70–120	1.03	1.0334	.5079	.4921	7600	70–120
.64	.6429	.7573	.2427	8400	70–120	1.04	1.0432	.5020	.4980	7400	70–120
.65	.6527	.7511	.2489	8400	70–120	1.05	1.0525	.4964	.5036	7200	70–120
.66	.6626	.7448	.2552	8400	70–120	1.06	1.0623	.4905	.5095	7026	70–120
.67	.6724	.7386	.2614	8400	70–120	1.07	1.0727	.4844	.5156	6852	70–120
.68	.6822	.7324	.2676	8400	70–120	1.08	1.0834	.4780	.5220	6678	70–120
.69	.6921	.7260	.2740	8400	70–120	1.09	1.0939	.4719	.5281	6504	70–120
.70	.7019	.7197	.2803	8400	70–120	1.10	1.1039	.4661	.5339	6330	70–120
.71	.7117	.7134	.2866	8400	70–120	1.11	1.1130	.4608	.5392	6119	70–120
.72	.7215	.7071	.2929	8400	70–120	1.12	1.1216	.4559	.5441	5908	70–120
.73	.7314	.7006	.2994	8400	70–120	1.13	1.1298	.4512	.5488	5697	70–120
.74	.7412	.6943	.3057	8400	70–120	1.14	1.1380	.4466	.5534	5486	70–120
.75	.7511	.6879	.3121	8400	70–120	1.15	1.1463	.4419	.5581	5275	70–120
.76	.7610	.6814	.3186	8400	70–120	1.16	1.1551	.4370	.5630	5014	70–120
.77	.7709	.6750	.3250	8400	70–120	1.17	1.1645	.4318	.5682	4753	70–120
.78	.7809	.6685	.3315	8400	70–120	1.175	1.1695	.4290	.5710	4623	70–120
.79	.7909	.6619	.3381	8400	70–120	1.18	1.1746	.4262	.5738	4492	70–120
.80	.8010	.6554	.3446	8400	70–120	1.185	1.1800	.4232	.5768	4361	70–120
.81	.8111	.6488	.3512	8400	70–120	1.19	1.1856	.4202	.5798	4231	70–120
.82	.8213	.6422	.3578	8400	70–120	1.195	1.1915	.4170	.5830	4100	70–120
.83	.8315	.6355	.3645	8400	70–120	1.20	1.1977	.4136	.5864	3970	70–120
.84	.8417	.6289	.3711	8400	70–120	With boundary layer suction (2 compressors)					
.85	.8520	.6222	.3778	8400	70–120	1.20	1.2030	0.4107	0.5893	7200	70–120
.86	.8622	.6156	.3844	8400	70–120	1.25	1.2592	.3813	.6187	5000	145–160
.87	.8724	.6090	.3910	8400	70–120	1.30	1.3054	.3583	.6417	5000	145–160
.88	.8825	.6025	.3975	8400	70–120	1.35	1.3708	.3274	.6726	2700	145–160
.89	.8926	.5960	.4040	8400	70–120						

Table I. Continued

(b) Calibration of 1989

M_∞	M_{tc}	$\frac{p_{tc}}{p_{t,\infty}}$	Reentry flap	Test section, in.	M_∞	M_{tc}	$\frac{p_{tc}}{p_{t,\infty}}$	Reentry flap	Test section, in.	M_∞	M_{tc}	$\frac{p_{tc}}{p_{t,\infty}}$	Reentry flap	Test section, in.
0.1000	0.1002	0.9930	8400	70–120	0.8100	0.8124	0.6480	8380	70–120	1.1200	1.1209	0.4563	5908	70–120
.1500	.1503	.9844	8400	70–120	.8200	.8224	.6414	8345	70–120	1.1300	1.1293	.4515	5697	70–120
.2000	.2004	.9724	8400	70–120	.8300	.8325	.6349	8299	70–120	1.1400	1.1377	.4467	5486	70–120
.2500	.2506	.9573	8400	70–120	.8400	.8426	.6283	8249	70–120	1.1500	1.1464	.4419	5275	70–120
.3000	.3008	.9392	8400	70–120	.8500	.8526	.6218	8197	70–120	1.1600	1.1554	.4368	5014	70–120
.3500	.3511	.9183	8400	70–120	.8600	.8626	.6153	8149	70–120	1.1700	1.1650	.4315	4753	70–120
.4000	.4013	.8950	8400	70–120	.8700	.8727	.6089	8105	70–120	1.1750	1.1701	.4286	4623	70–120
.4500	.4515	.8695	8400	70–120	.8800	.8827	.6024	8068	70–120	1.1800	1.1754	.4258	4492	70–120
.5000	.5017	.8421	8400	70–120	.8900	.8927	.5959	8035	70–120	1.1850	1.1809	.4227	4361	70–120
.5500	.5519	.8130	8400	70–120	.9000	.9028	.5895	8006	70–120	1.1900	1.1867	.4196	4231	70–120
.6000	.6021	.7827	8400	70–120	.9100	.9128	.5830	7978	70–120	1.1950	1.1927	.4163	4100	70–120
.6100	.6121	.7765	8400	70–120	.9200	.9229	.5766	7948	70–120	1.2000	1.1990	.4129	3970	70–120
.6200	.6222	.7703	8400	70–120	.9300	.9331	.5702	7914	70–120	With boundary layer suction				
.6300	.6322	.7640	8400	70–120	.9400	.9432	.5638	7873	70–120	1.1000	1.1030	0.4666	7200	70–120[a]
.6400	.6422	.7577	8400	70–120	.9500	.9533	.5574	7824	70–120	1.1100	1.1110	.4620	7200	70–120[a]
.6500	.6523	.7514	8400	70–120	.9600	.9635	.5510	7766	70–120	1.1200	1.1192	.4573	7200	70–120[a]
.6600	.6623	.7451	8400	70–120	.9700	.9736	.5447	7699	70–120	1.1300	1.1275	.4525	7200	70–120[a]
.6700	.6723	.7387	8400	70–120	.9800	.9836	.5384	7627	70–120	1.1400	1.1361	.4477	7200	70–120[a]
.6800	.6823	.7323	8400	70–120	.9900	.9934	.5324	7552	70–120	1.1500	1.1452	.4425	7200	70–120[a]
.6900	.6923	.7259	8400	70–120	1.0000	1.0032	.5263	7477	70–120	1.1600	1.1548	.4371	7100	70–120
.7000	.7023	.7194	8400	70–120	1.0100	1.0135	.5200	7408	70–120	1.1700	1.1650	.4315	7000	70–120
.7100	.7123	.7130	8400	70–120	1.0200	1.0236	.5138	7346	70–120	1.1750	1.1703	.4286	6950	70–120
.7200	.7223	.7066	8400	70–120	1.0300	1.0334	.5079	7293	70–120	1.1800	1.1757	.4256	6900	70–120
.7300	.7323	.7001	8400	70–120	1.0400	1.0432	.5019	7247	70–120	1.1850	1.1812	.4226	6850	70–120
.7400	.7422	.6936	8400	70–120	1.0500	1.0533	.4959	7200	70–120	1.1900	1.1867	.4196	6800	70–120
.7500	.7522	.6871	8400	70–120	1.0600	1.0636	.4897	7025	70–120	1.1950	1.1923	.4165	6750	70–120
.7600	.7622	.6806	8400	70–120	1.0700	1.0740	.4836	6855	70–120	1.2000	1.1980	.4135	6700	70–120
.7700	.7722	.6741	8400	70–120	1.0800	1.0843	.4775	6680	70–120	1.22	1.22		6500	70–120
.7800	.7822	.6676	8400	70–120	1.0900	1.0943	.4717	6510	70–120	1.22+	1.23		5900	140–165
.7900	.7923	.6611	8400	70–120	1.1000	1.1036	.4663	6330	70–120	1.2500	1.2584	.3818	6000	140–165
.8000	.8023	.6545	8400	70–120	1.1100	1.1124	.4612	6119	70–120	1.3000	1.3032	.3593	5750	140–165
										1.3150	1.3205	.3510	4800	140–165

[a]Compressors at less than 50 percent suction for $M = 1.1$; extreme gradient at $x = 130$ in. for $M = 1.15$ with full suction.

Table I. Concluded

(c) Closed-slot calibration of 1978

[Reentry flaps closed ($f_R = 8400$)]

M_∞	M_{set}	$\frac{p_{set}}{p_{t,\infty}}$
0.200	0.2015	0.9721
.300	.3025	.9385
.400	.4035	.8939
.500	.5044	.8405
.600	.6053	.7807
.700	.7062	.7169
.800	.8070	.6515
.900	.9155	.5813

(d) Extended test section calibration of 1991

M_∞	M_{tc}	$\frac{p_{tc}}{p_{t,\infty}}$	Reentry flap	Test section, in.	M_∞	M_{tc}	$\frac{p_{tc}}{p_{t,\infty}}$	Reentry flap	Test section, in.
0.1000	0.1000	0.9930	8400	50–150	0.7500	0.7523	0.6871	8400	50–150
.1500	.1501	.9844	8400	50–150	.7600	.7622	.6806	8400	50–150
.2000	.2003	.9724	8400	50–150	.7700	.7722	.6741	8400	50–150
.2500	.2506	.9573	8400	50–150	.7800	.7822	.6676	8400	50–150
.3000	.3010	.9391	8400	50–150	.7900	.7922	.6611	8400	50–150
.3500	.3513	.9182	8400	50–150	.8000	.8022	.6546	8400	50–150
.4000	.4015	.8949	8400	50–150	.8100	.8122	.6481	8380	50–150
.4500	.4518	.8693	8400	50–150	.8200	.8223	.6415	8345	50–150
.5000	.5021	.8418	8400	50–150	.8300	.8323	.6350	8299	50–150
.5500	.5523	.8128	8400	50–150	.8400	.8424	.6284	8249	50–150
.6000	.6025	.7825	8400	50–150	.8500	.8524	.6220	8197	50–150
.6100	.6125	.7763	8400	50–150	.8600	.8624	.6155	8149	50–150
.6200	.6225	.7701	8400	50–150	.8700	.8724	.6090	8105	50–150
.6300	.6326	.7638	8400	50–150	.8800	.8824	.6026	8068	50–150
.6400	.6426	.7575	8400	50–150	.8900	.8924	.5961	8035	50–150
.6500	.6526	.7512	8400	50–150	.9000	.9023	.5898	8006	50–150
.6600	.6626	.7448	8400	50–150	.9100	.9124	.5833	7978	50–150
.6700	.6726	.7385	8400	50–150	.9200	.9224	.5769	7948	50–150
.6800	.6825	.7322	8400	50–150	.9300	.9325	.5705	7914	50–150
.6900	.6925	.7257	8400	50–150	.9400	.9427	.5641	7873	50–150
.7000	.7025	.7193	8400	50–150	.9500	.9531	.5575	7824	50–150
.7100	.7125	.7129	8400	50–150	.9600	.9635	.5510	7766	50–150
.7200	.7224	.7065	8400	50–150	.9700	.9738	.5445	7699	50–150
.7300	.7324	.7000	8400	50–150	.9800	.9839	.5382	7627	50–150
.7400	.7423	.6936	8400	50–150	.9900	.9937	.5322	7552	50–150

Table II. Test Section Wall Boundary Layer

[Summary of boundary layer data taken at 52-in. test station on vertical center of west wall]

M_∞	R/l, ft^{-1}	$T_{t,\infty}$, °F	y_e, in.	δ^*, in.	θ, in.	H
1.196	3.190×10^6	99.3	2.015	0.229	0.126	1.824
1.197	3.190	99.2	2.015	.227	.125	1.822
1.100	3.170	99.5	2.015	.262	.148	1.769
1.002	3.120	97.7	2.520	.298	.176	1.693
.900	3.000	99.9	2.520	.308	.191	1.611
.799	2.840	99.5	2.520	.311	.203	1.534
.700	2.650	97.0	2.520	.313	.213	1.473
.599	2.400	97.2	3.780	.325	.229	1.419
.500	2.090	99.1	3.050	.327	.238	1.376
.402	1.740	99.9	3.780	.338	.253	1.332
.299	1.350	96.3	3.780	.356	.272	1.307
.200	.922	96.7	3.780	.392	.303	1.294

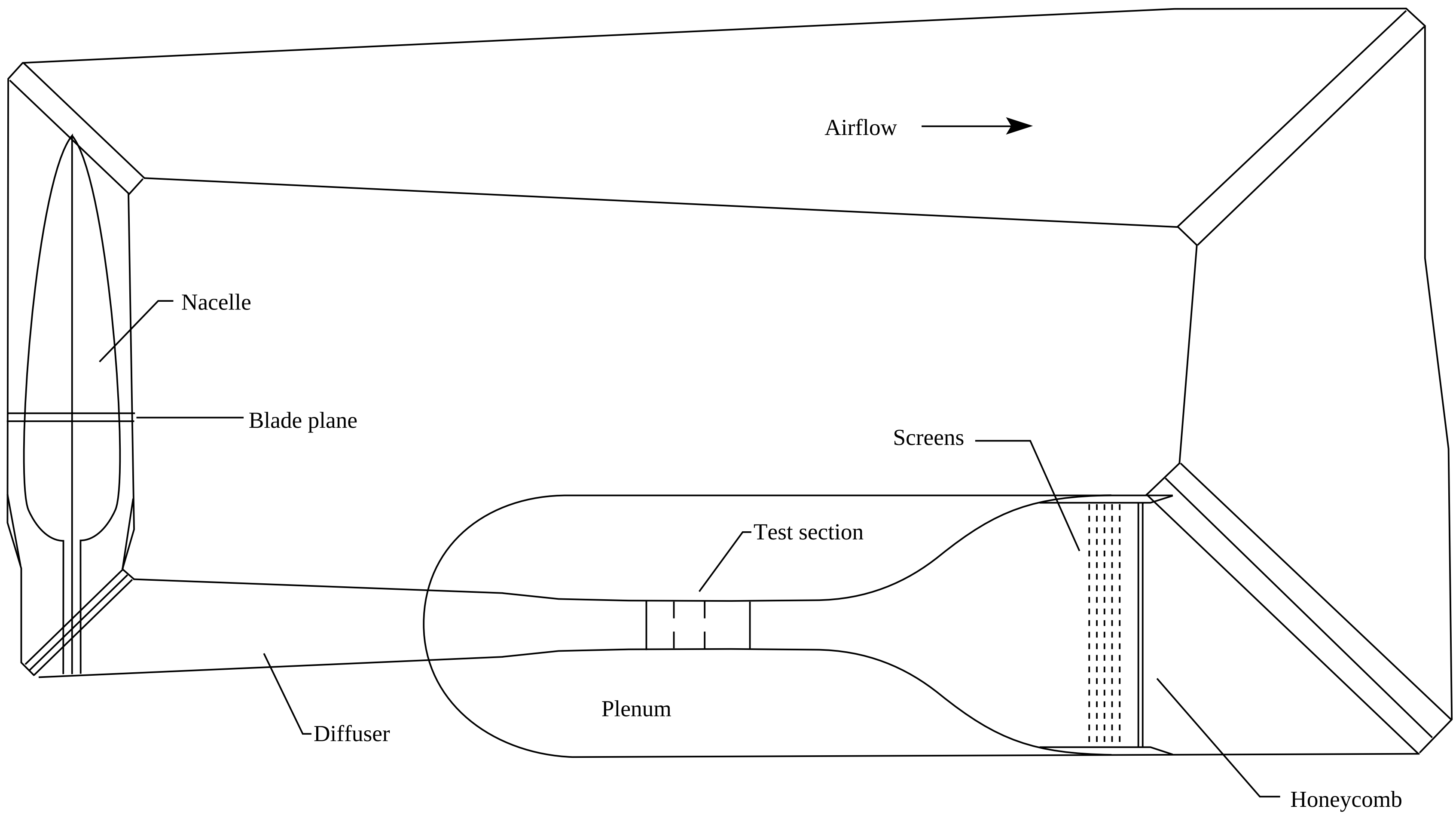

(b) Plan view of tunnel circuit.

Figure 1. Continued.

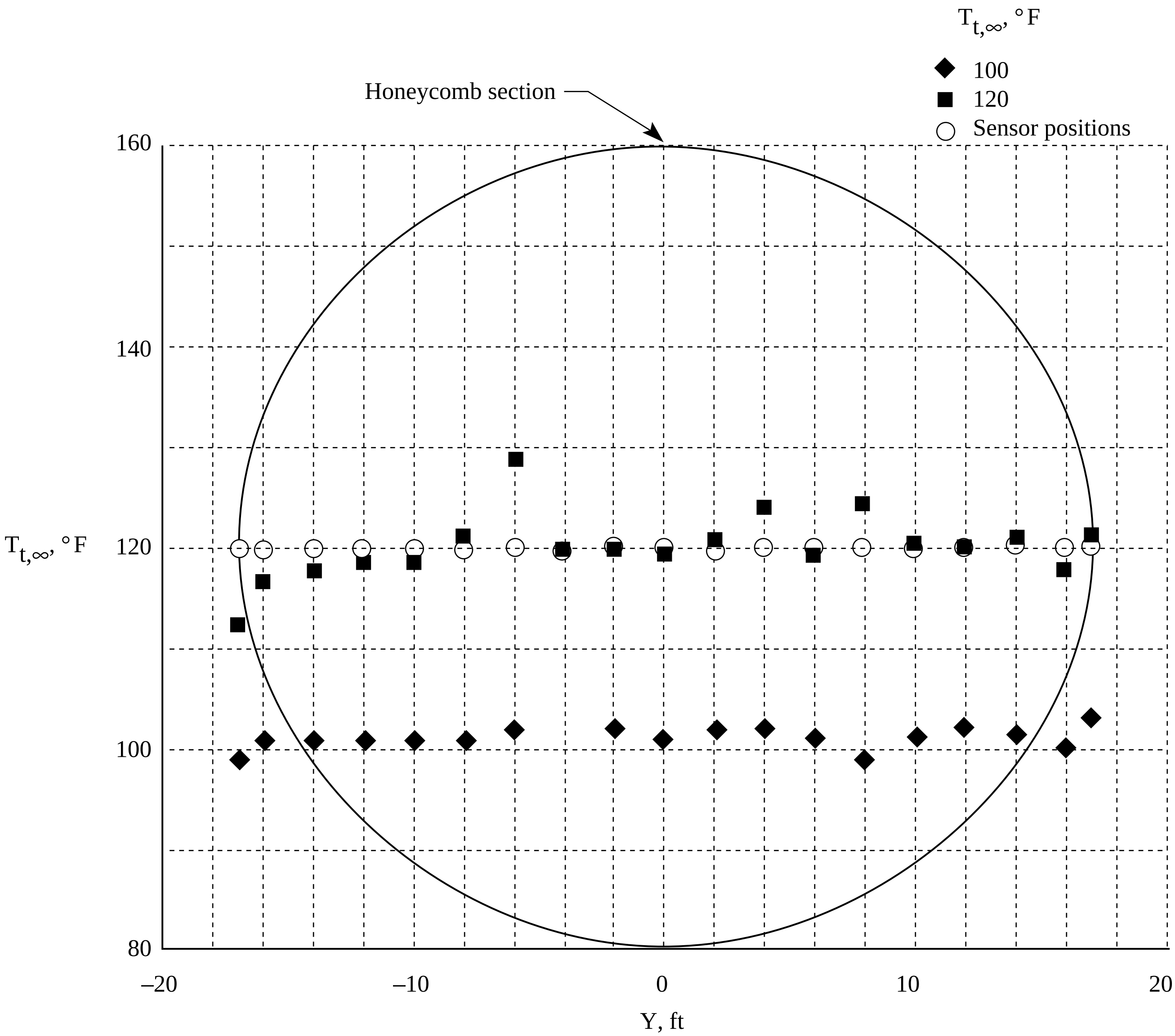

Figure 2. Typical total temperature distribution on upstream face of honeycomb.

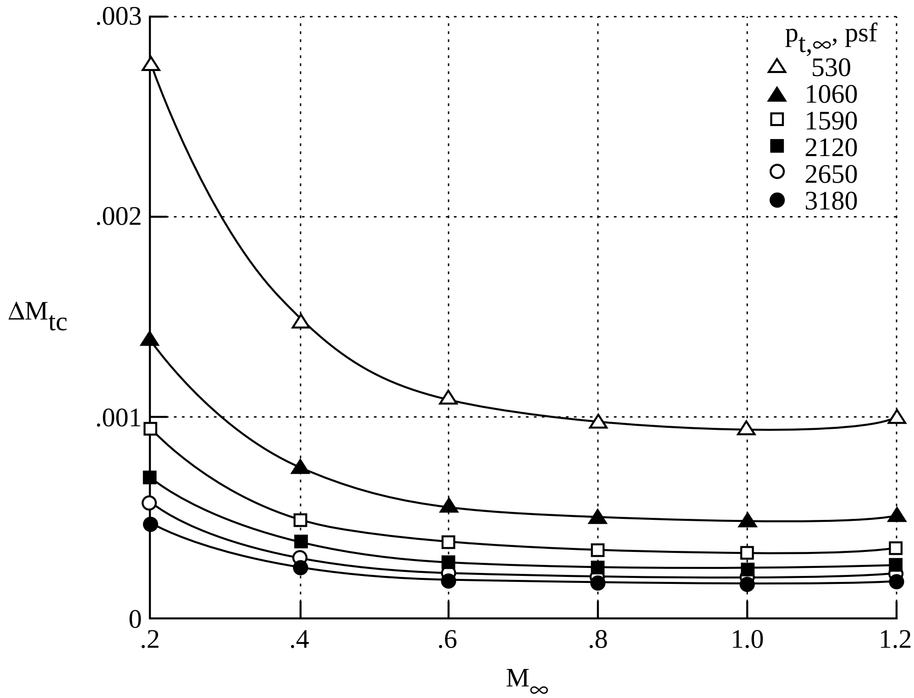

(a) Variation of error in M_{tc} with $p_{t,\infty}$ based on 0.2-psf instrument error in both $p_{t,\infty}$ and $p_{t,c}$, worst-case combination of errors.

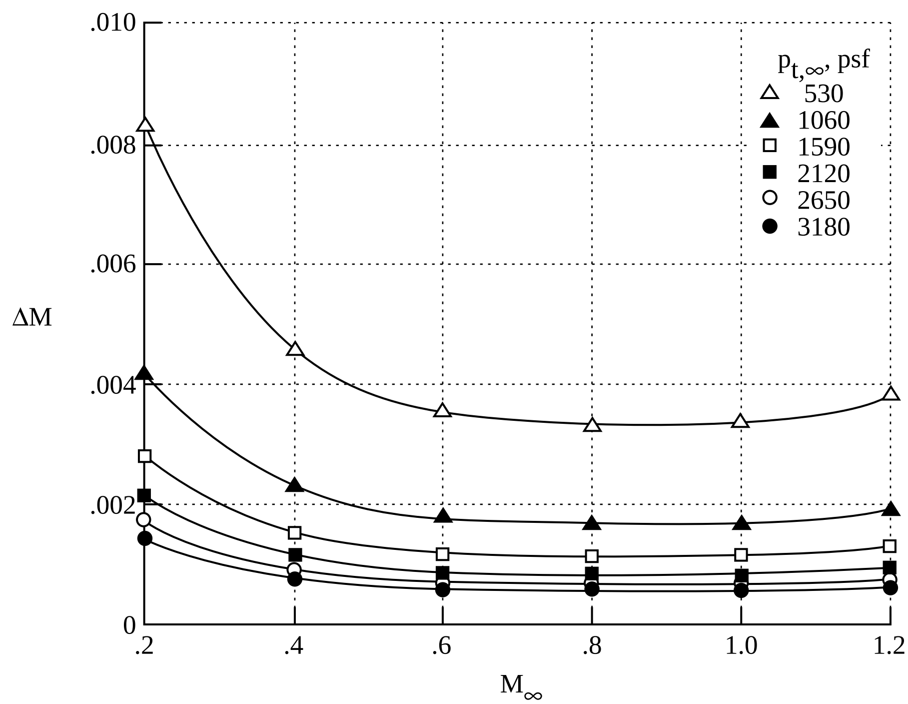

(b) Variation of error in local M with $p_{t,\infty}$ based on 1-psf instrument error in p_{local} and 0.2-psf error in $p_{t,\infty}$, worst-case combination of errors.

Figure 3. Error in Mach number as a function of total pressure.

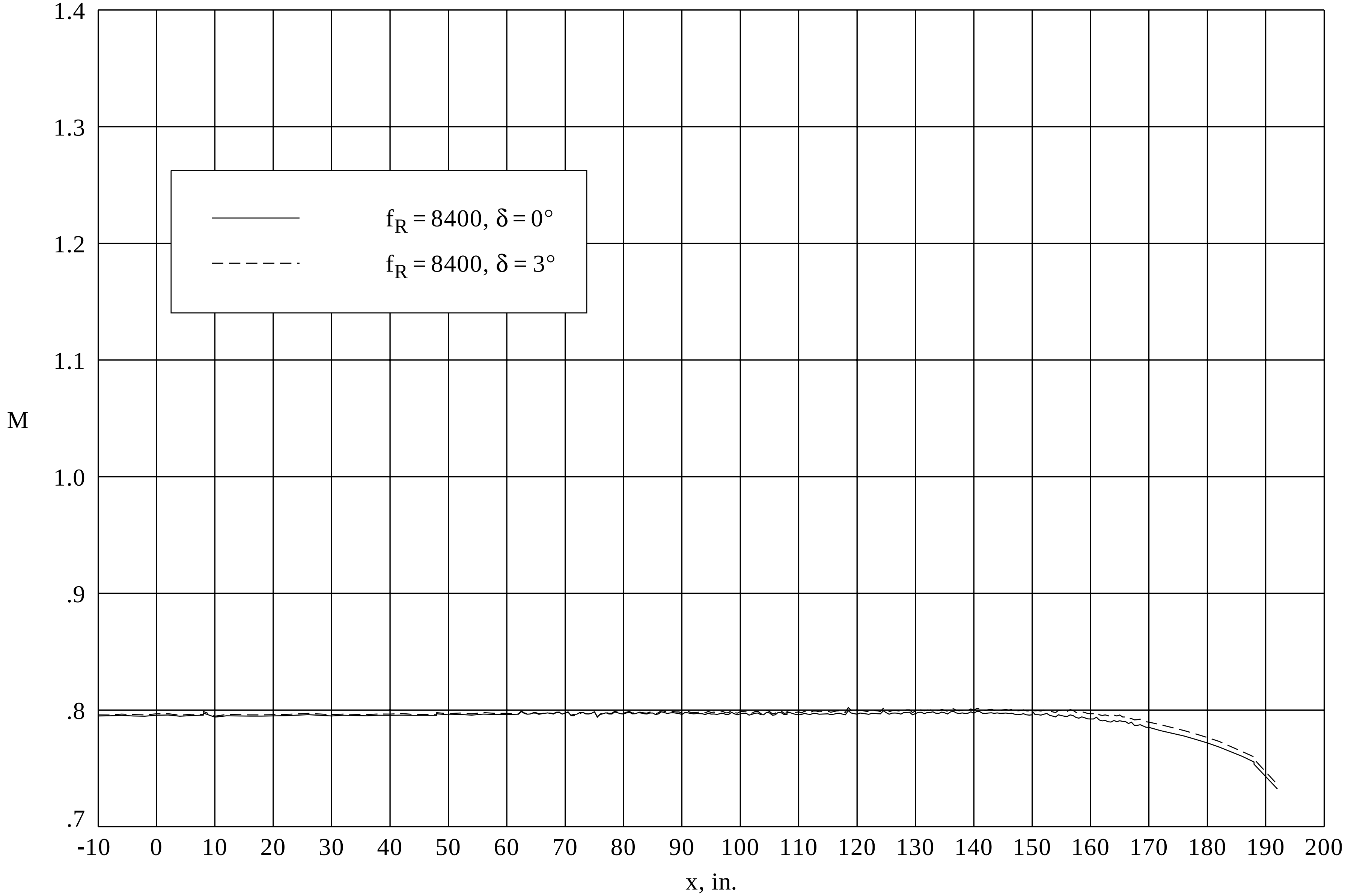

(a) Effect of diffuser spoiler at *M* = 0.800.

Figure 4. Mach number distribution along tunnel centerline at 1-atm stagnation pressure.

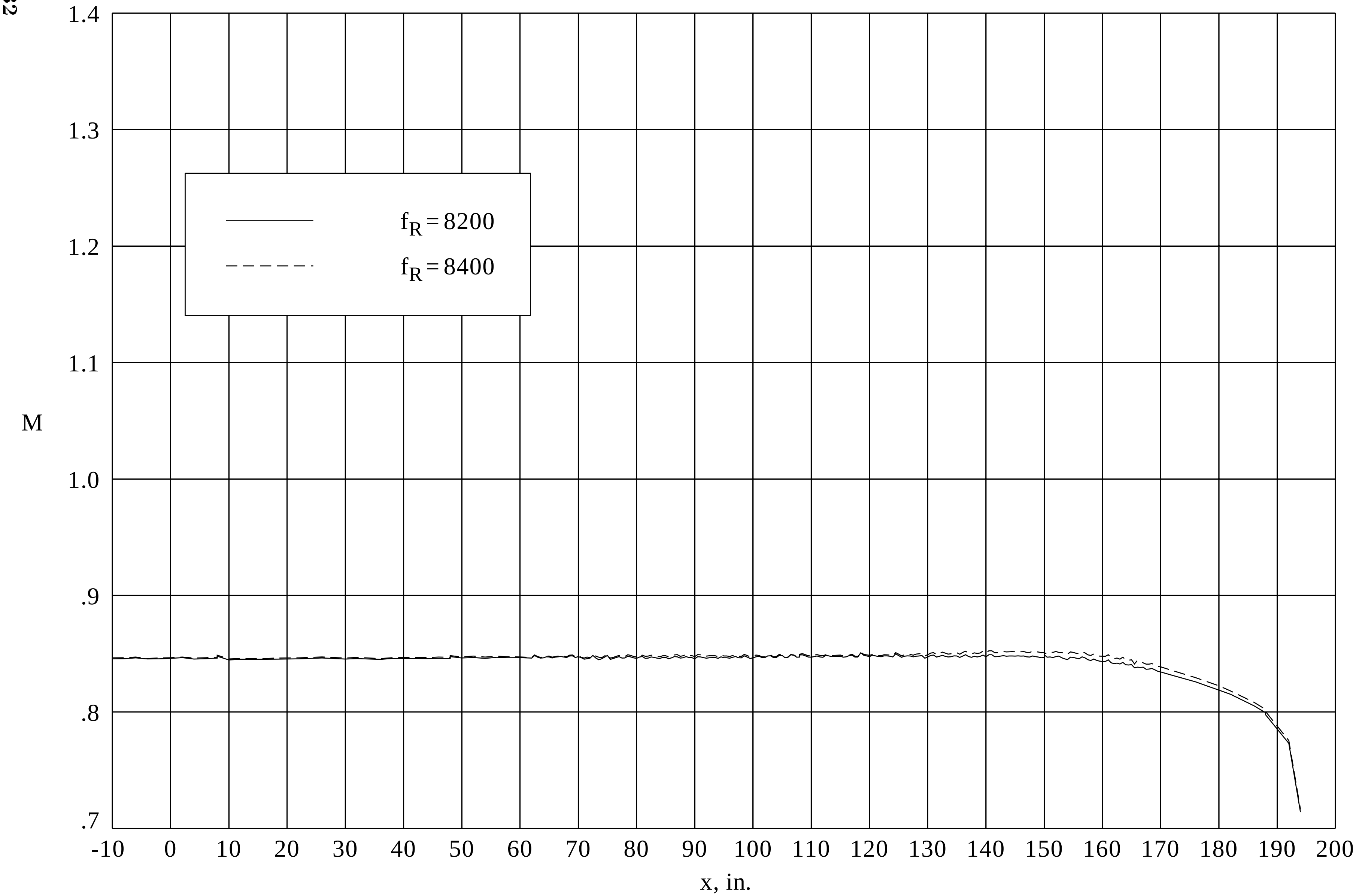

(b) Effect of reentry flap at M = 0.850.

Figure 4. Continued.

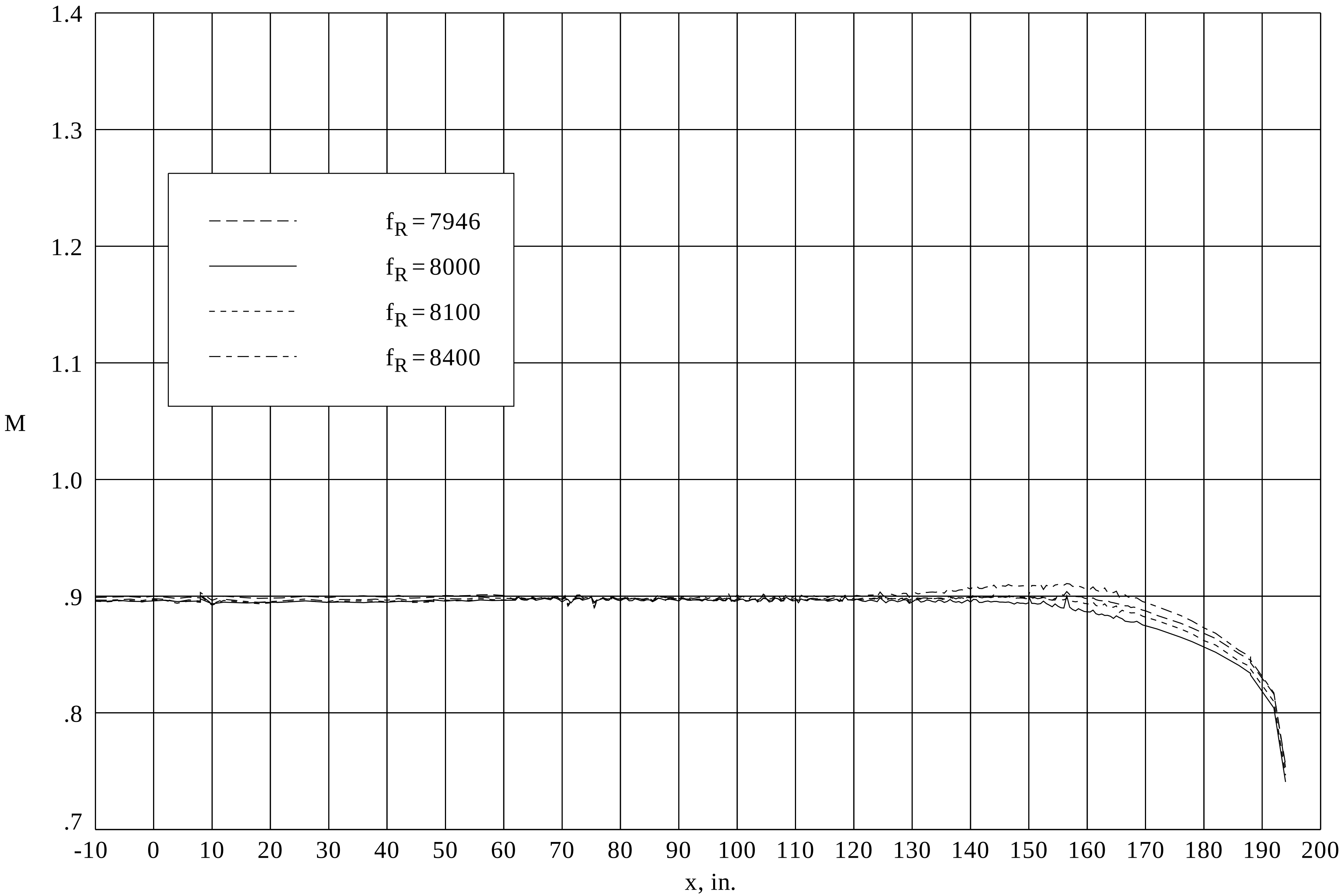

(c) Effect of reentry flap at *M* = 0.900.

Figure 4. Continued.

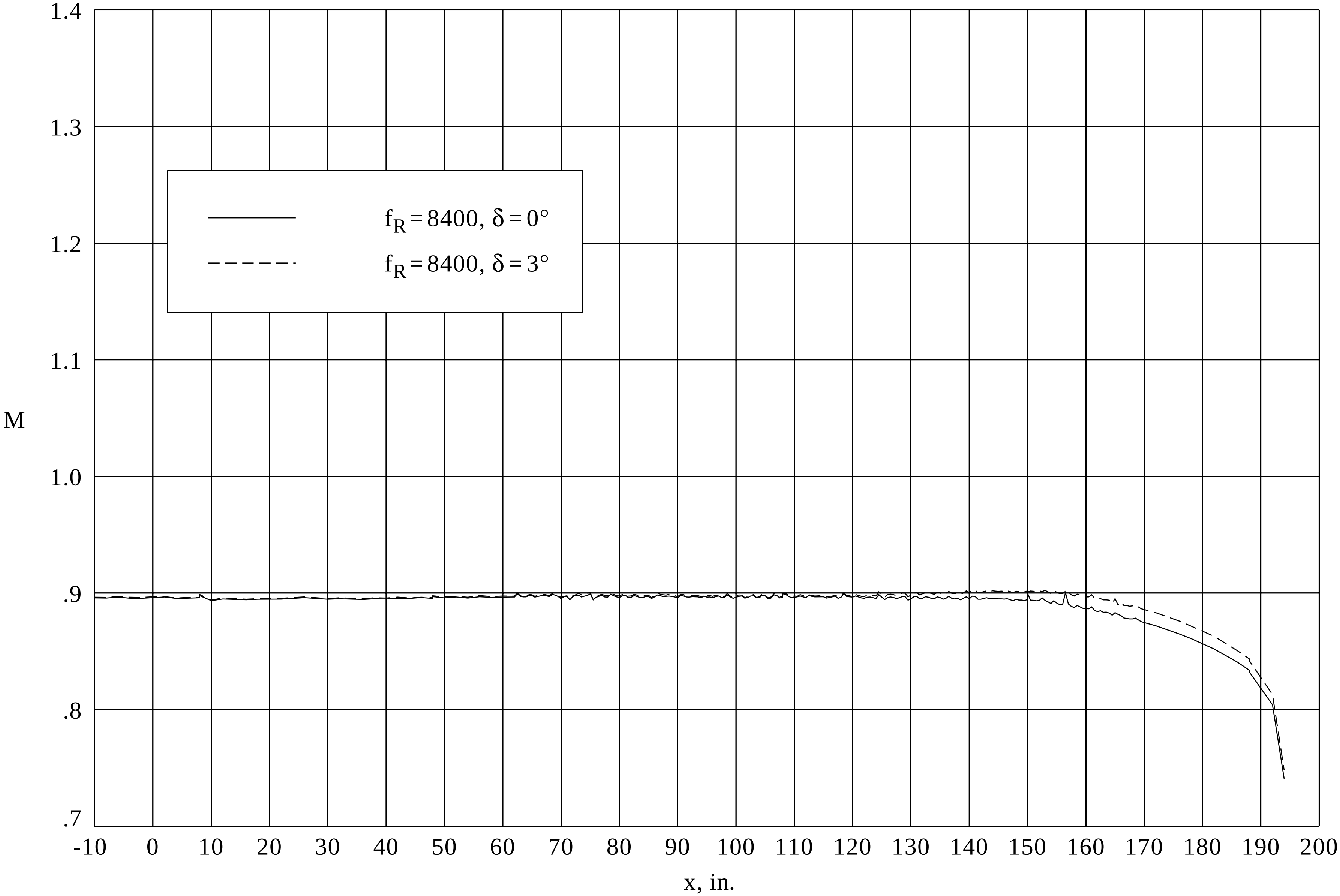

(d) Effect of diffuser spoiler at *M* = 0.900.

Figure 4. Continued.

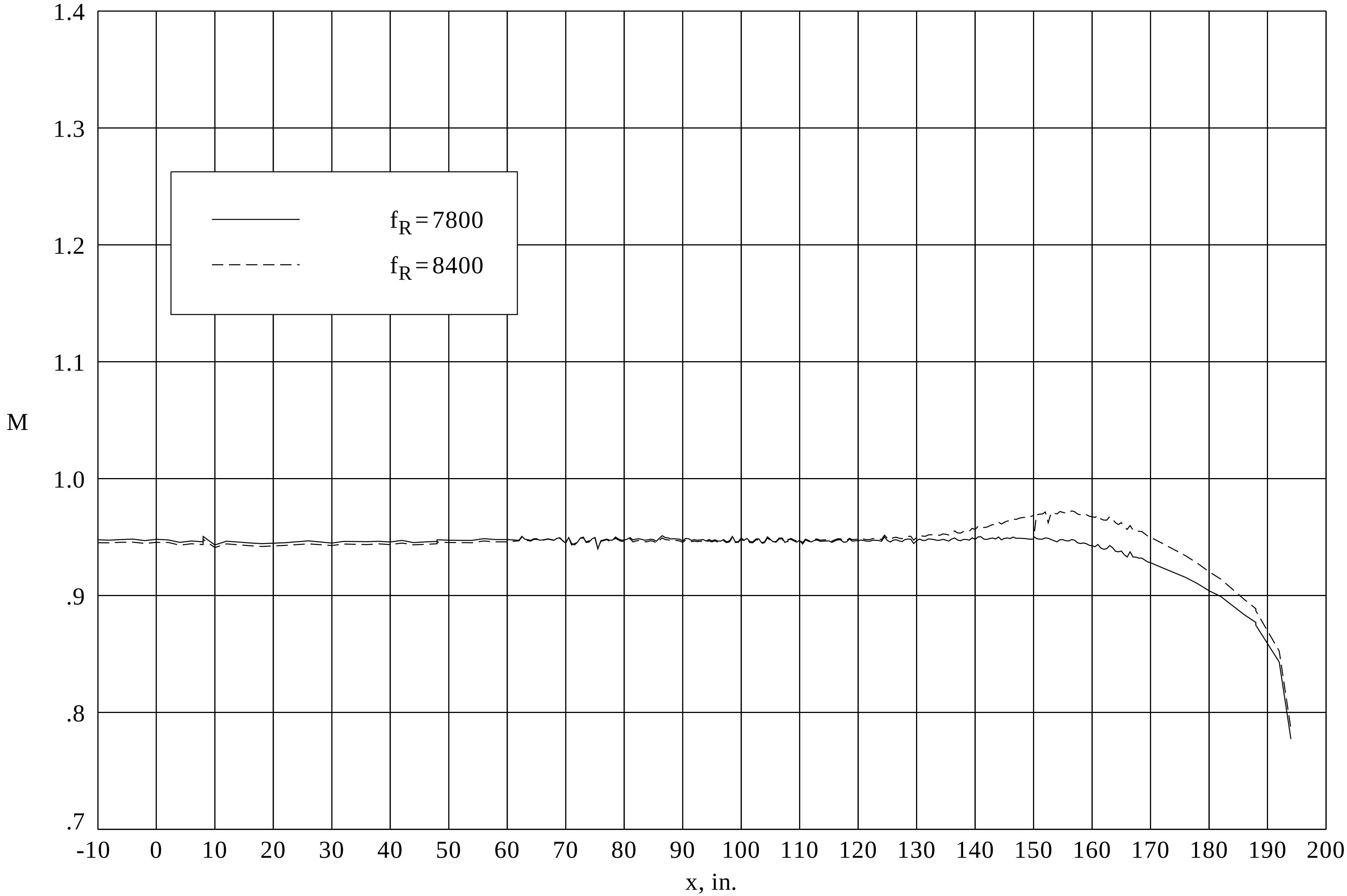

(e) Effect of reentry flap at M = 0.950.

Figure 4. Continued.

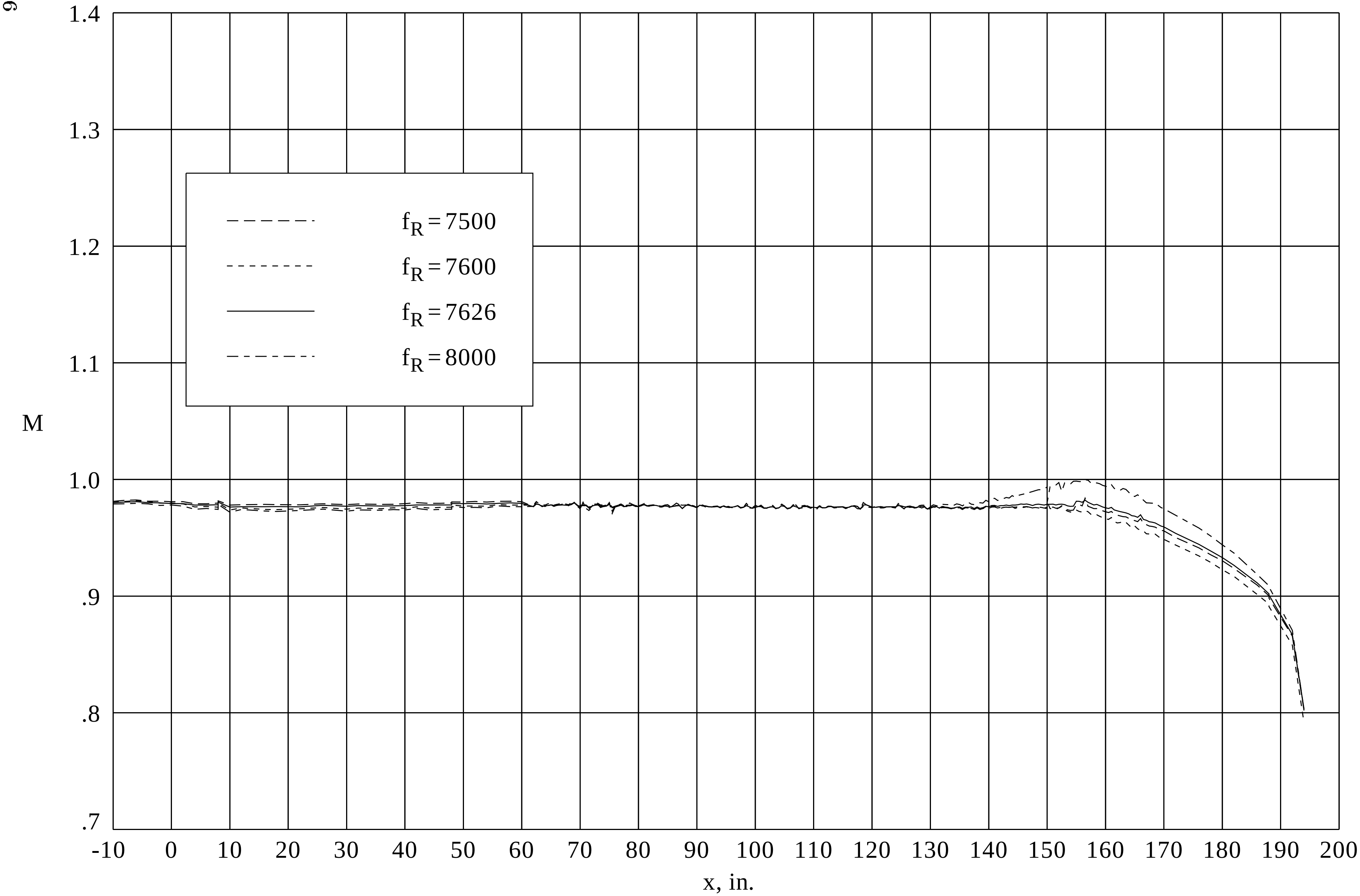

(f) Effect of reentry flap at M = 0.980.

Figure 4. Continued.

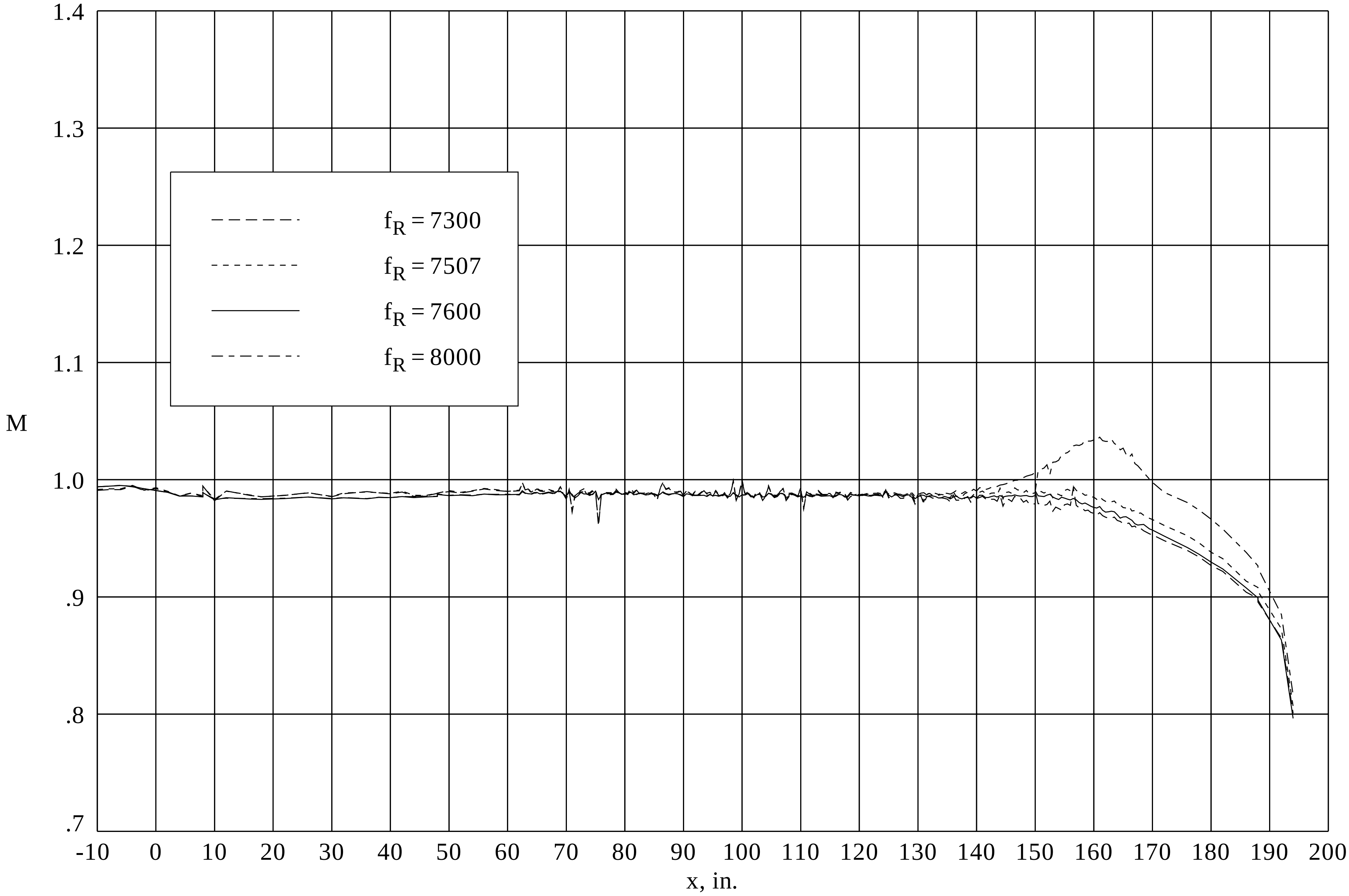

(g) Effect of reentry flap at M = 0.990.

Figure 4. Continued.

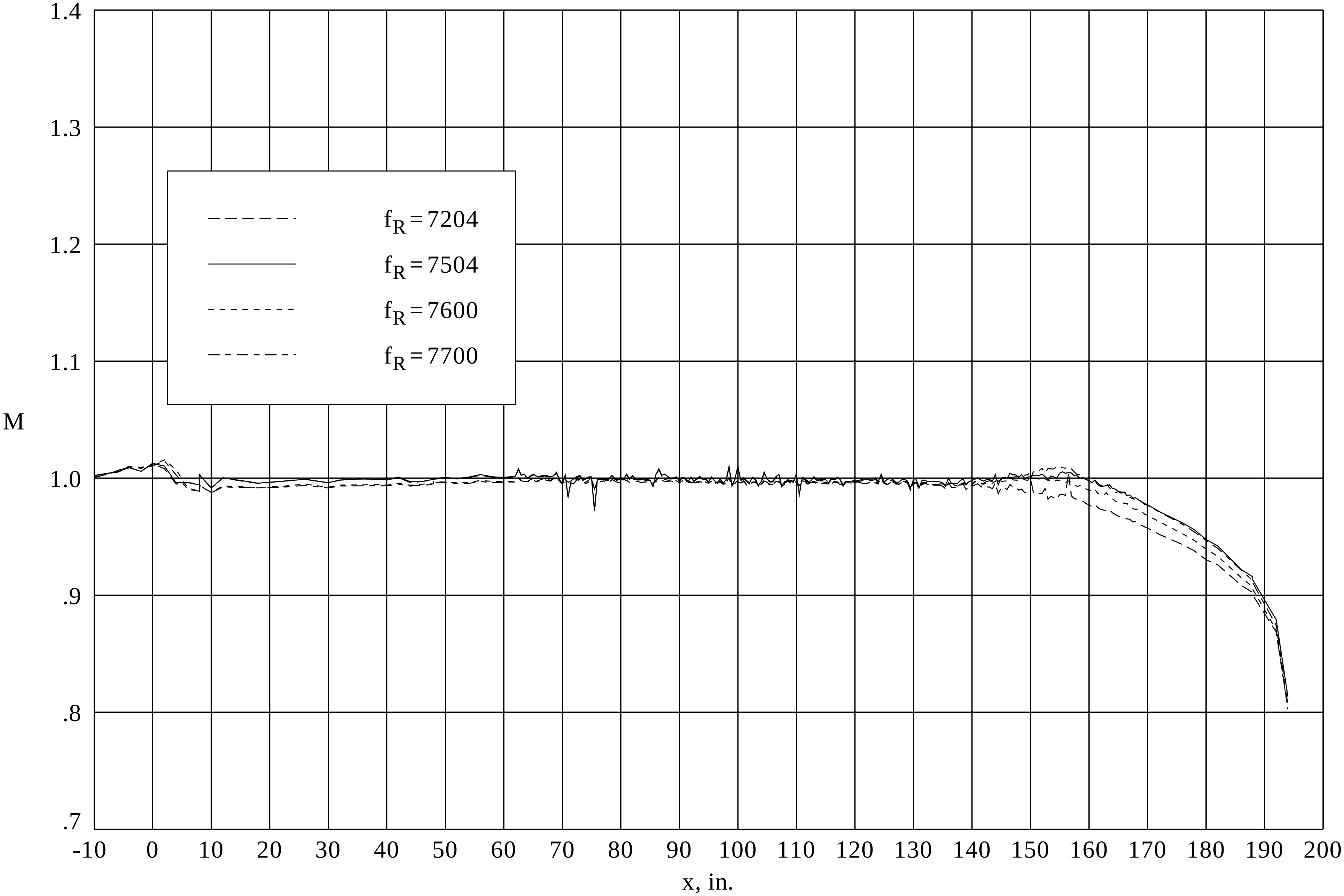

(h) Effect of reentry flap at *M* = 1.000.

Figure 4. Continued.

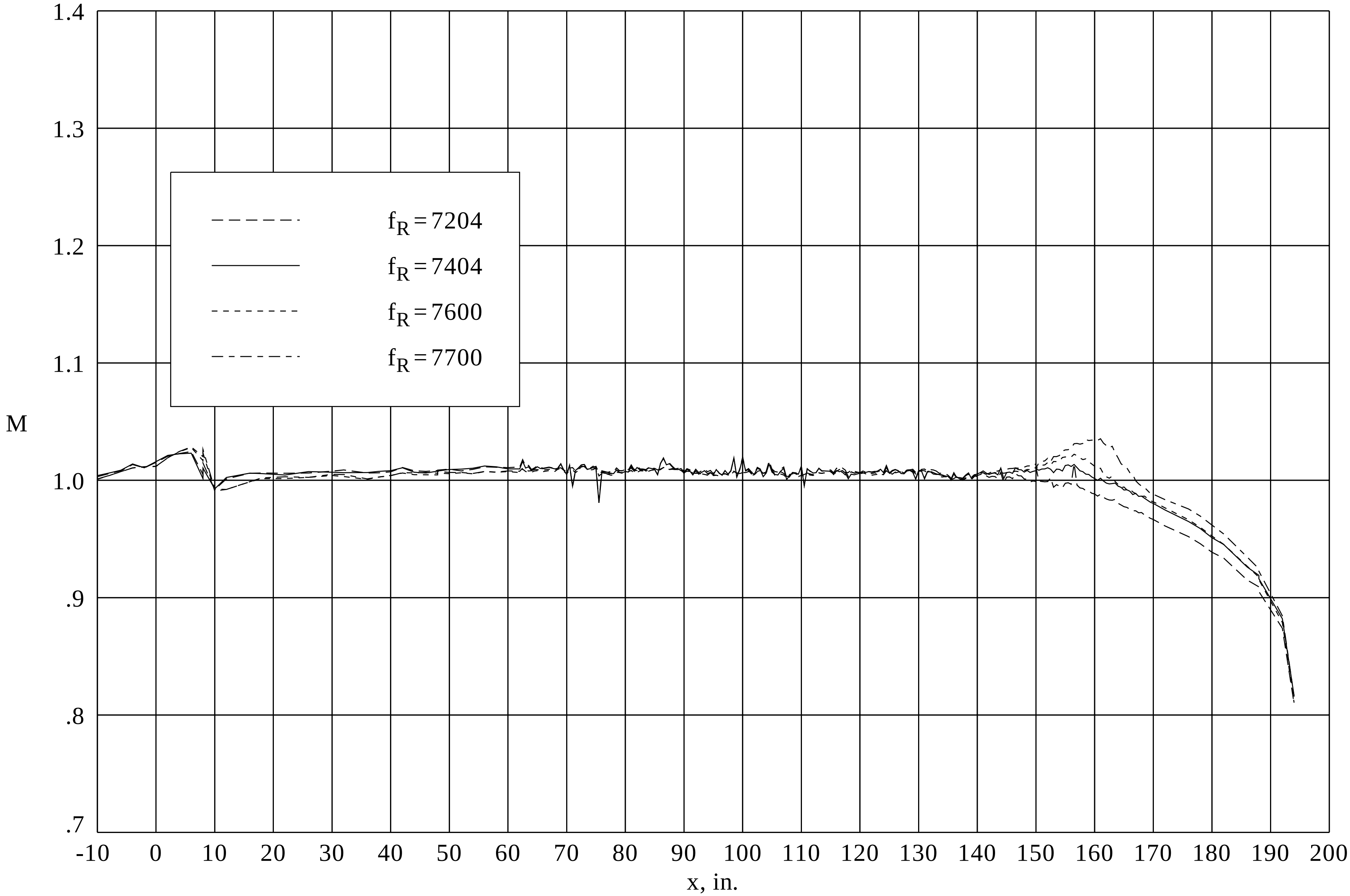

(i) Effect of reentry flap at M = 1.010.

Figure 4. Continued.

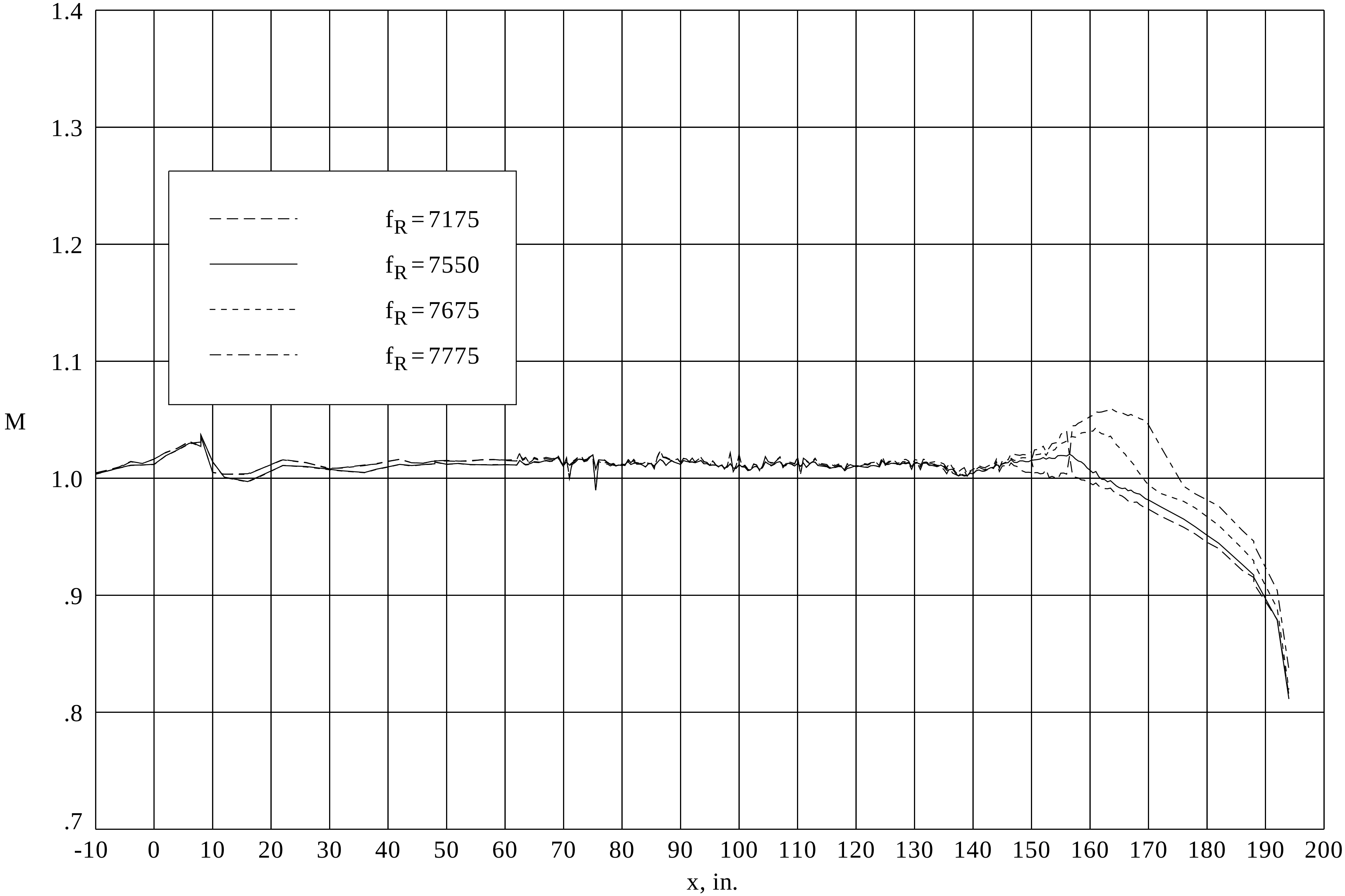

(j) Effect of reentry flap at M = 1.015.

Figure 4. Continued.

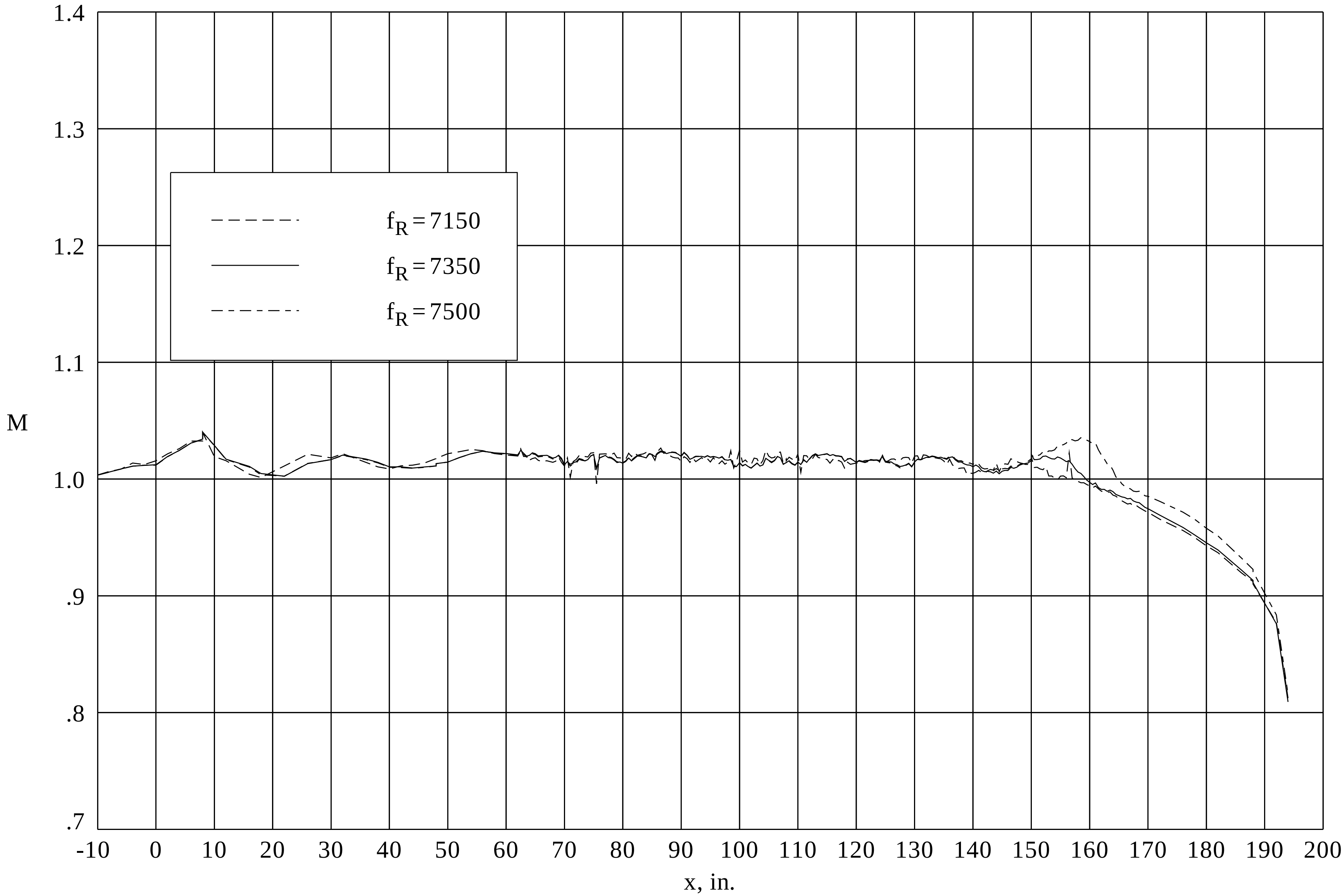

(k) Effect of reentry flap at M = 1.020.

Figure 4. Continued.

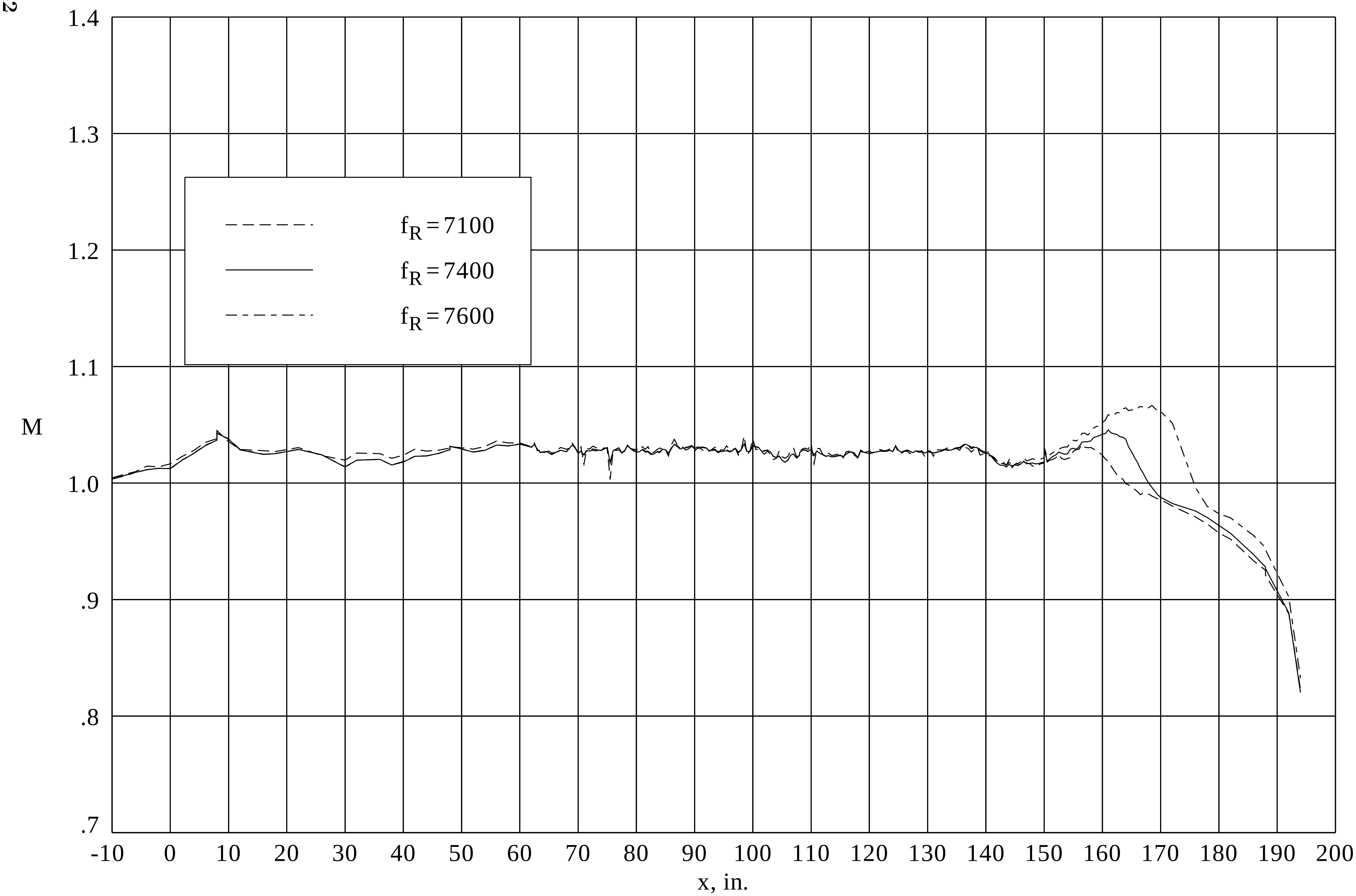

(l) Effect of reentry flap at M = 1.030.

Figure 4. Continued.

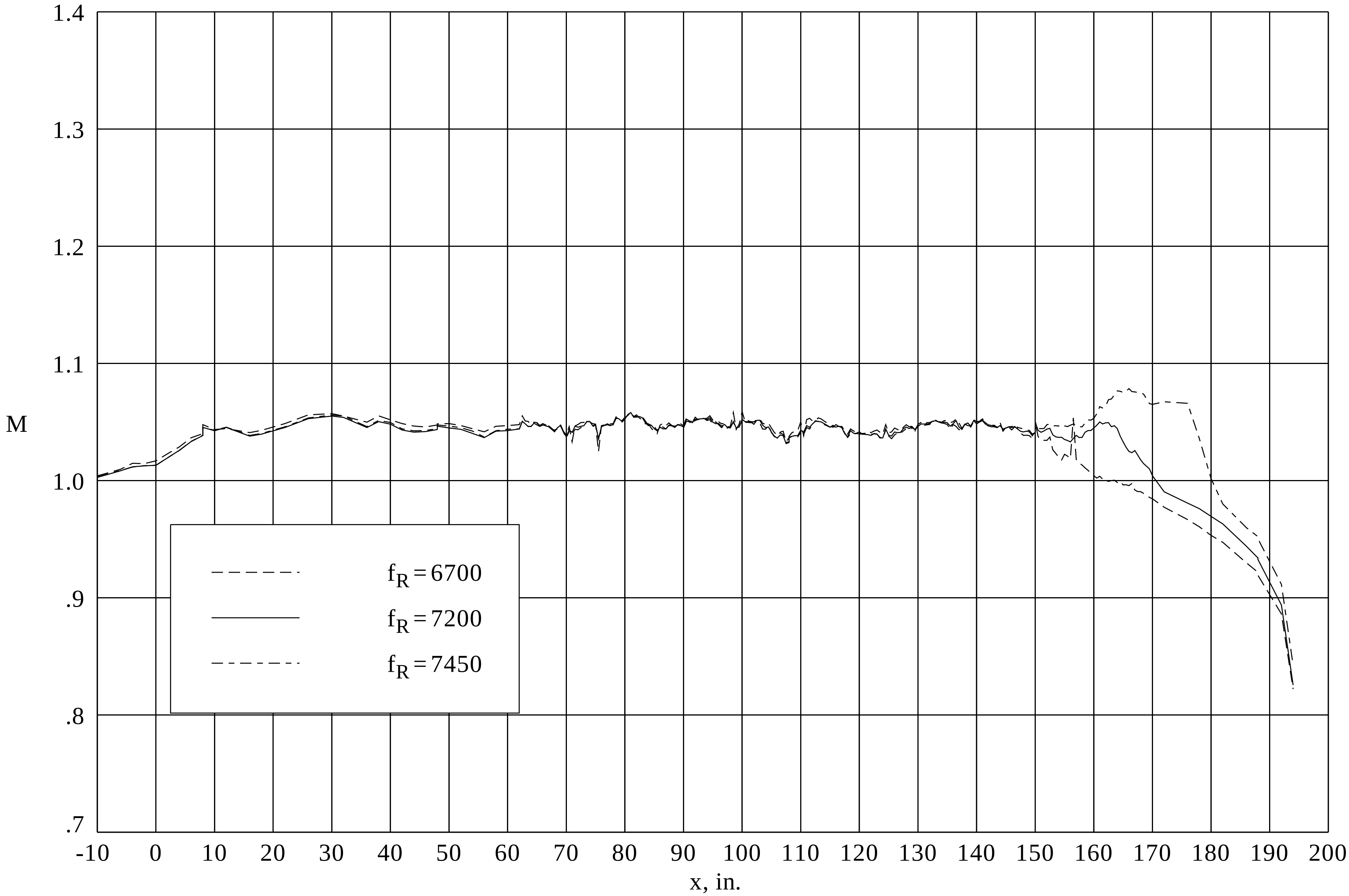

(m) Effect of reentry flap at M = 1.050.

Figure 4. Continued.

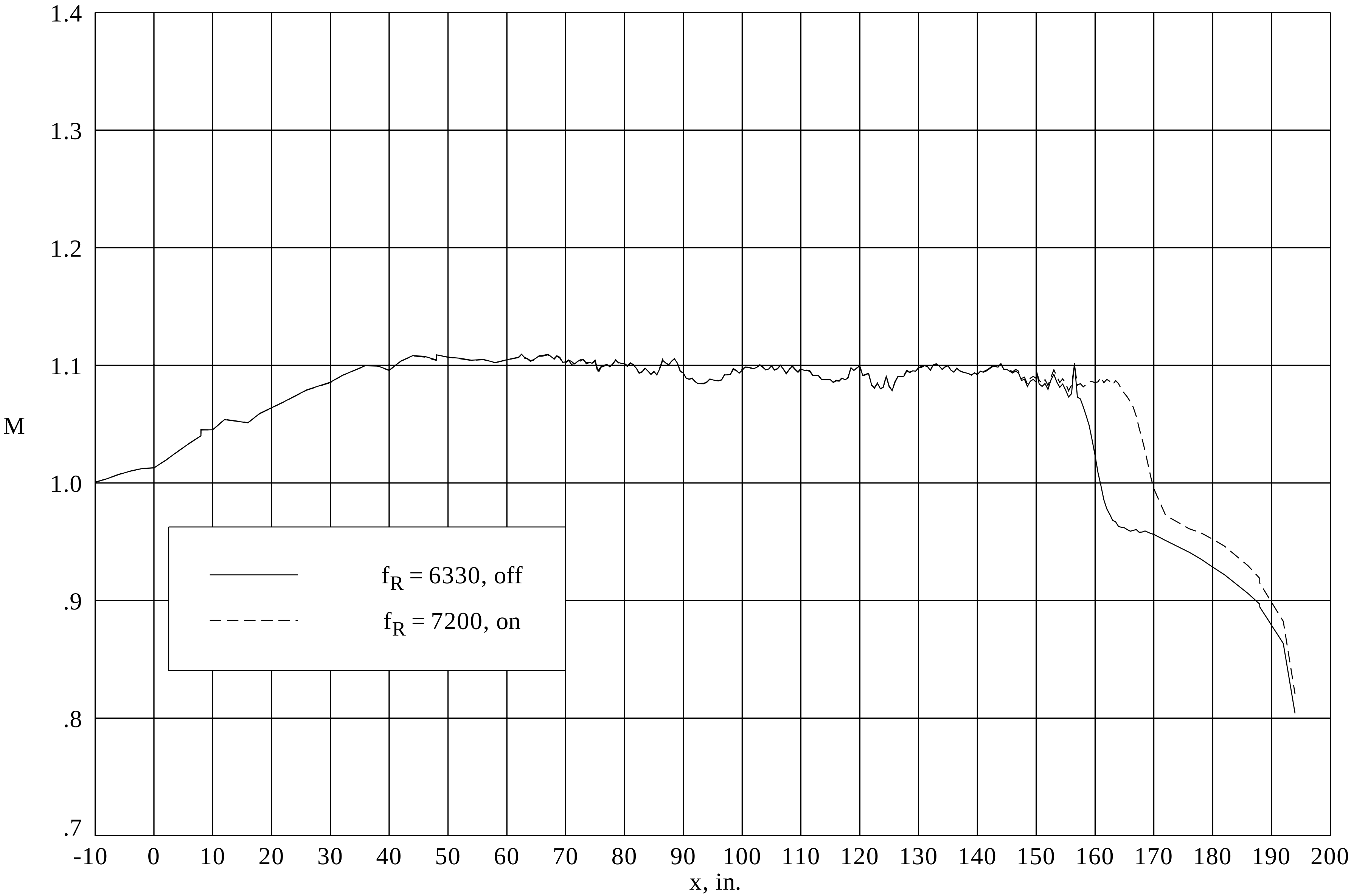

(n) Effect of reentry flap and boundary layer suction at M = 1.100.

Figure 4. Continued.

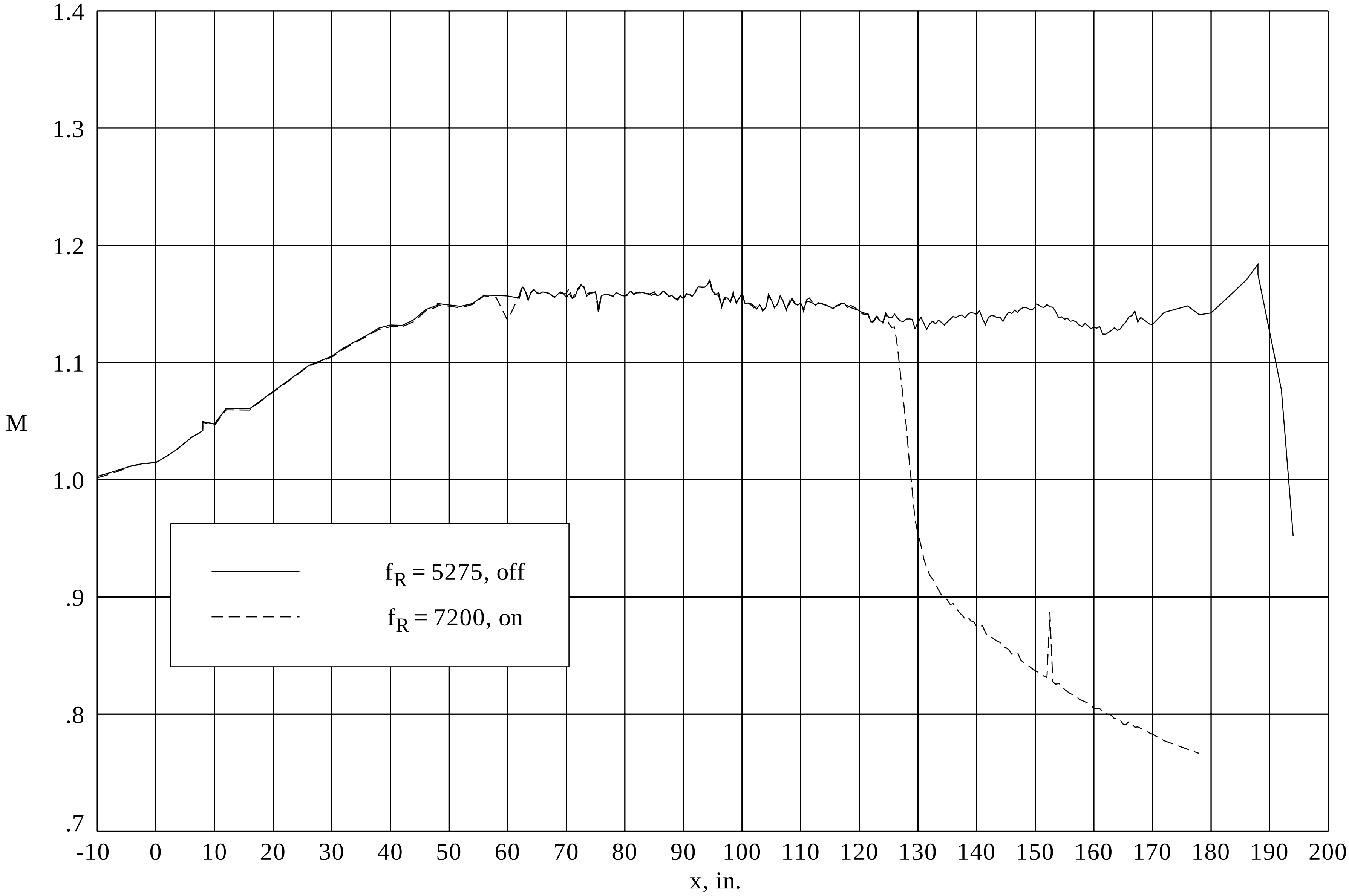

(o) Effect of reentry flap and boundary layer suction at *M* = 1.150.

Figure 4. Continued.

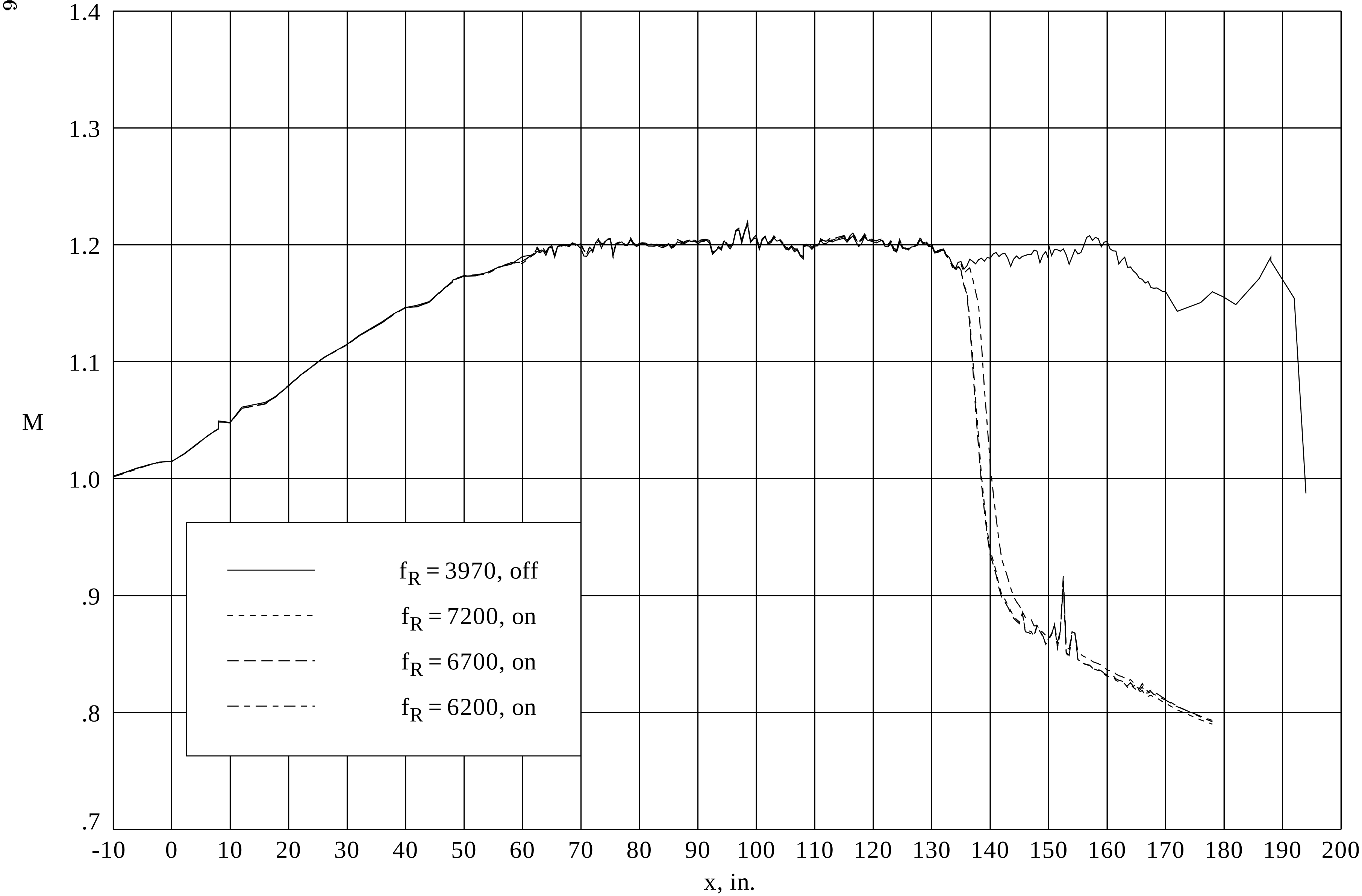

(p) Effect of reentry flap and boundary layer suction at M = 1.200.

Figure 4. Continued.

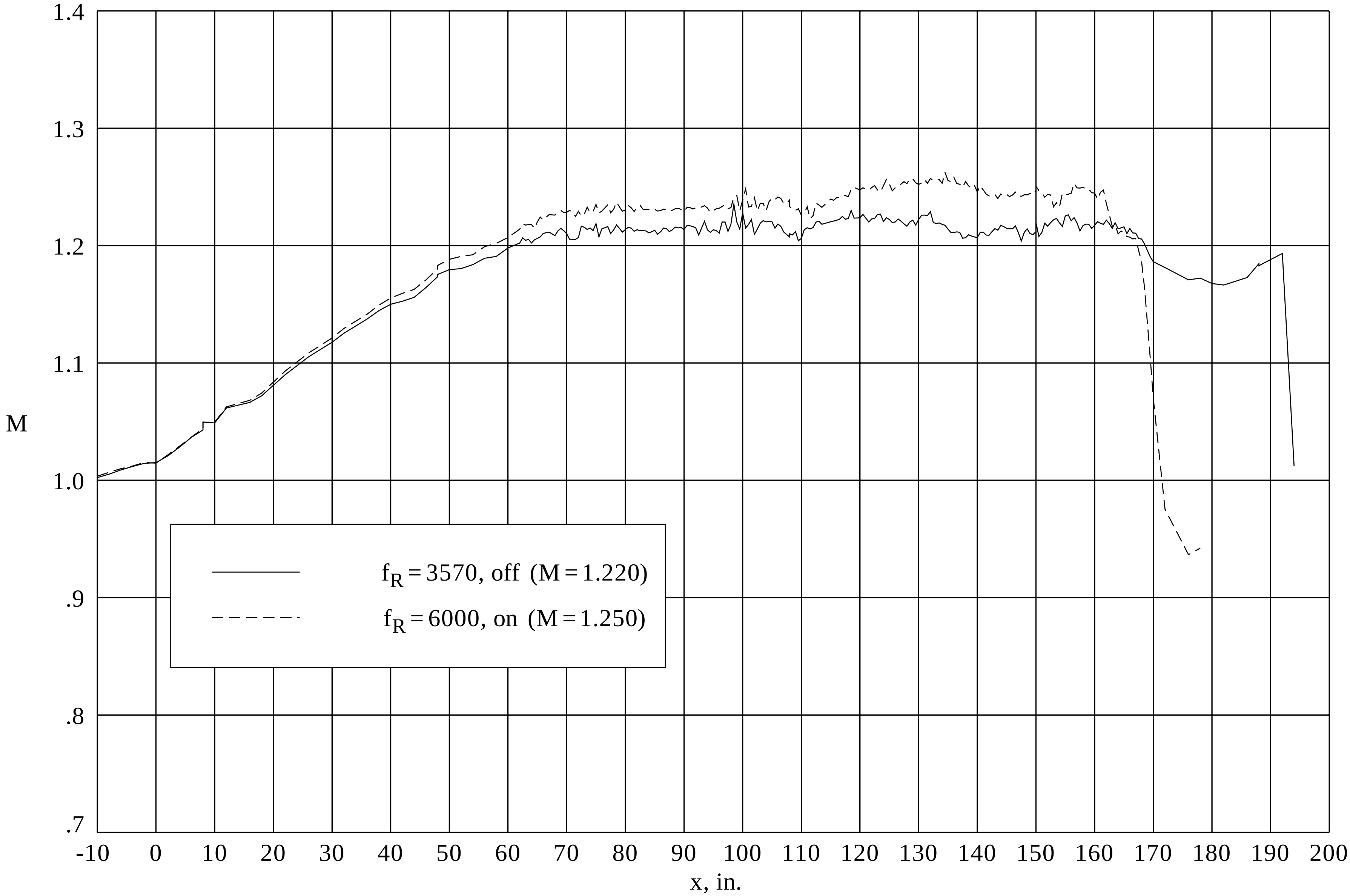

(q) Effect of reentry flap and boundary layer suction at *M* > 1.200.

Figure 4. Continued.

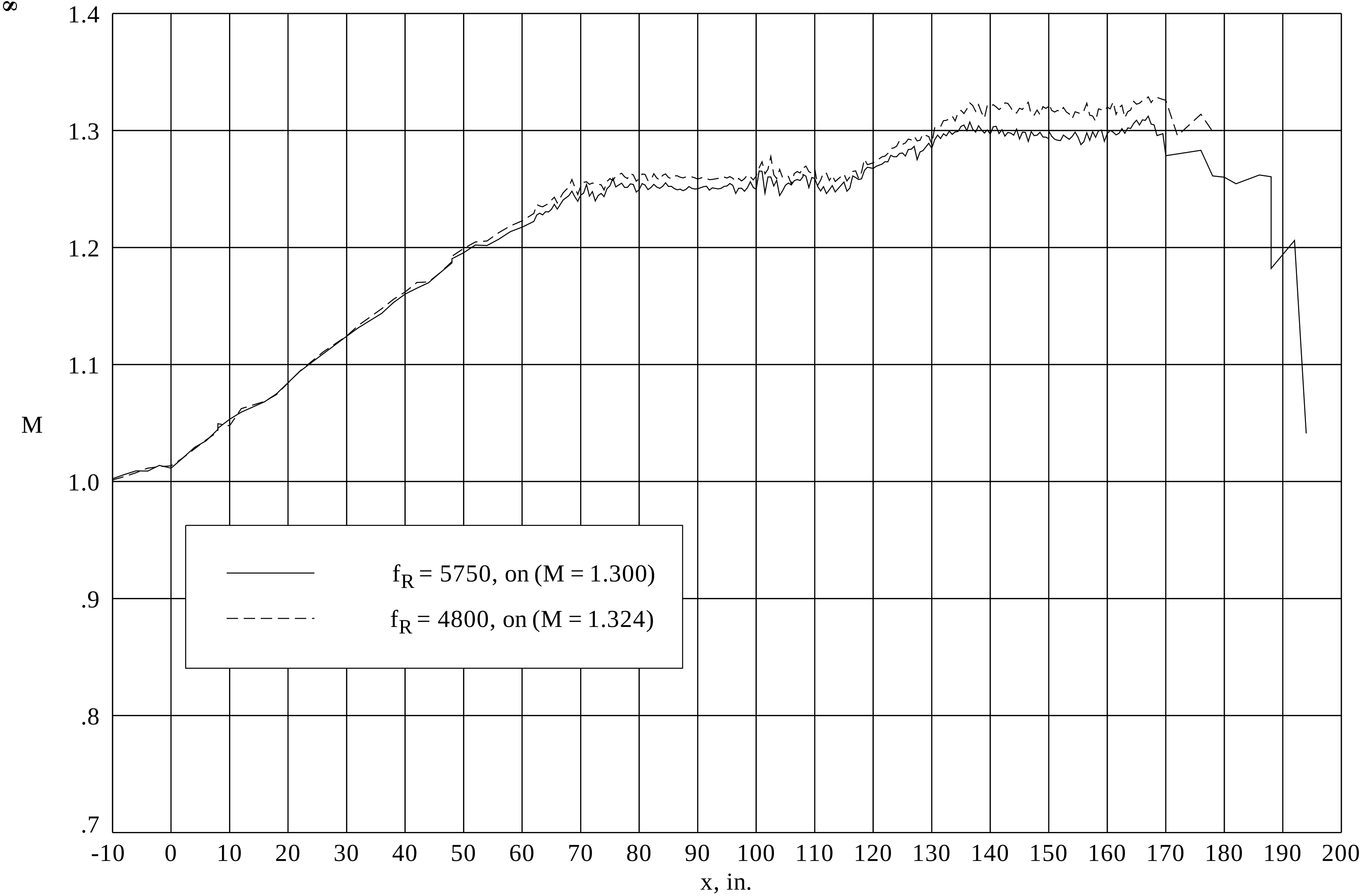

(r) Effect of reentry flap and boundary layer suction at $M \approx 1.300$.

Figure 4. Concluded.

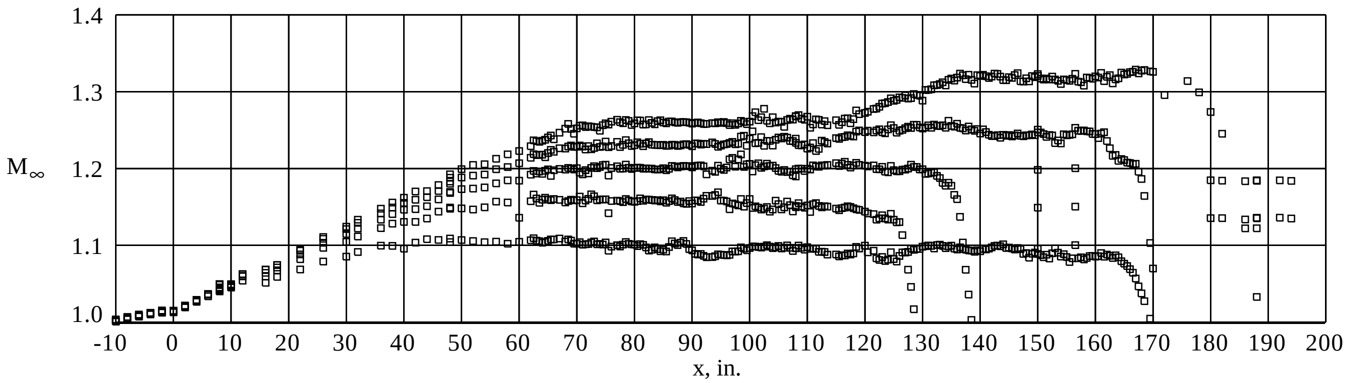

(a) Calibration distributions. $1.10 < M < 1.324$; boundary layer suction on.

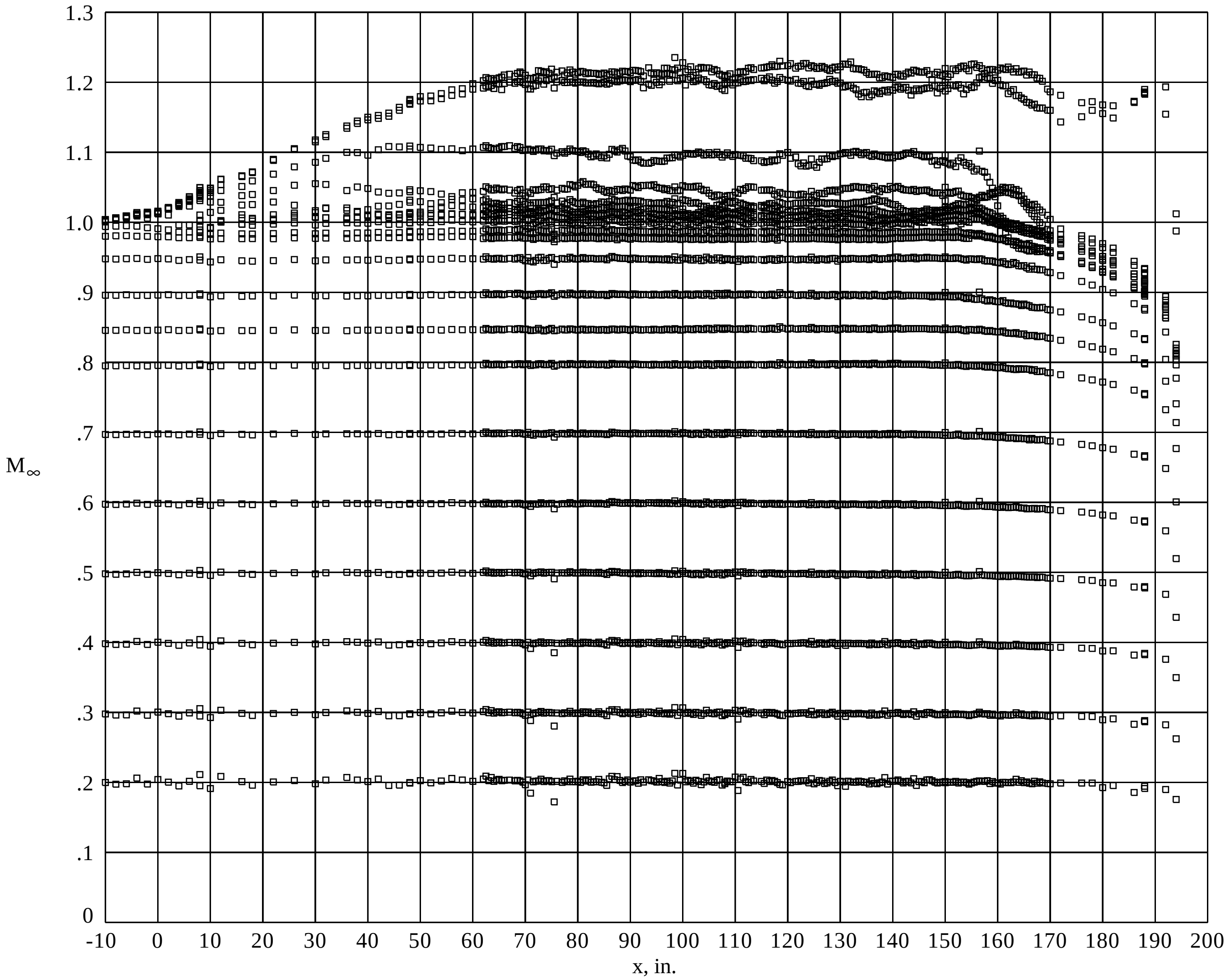

(b) Calibration distributions. $0.20 < M < 1.22$; boundary layer suction off.

Figure 5. Mach number distribution along tunnel centerline selected as defining calibration.

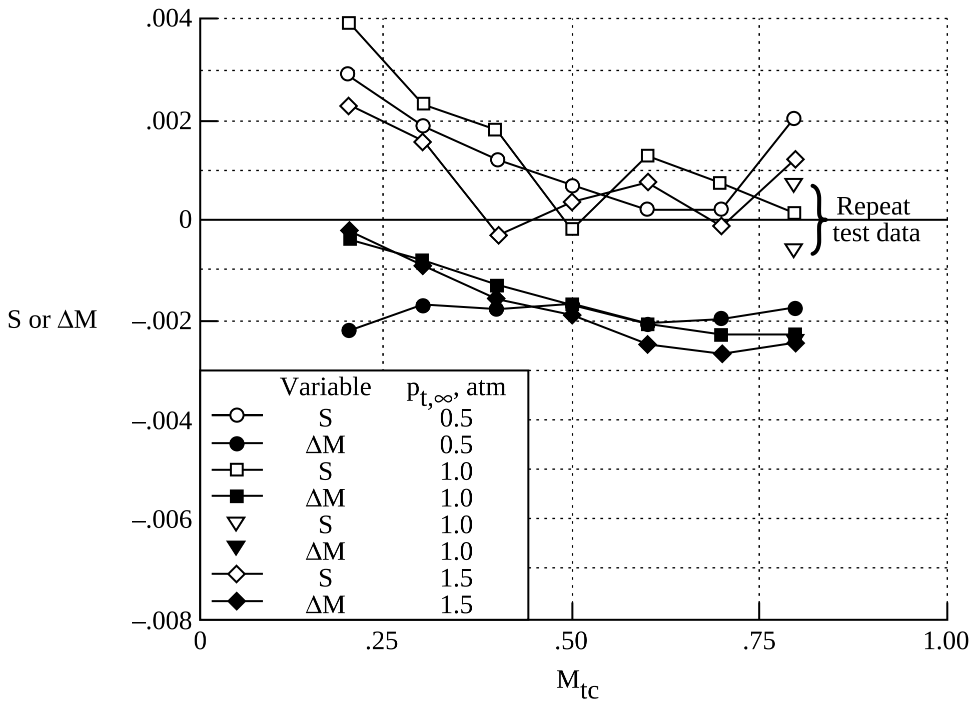

(a) Effect of $M \leq 0.80$; reentry flaps closed; 1989 data.

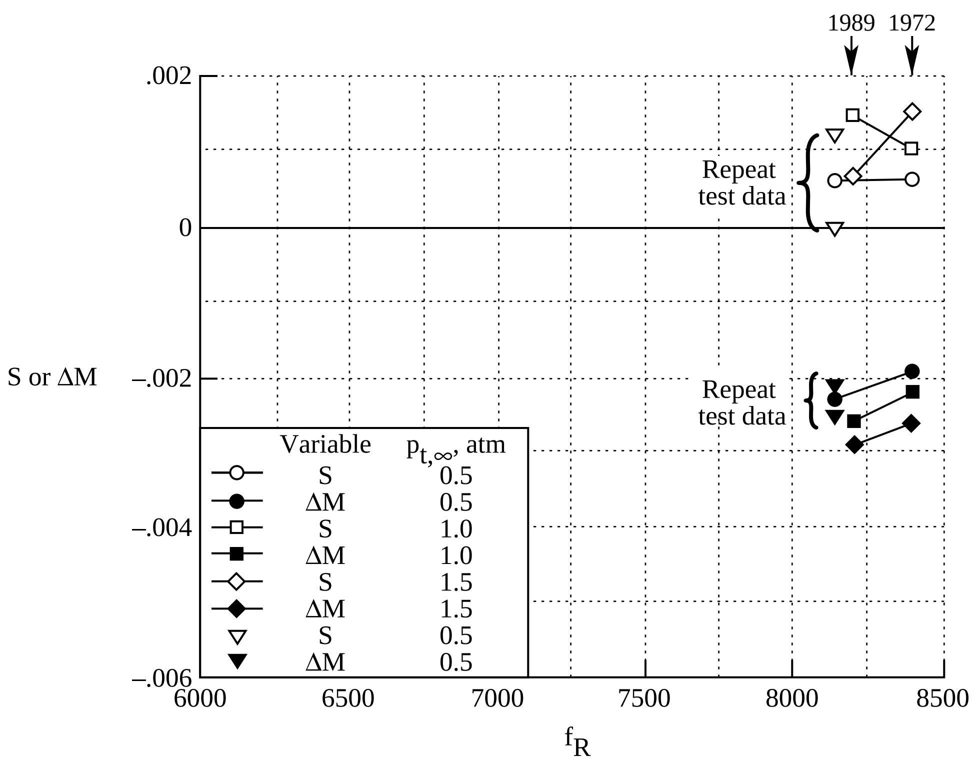

(b) Effect of reentry flaps at $M = 0.85$.

Figure 6. Variation of Mach number gradient parameter and Mach number correction with various control parameters; three levels of stagnation pressure.

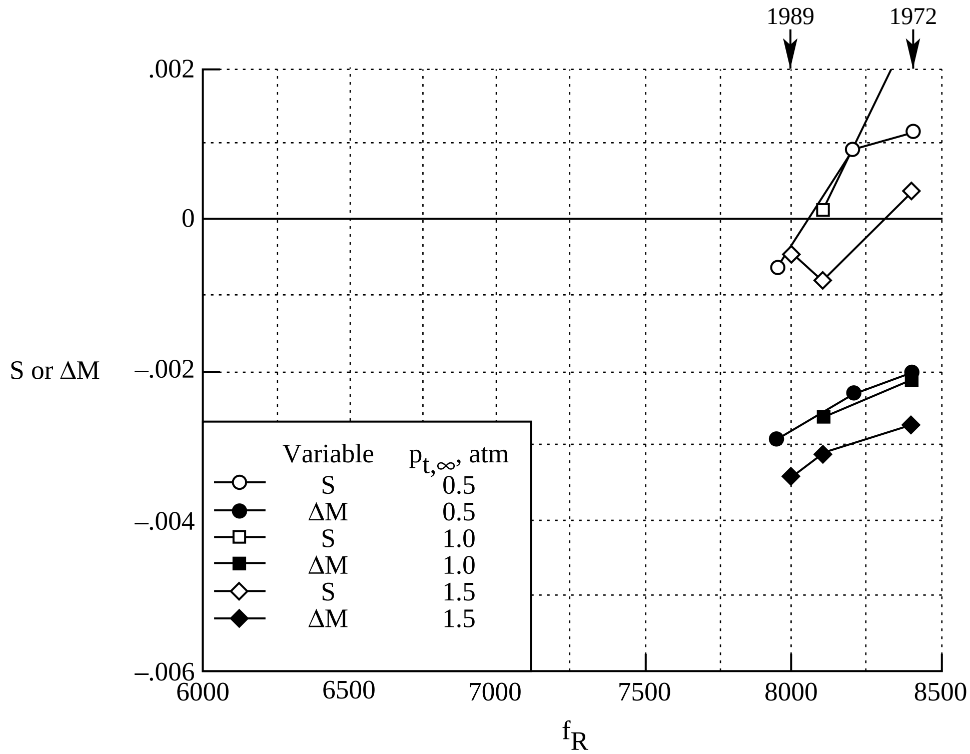

(c) Effect of reentry flaps at $M = 0.90$.

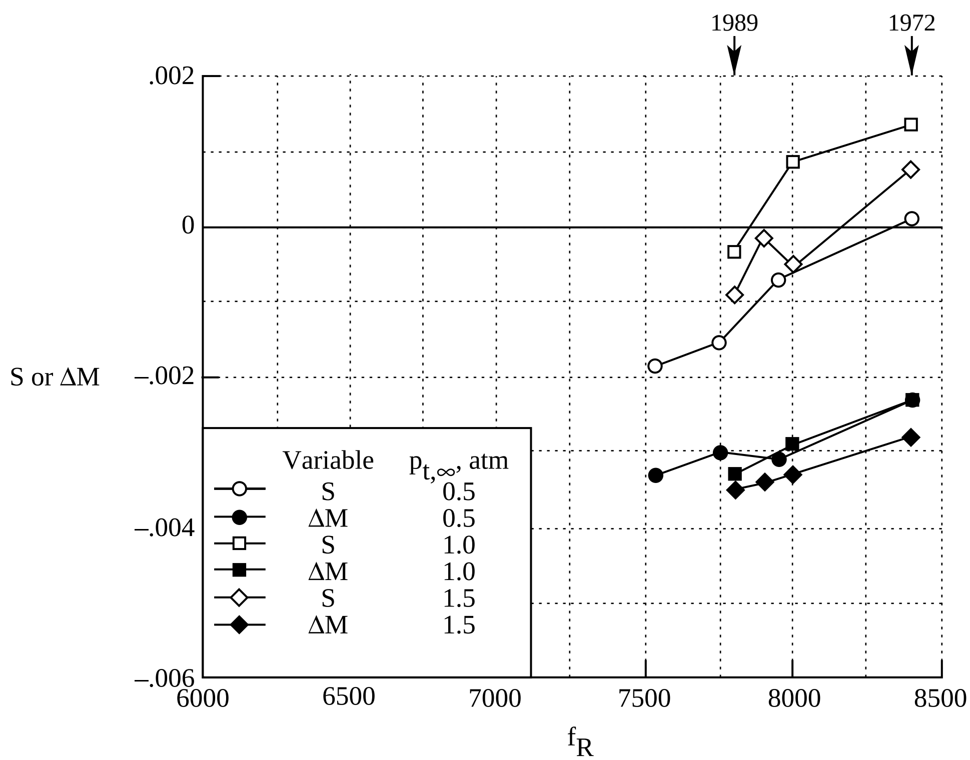

(d) Effect of reentry flaps at $M = 0.95$.

Figure 6. Continued.

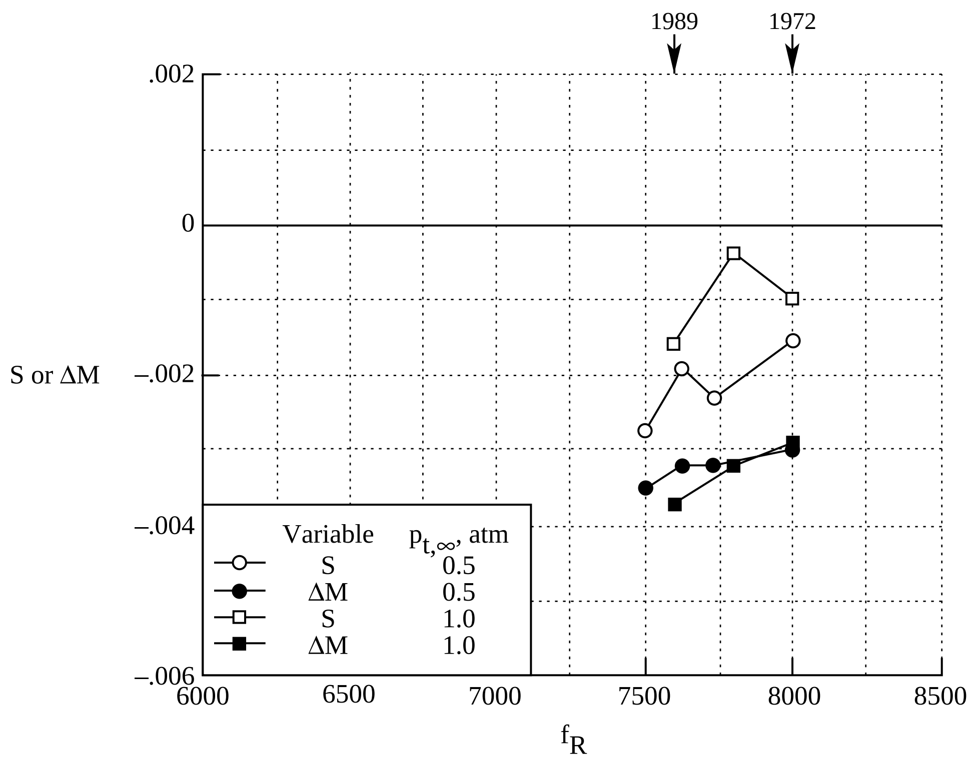

(e) Effect of reentry flaps at $M = 0.98$.

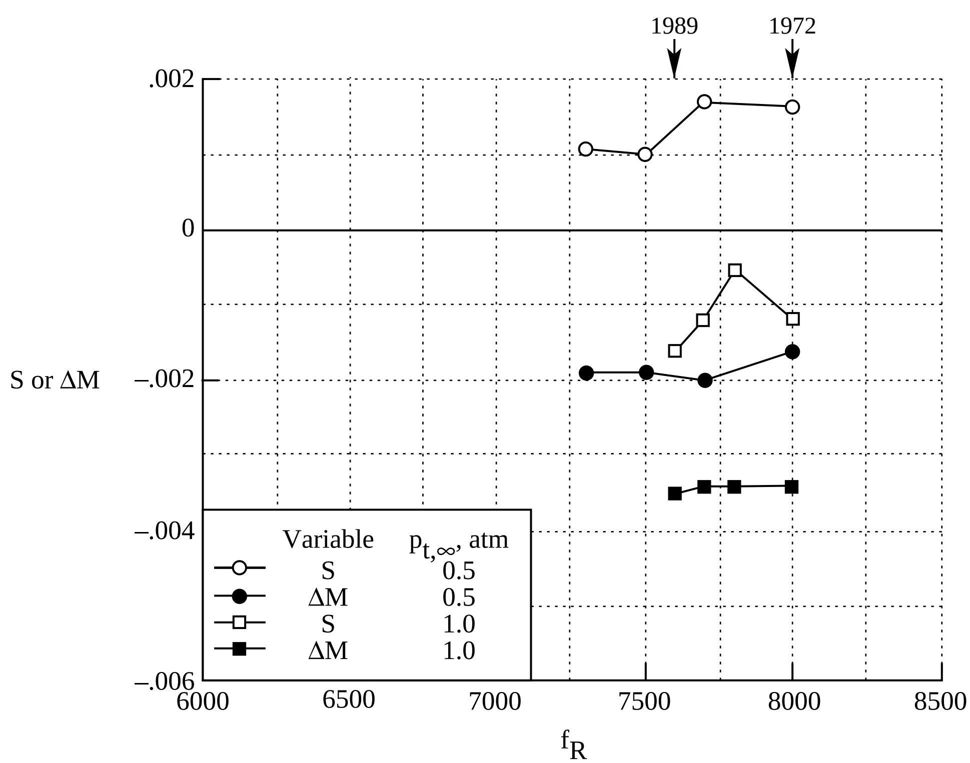

(f) Effect of reentry flaps at $M = 0.99$.

Figure 6. Continued.

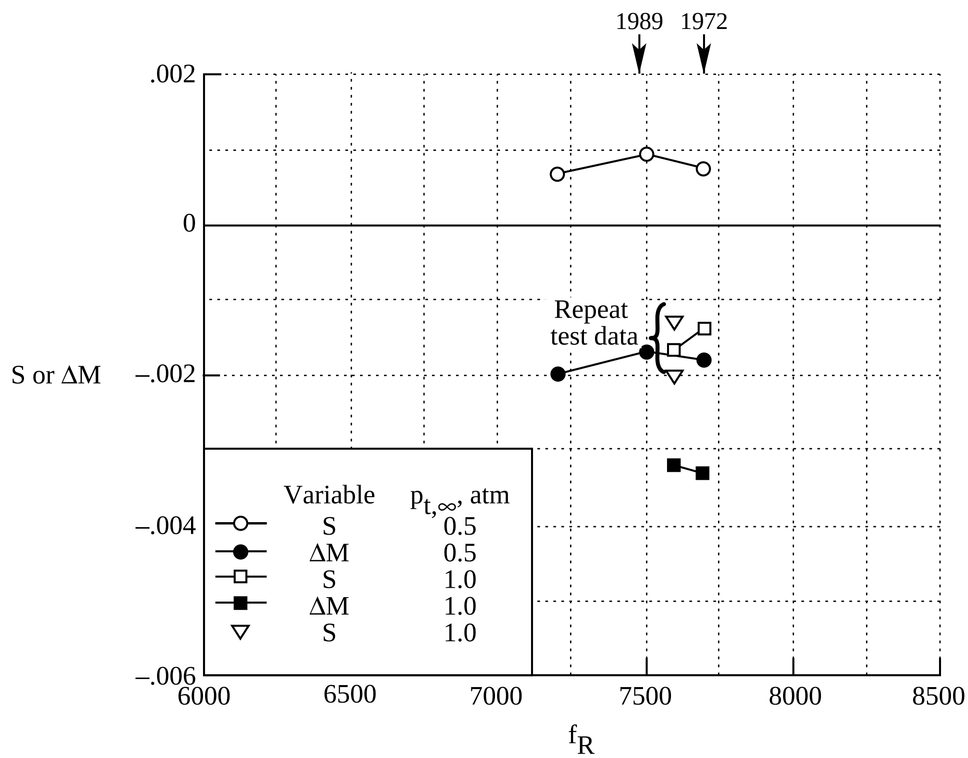

(g) Effect of reentry flaps at $M = 1.00$.

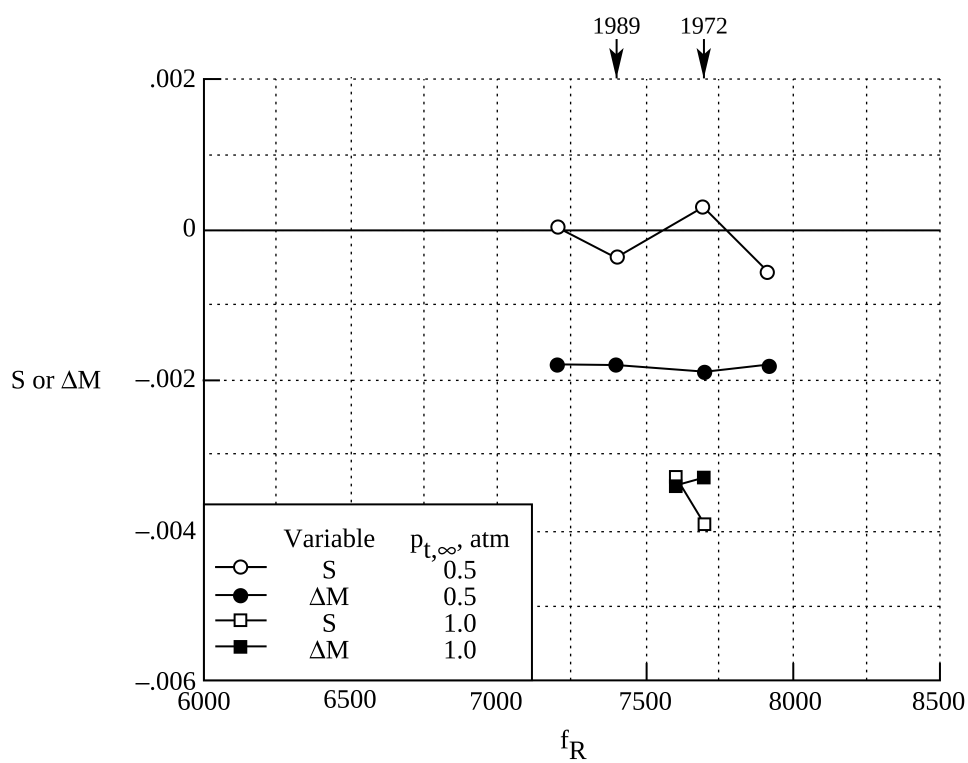

(h) Effect of reentry flaps at $M = 1.01$.

Figure 6. Continued.

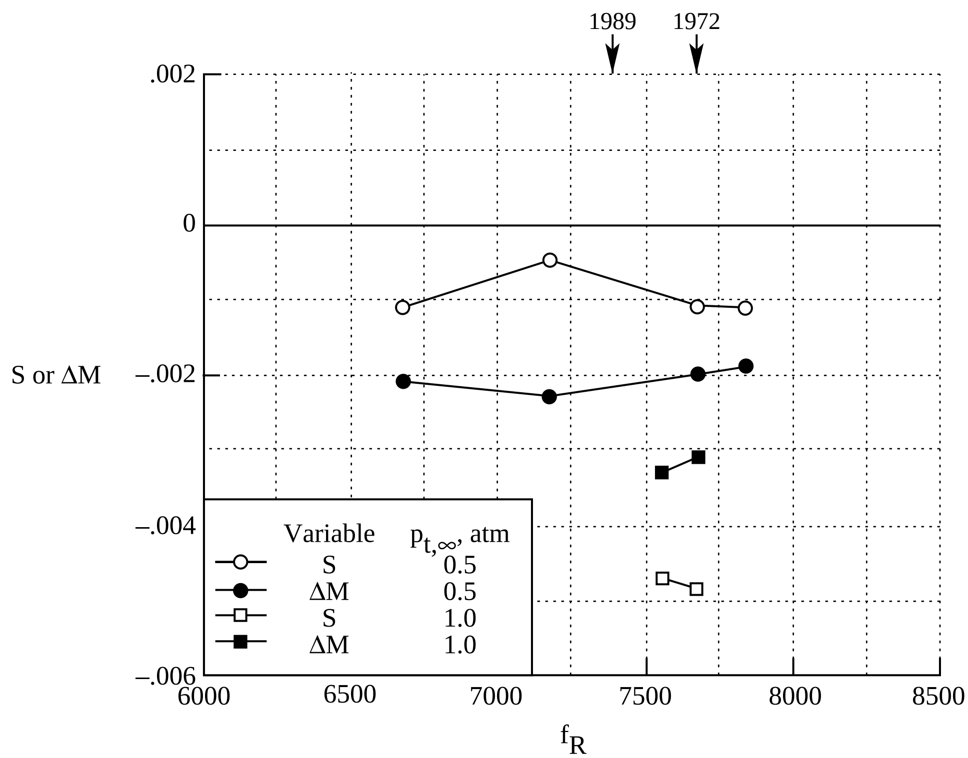

(i) Effect of reentry flaps at $M = 1.015$.

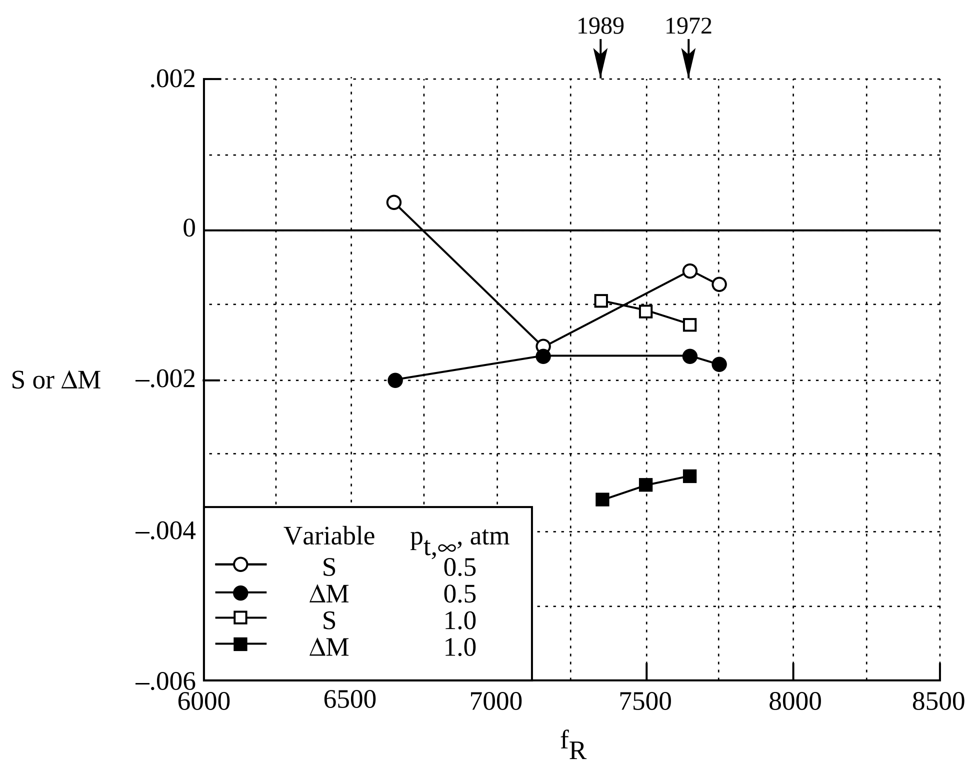

(j) Effect of reentry flaps at $M = 1.02$.

Figure 6. Continued.

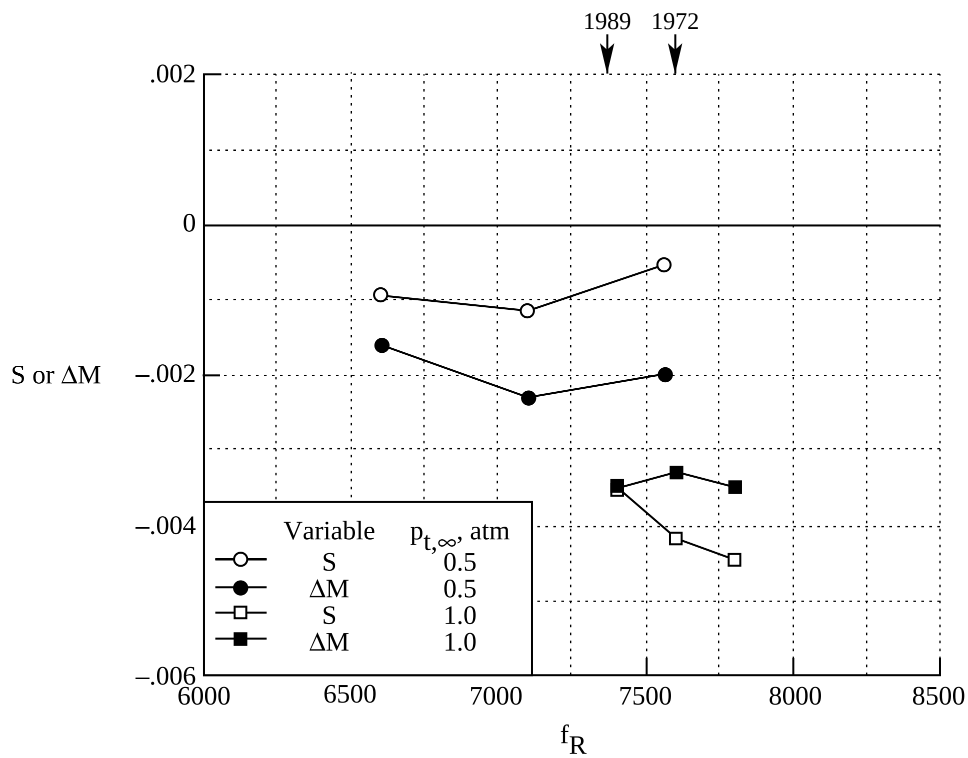

(k) Effect of reentry flaps at $M = 1.03$.

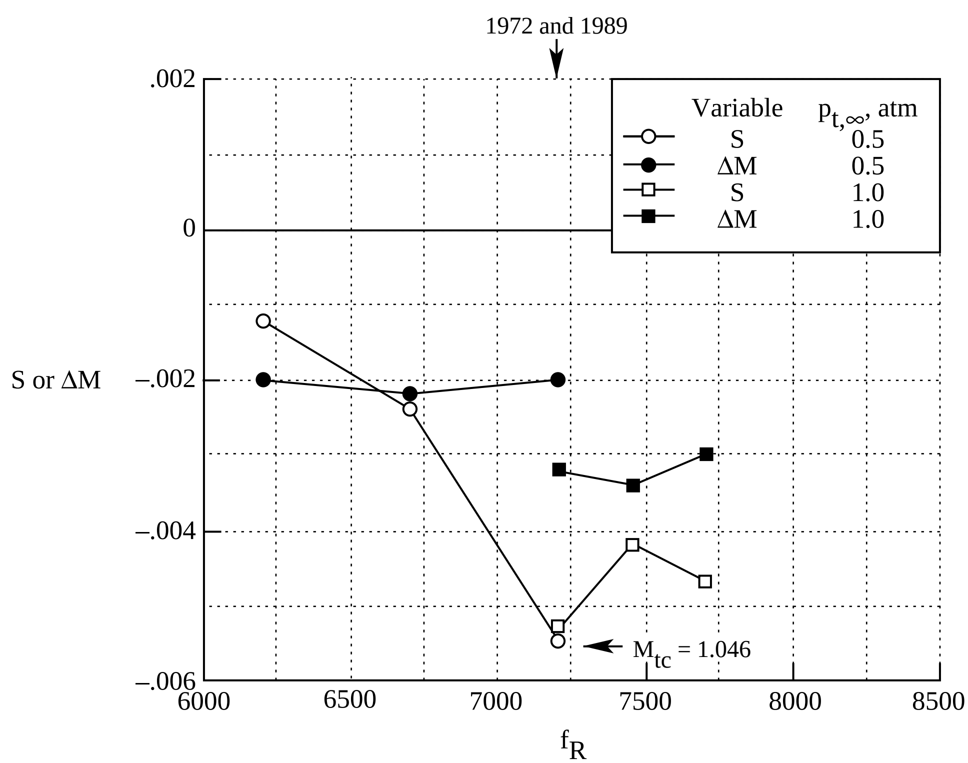

(l) Effect of reentry flaps at $M = 1.05$.

Figure 6. Continued.

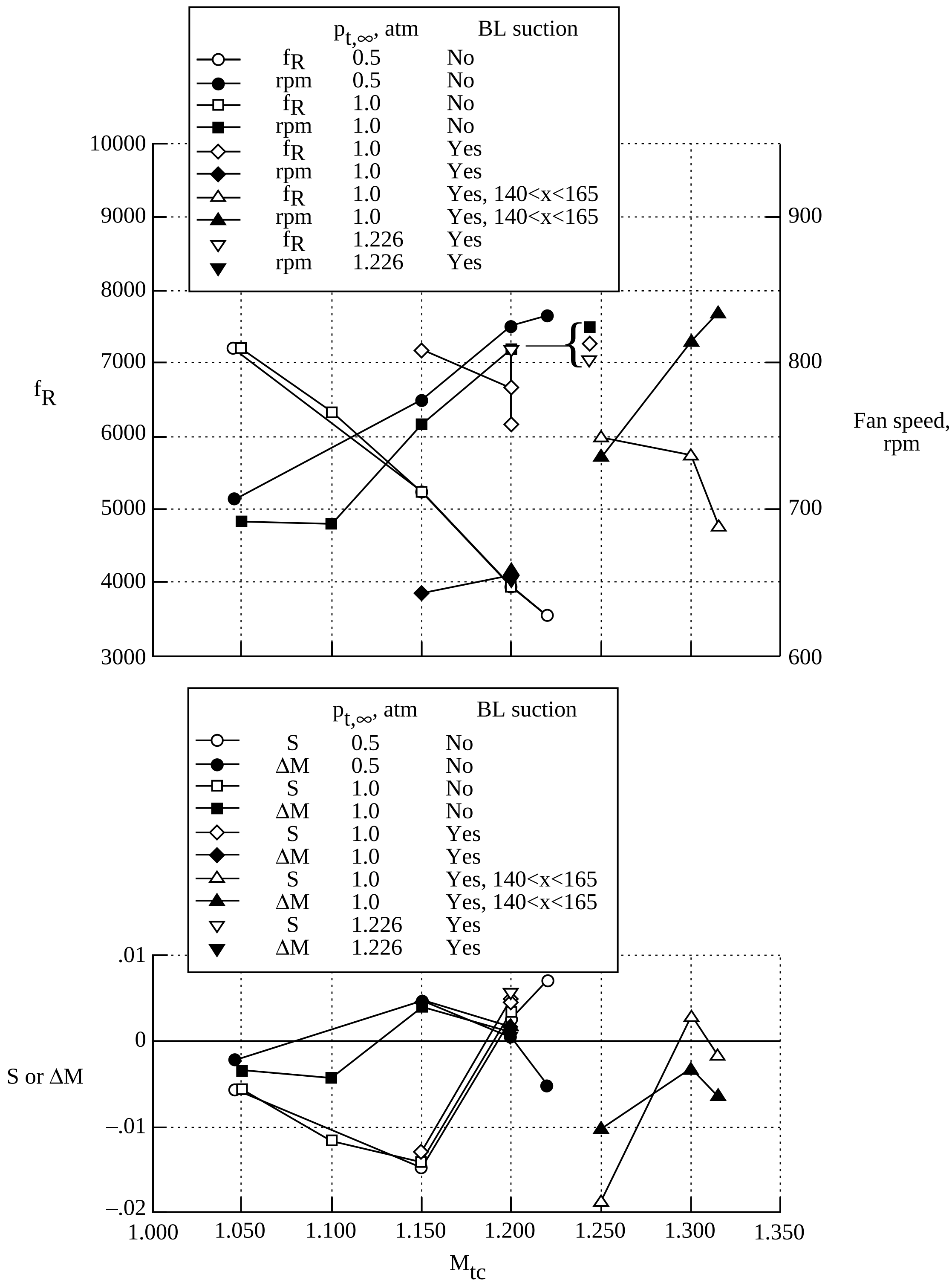

(m) Effect of reentry flaps, Mach number, and boundary layer suction for $M > 1.00$.

Figure 6. Concluded.

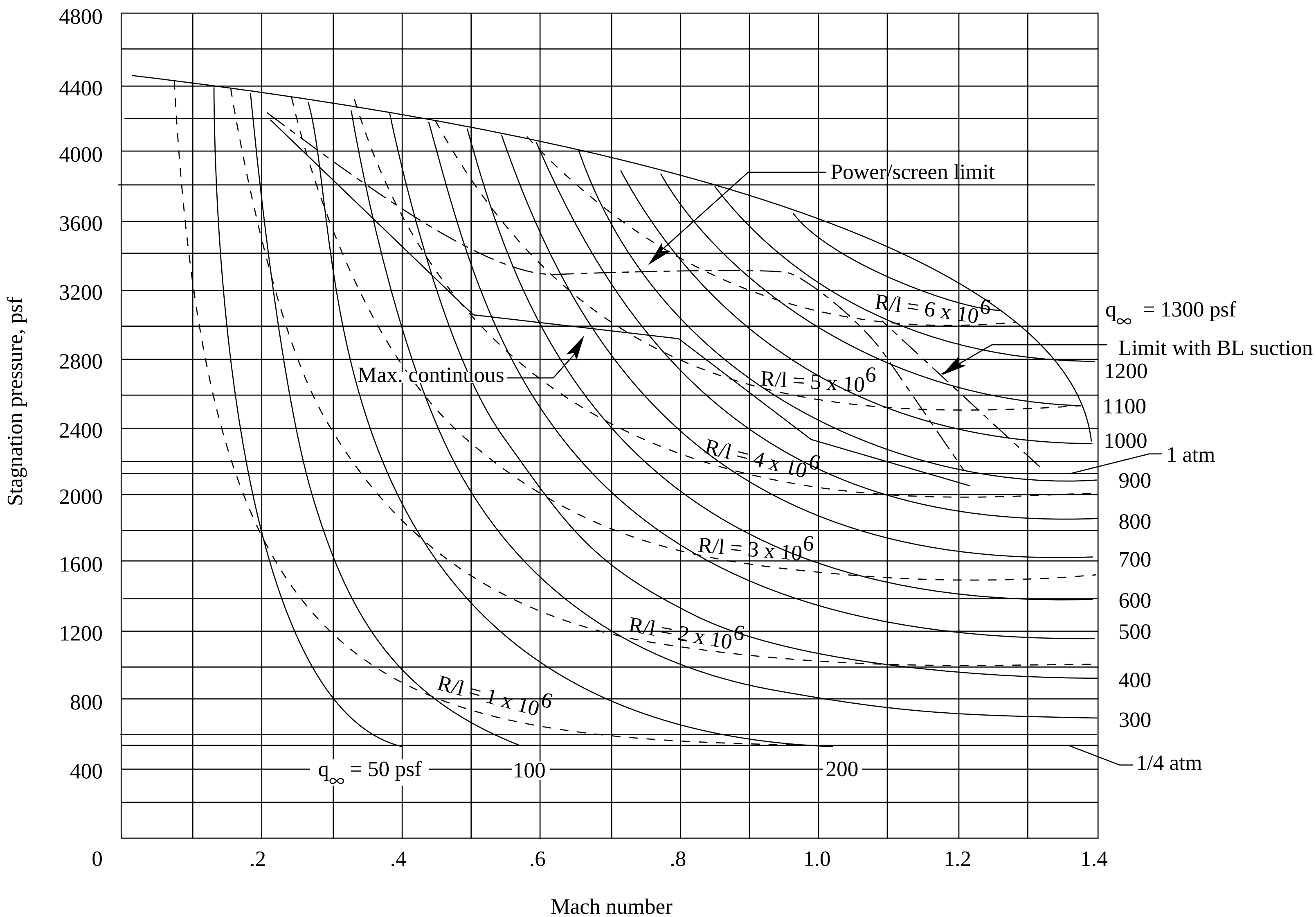

Figure 7. Operational envelope showing lines of constant unit Reynolds number and dynamic pressure q_∞.

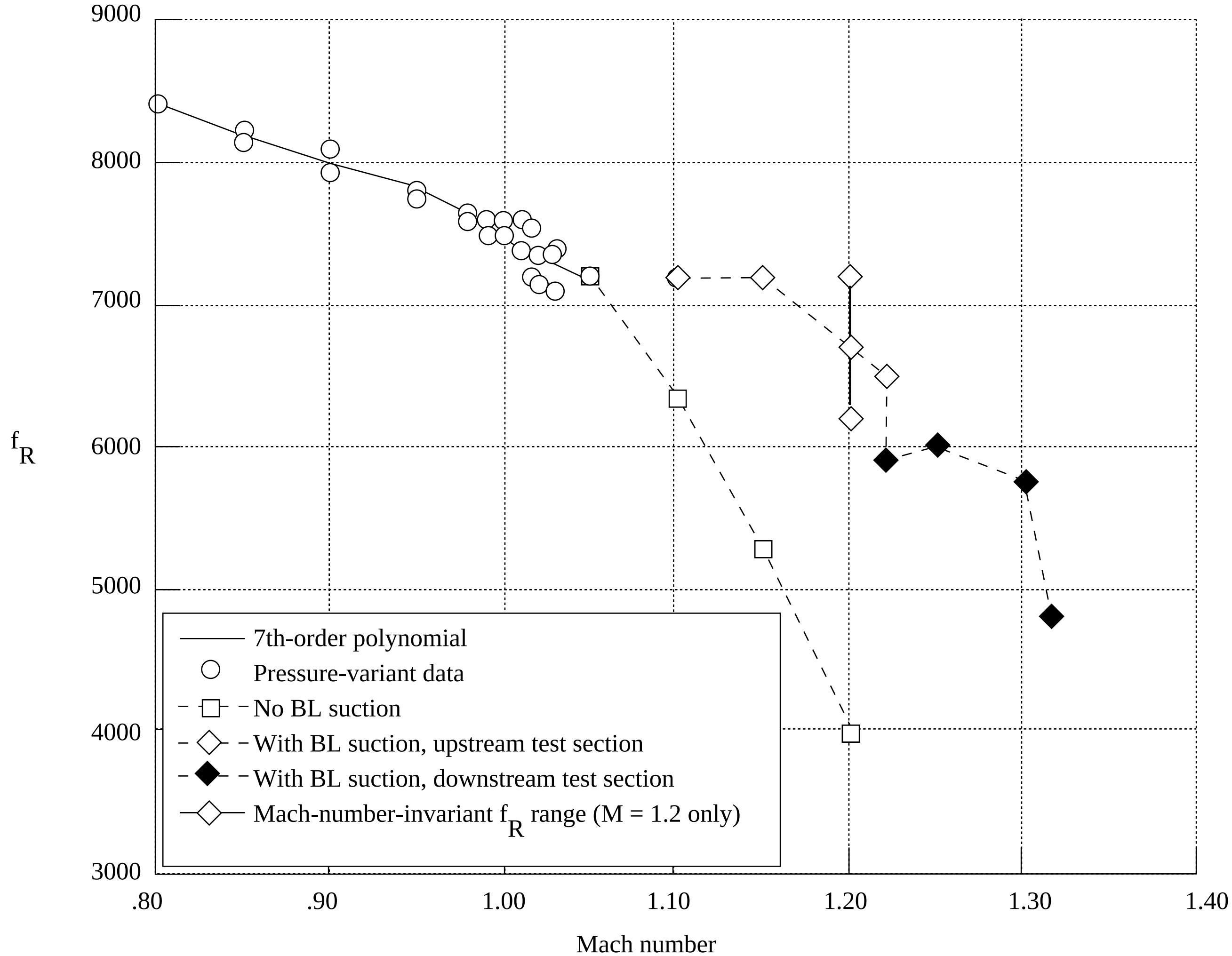

(a) Reentry flap variation in counts for $M > 0.80$.

Figure 8. Reentry flap position versus Mach number; effect of pressure and boundary layer suction variations.

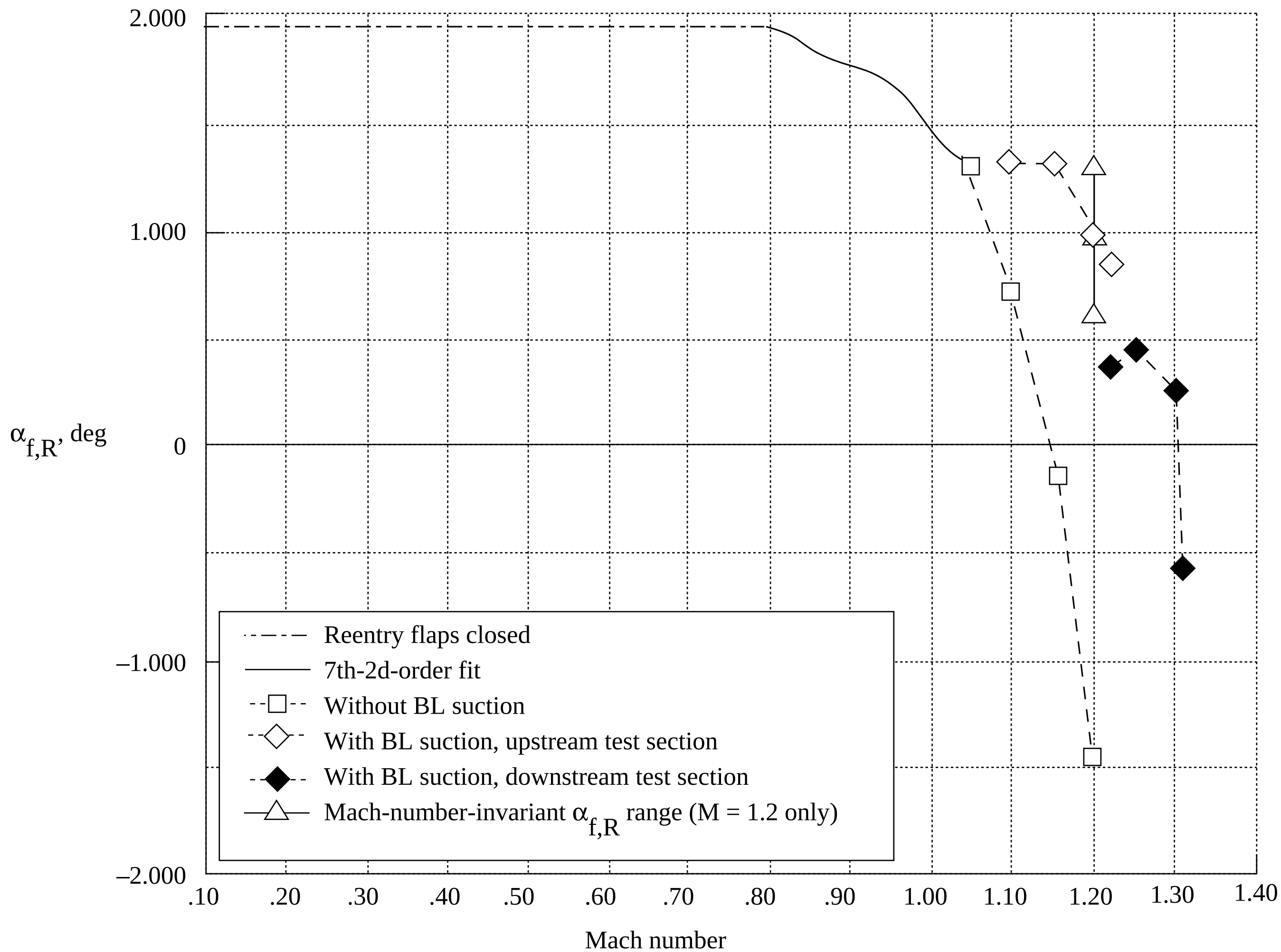

(b) Reentry flap position versus Mach number.

Figure 8. Concluded.

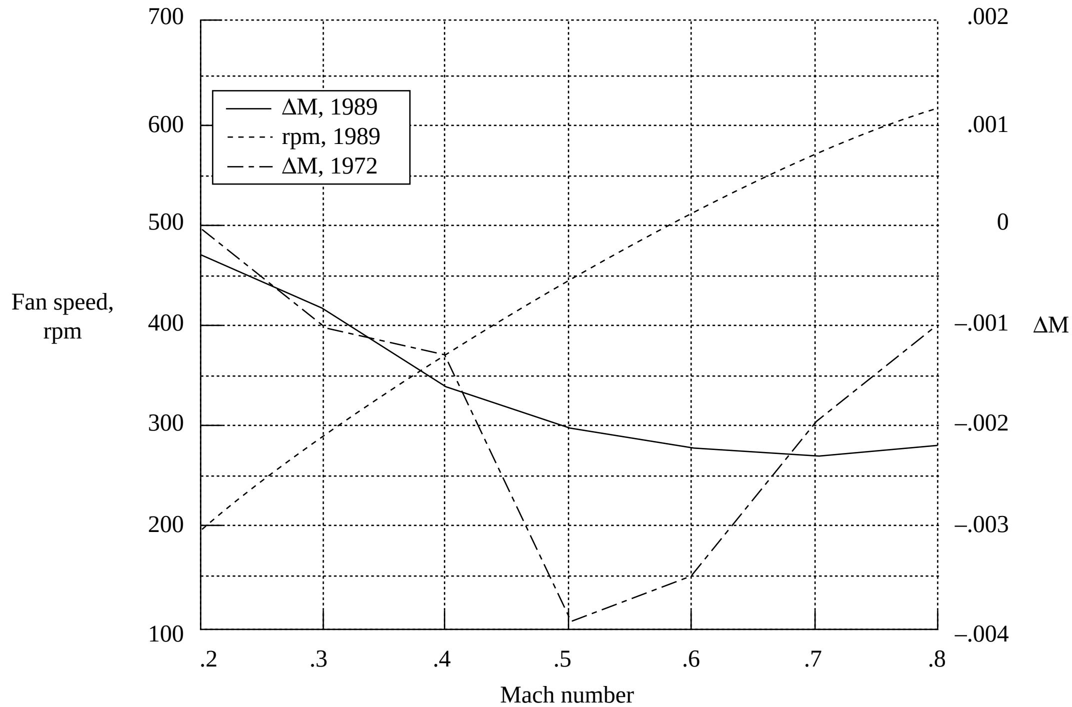

(a) $M < 0.80$.

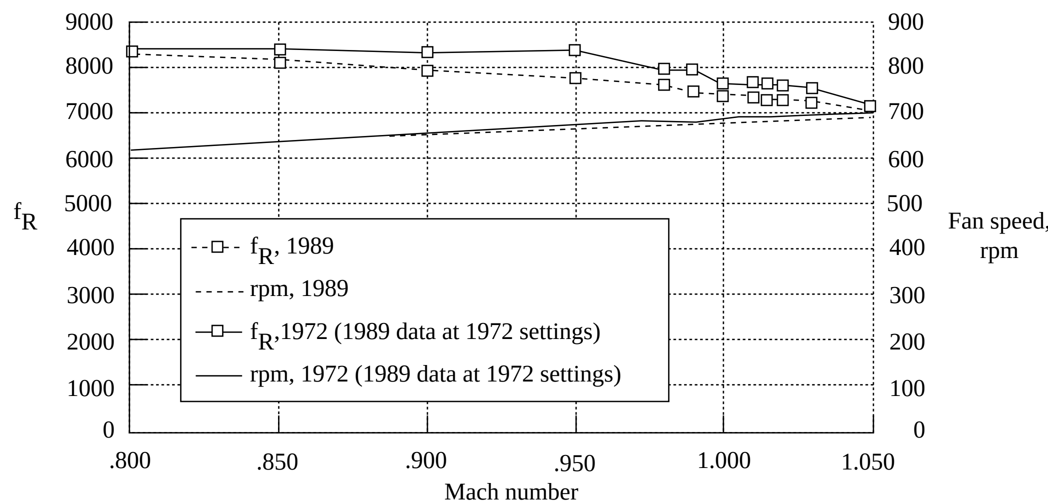

(b) Reentry flap setting and fan speed at $M = 0.80$ to 1.05.

Figure 9. Effect of Mach number on required fan speed, reentry flap setting, and Mach number correction compared with 1972 calibration.

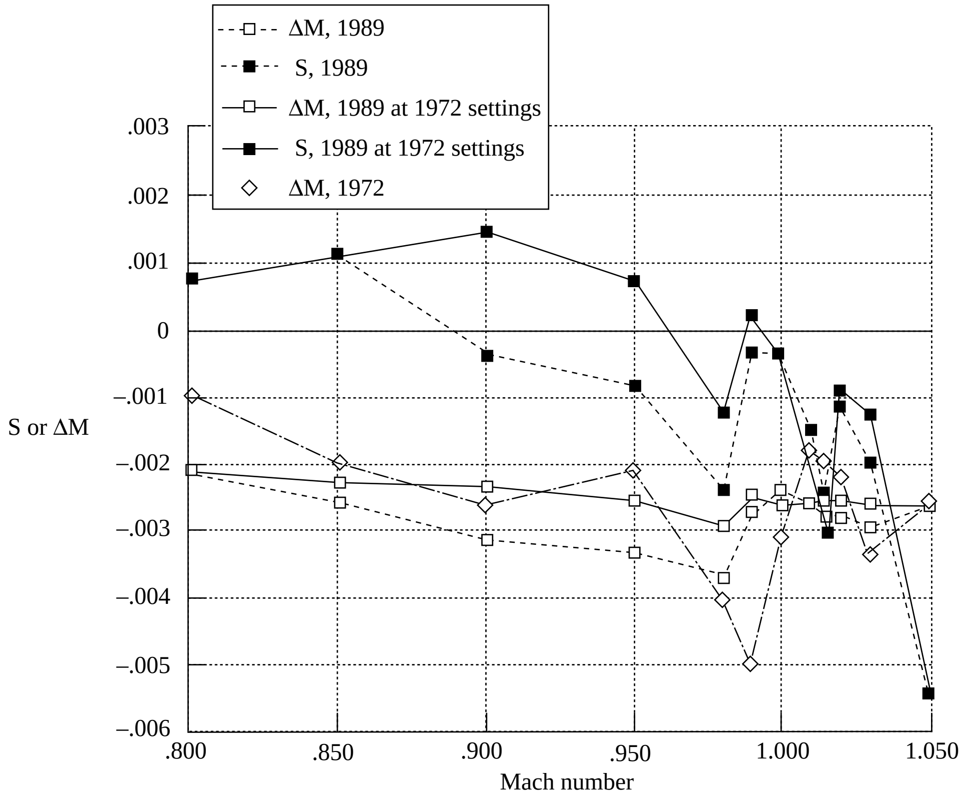

(c) Gradient parameter and Mach number correction at $M = 0.80$ to 1.05.

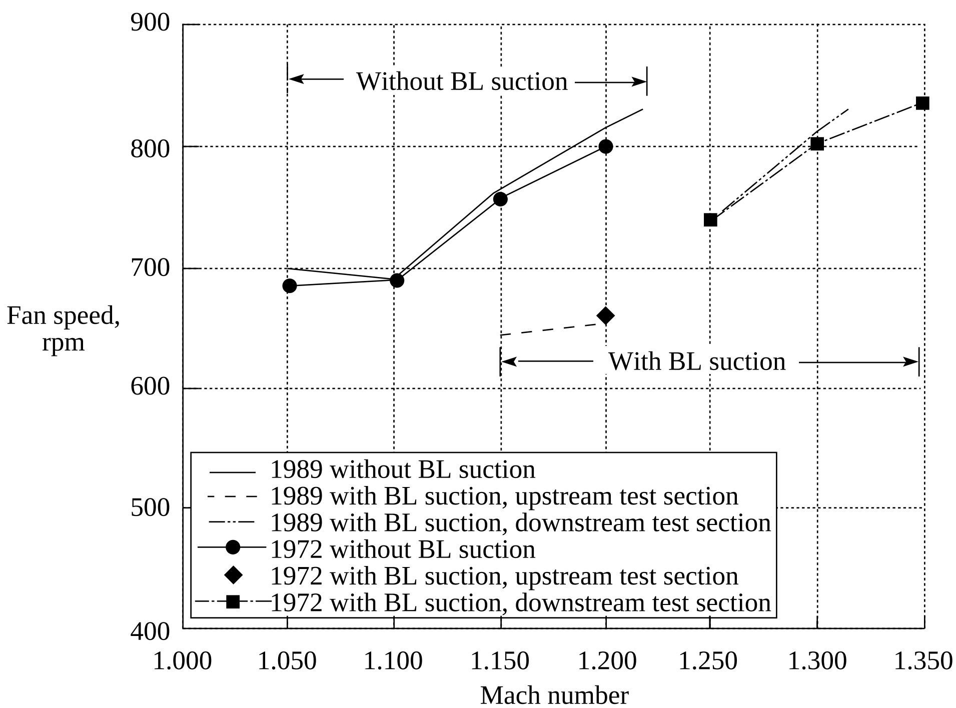

(d) Fan speed at $M > 1.05$.

Figure 9. Continued.

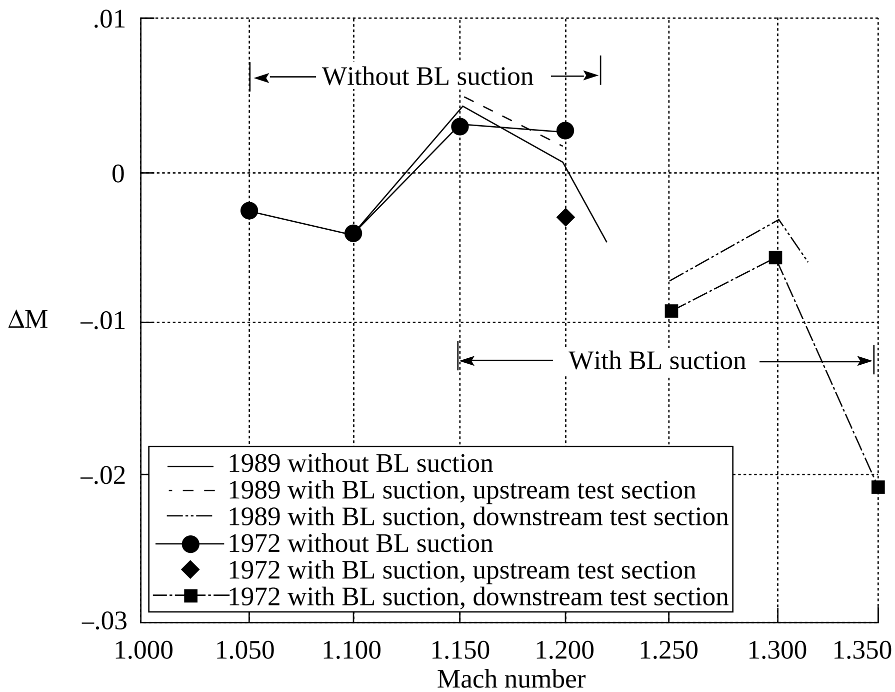

(e) Mach number correction at $M > 1.05$.

Figure 9. Concluded.

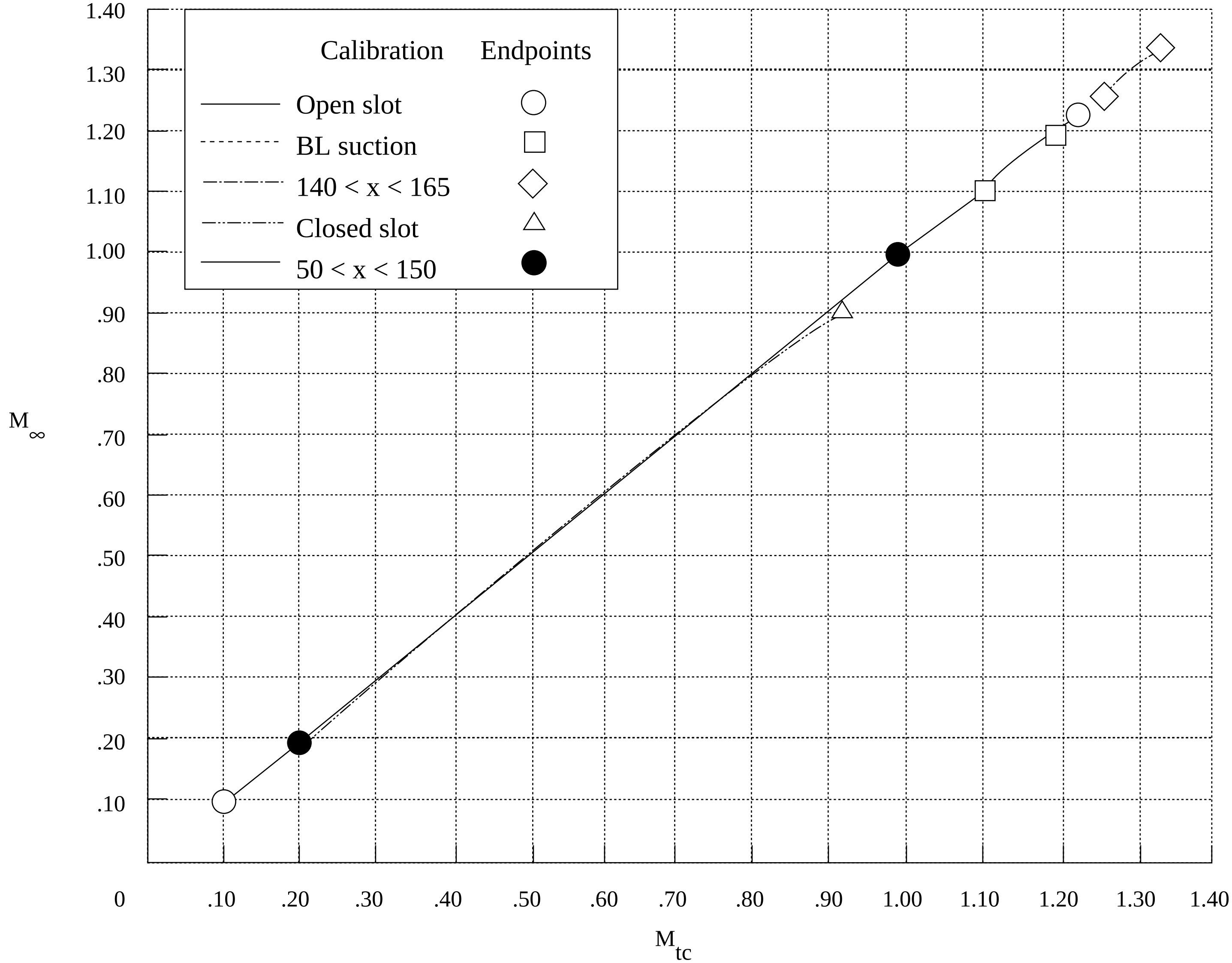

(a) Complete Mach number range.

Figure 10. Free-stream Mach number versus plenum Mach number for various test section calibrations.

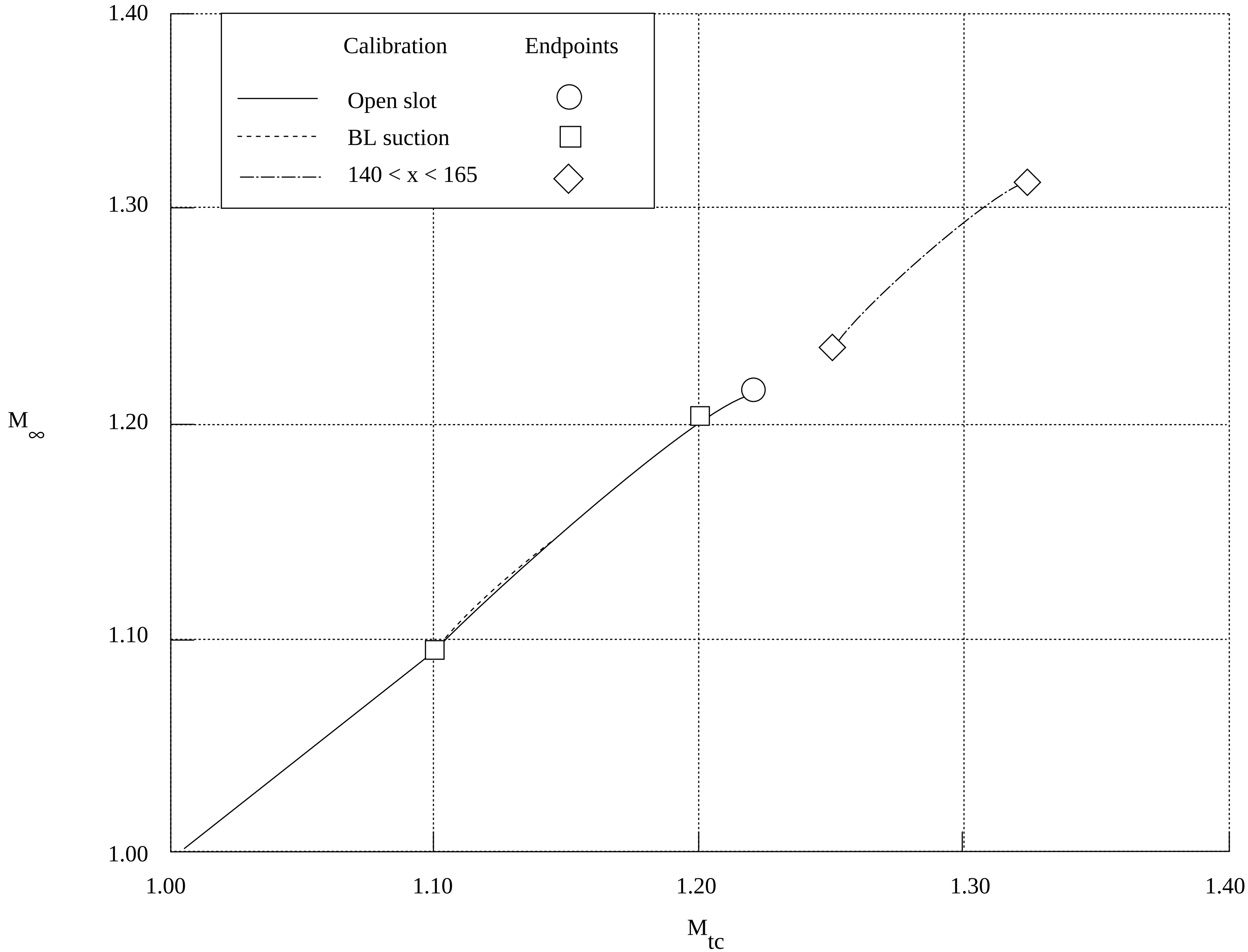

(b) Supersonic Mach number range.

Figure 10. Concluded.

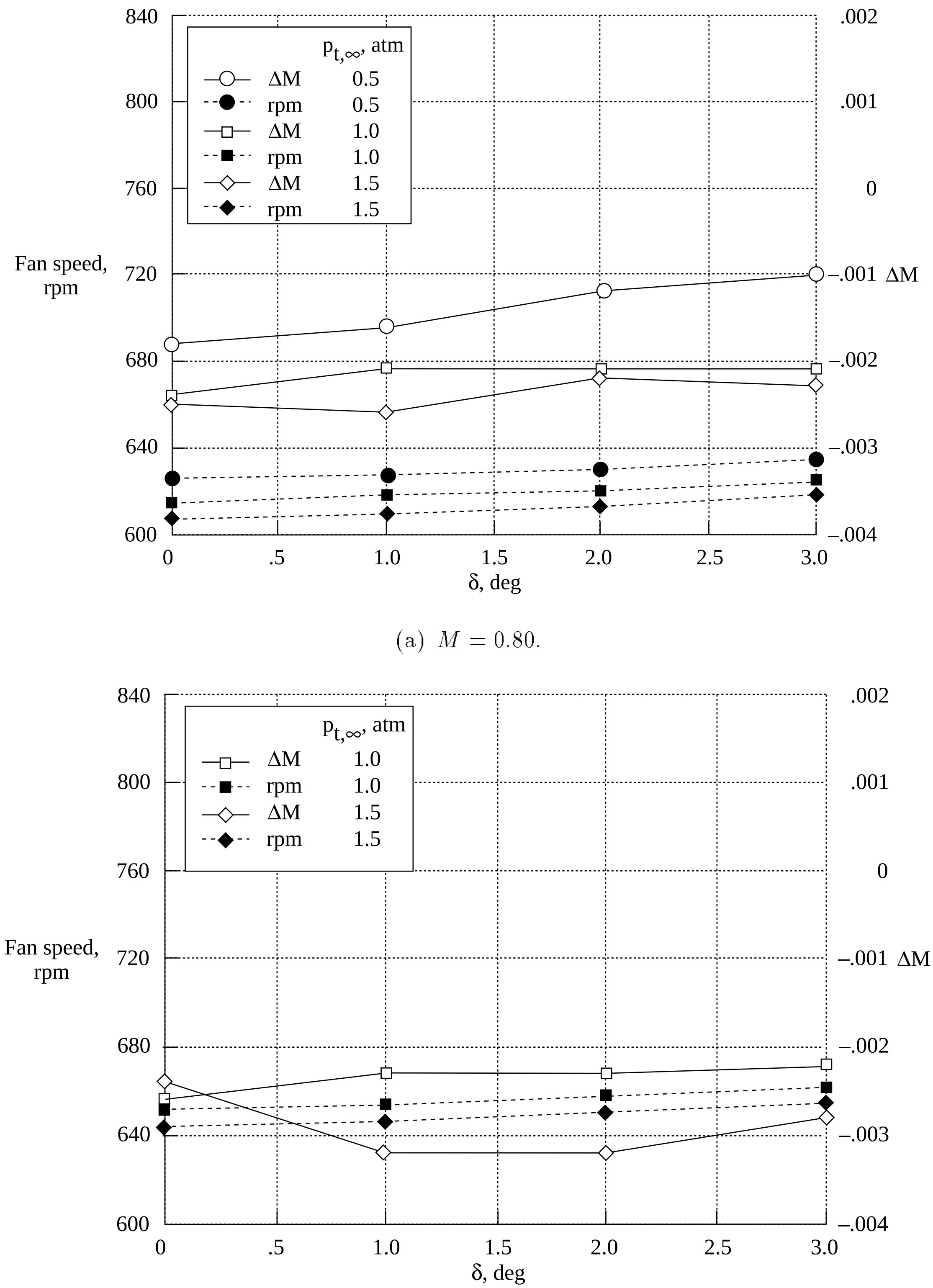

(a) $M = 0.80$.

(b) $M = 0.90$.

Figure 11. Typical effect of diffuser spoiler angle δ on Mach number correction and required fan speed.

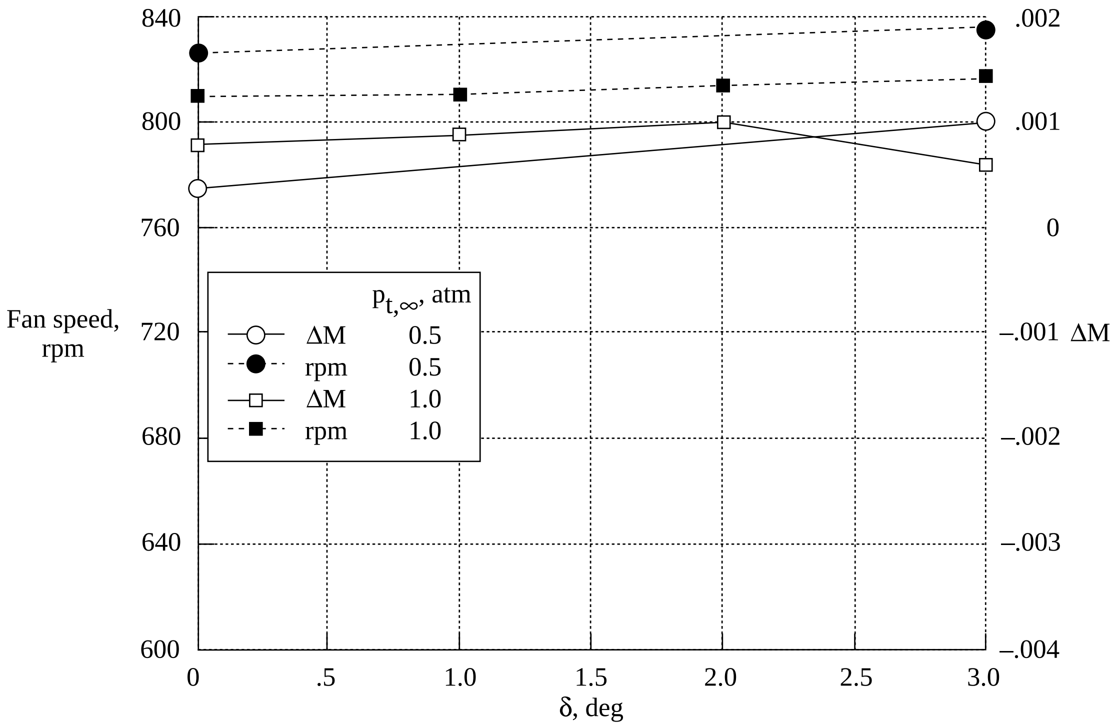

(c) $M = 1.20$.

Figure 11. Concluded.

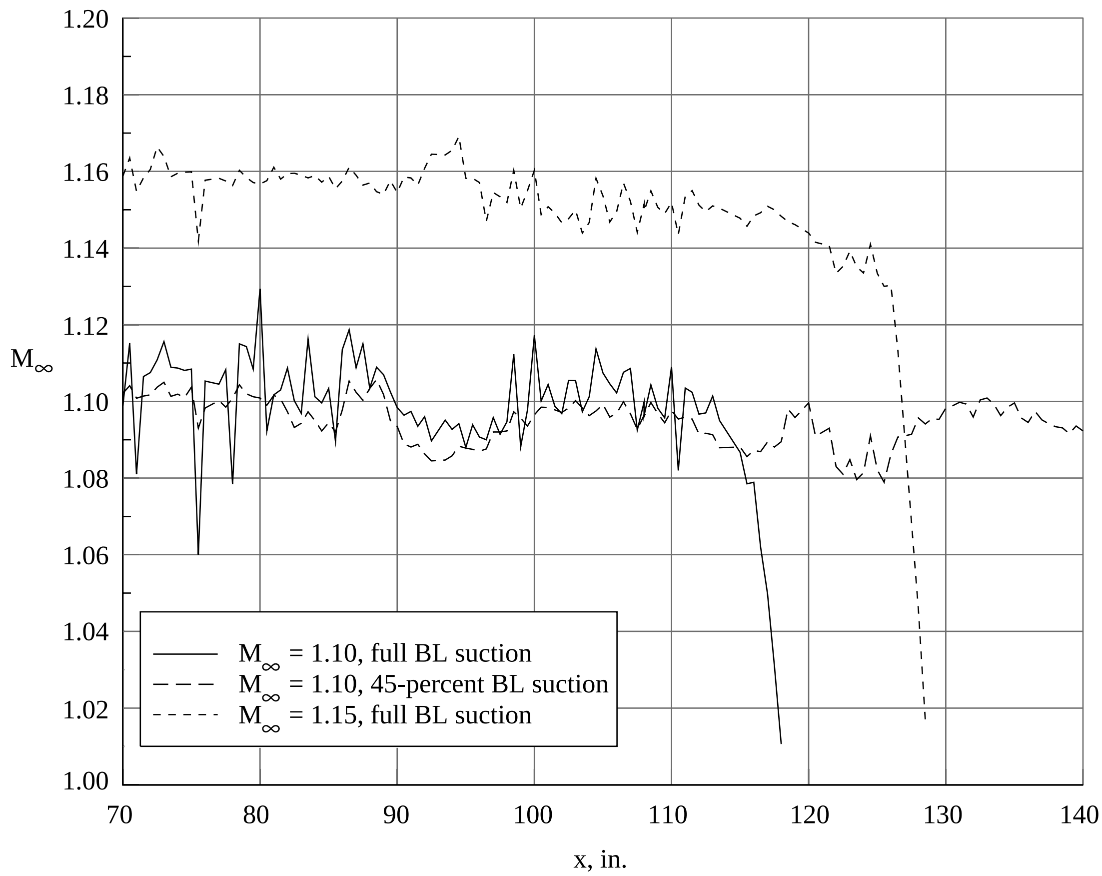

Figure 12. Effect of suction on downstream Mach number gradient at lower end of range for boundary layer suction.

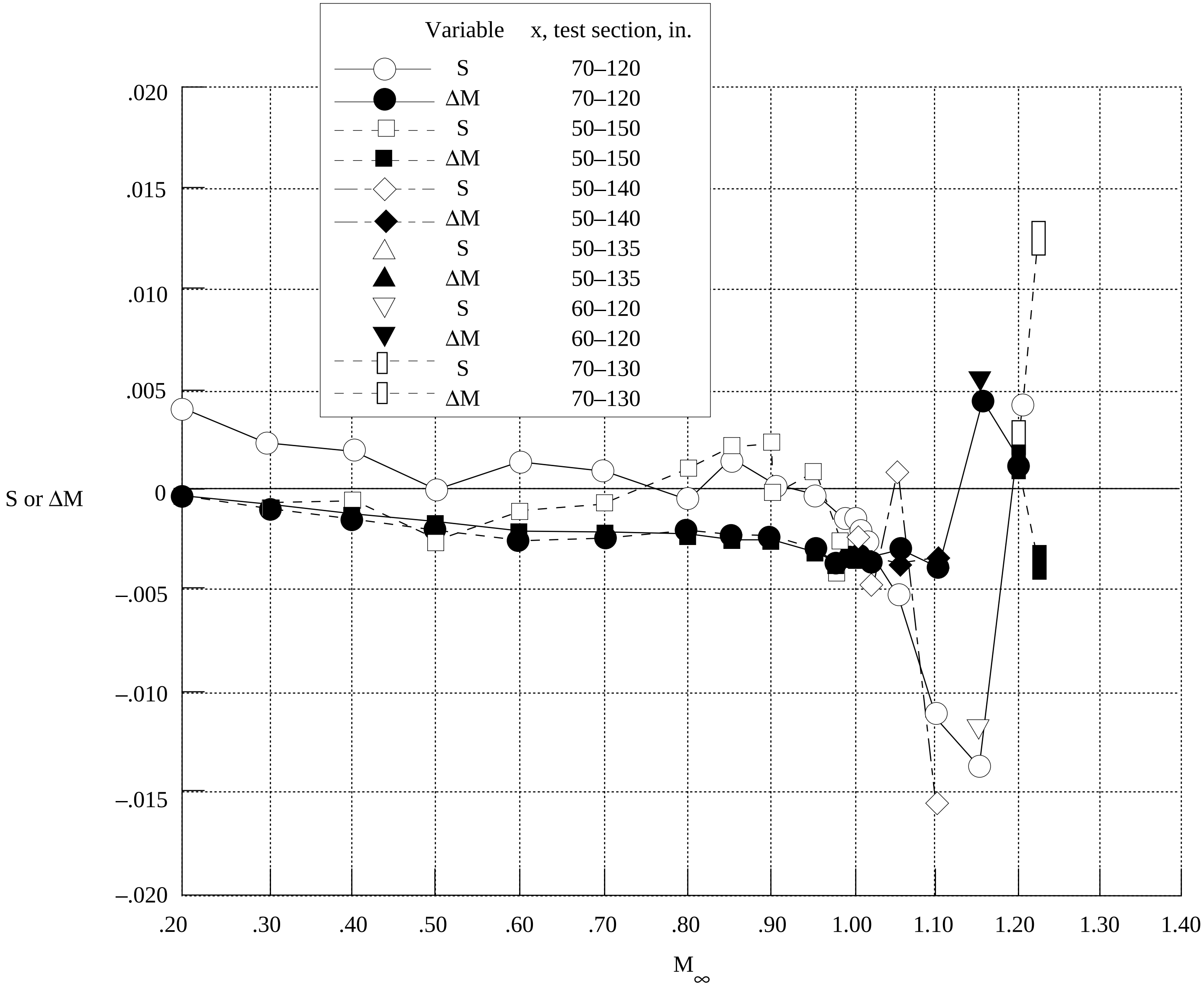

(a) Complete Mach number range without boundary layer suction.

Figure 13. Mach number gradient parameter and Mach number correction versus Mach number for various test sections.

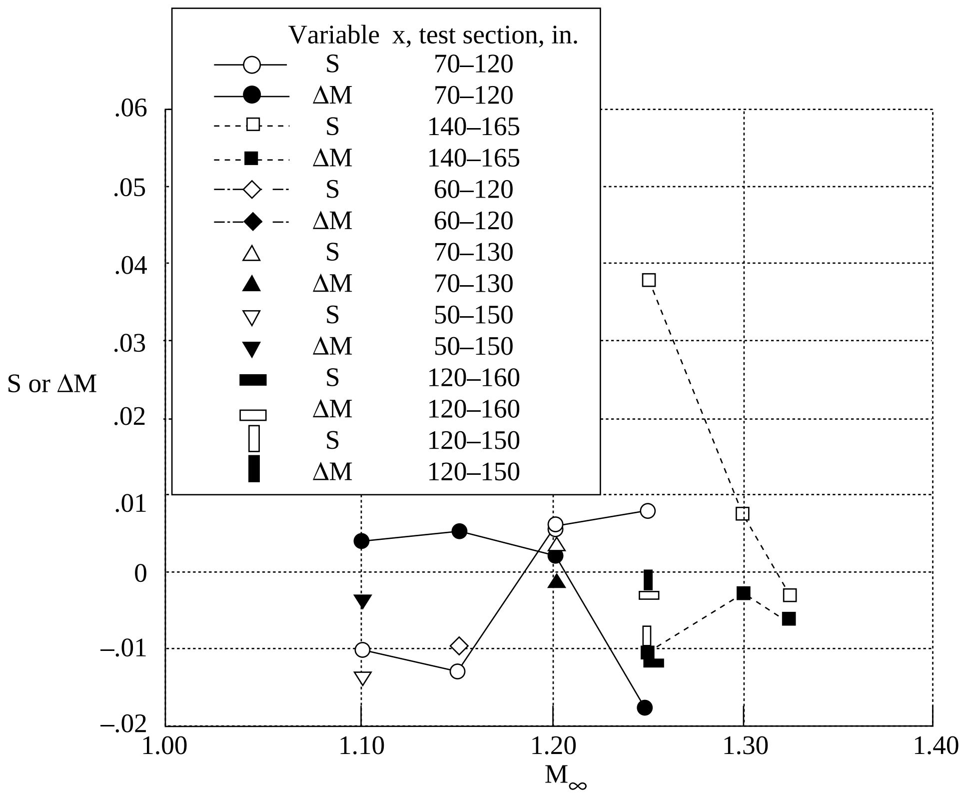

(b) $M > 1.1$ with boundary layer suction.

Figure 13. Concluded.

L-92-11237

(a) Tunnel view from the west. All linear dimensions in inches except strut travel.

Figure 1. Slotted-throat and diffuser entrance sections of 8-Foot Transonic Pressure Tunnel.

L-89-04368

(c) Calibration probe, looking upstream.

Figure 1. Continued.

L-89-04367

(d) Calibration probe, looking downstream.

Figure 1. Concluded.

REPORT DOCUMENTATION PAGE	*Form Approved* *OMB No. 0704-0188*

1. AGENCY USE ONLY *(Leave blank)*	2. REPORT DATE	3. REPORT TYPE AND DATES COVERED
	August 1994	Technical Paper

4. TITLE AND SUBTITLE
The NASA Langley 8-Foot Transonic Pressure Tunnel Calibration

5. FUNDING NUMBERS
WU 505-59-10-30

6. AUTHOR(S)
Cuyler W. Brooks, Jr., Charles D. Harris, and Patricia G. Reagon

7. PERFORMING ORGANIZATION NAME(S) AND ADDRESS(ES)
NASA Langley Research Center
Hampton, VA 23681-0001

8. PERFORMING ORGANIZATION REPORT NUMBER
L-17322

9. SPONSORING/MONITORING AGENCY NAME(S) AND ADDRESS(ES)
National Aeronautics and Space Administration
Washington, DC 20546-0001

10. SPONSORING/MONITORING AGENCY REPORT NUMBER
NASA TP-3437

11. SUPPLEMENTARY NOTES

12a. DISTRIBUTION/AVAILABILITY STATEMENT
Unclassified–Unlimited

Subject Category 02

12b. DISTRIBUTION CODE

13. ABSTRACT *(Maximum 200 words)*
The NASA Langley 8-Foot Transonic Pressure Tunnel is a continuous-flow, variable-pressure wind tunnel with control capability to independently vary Mach number, stagnation pressure, stagnation temperature, and humidity. The top and bottom walls of the test section are axially slotted to permit continuous variation of the test section Mach number from 0.2 to 1.2; the slot-width contour provides a gradient-free test section 50 in. long for Mach numbers equal to or greater than 1.0 and 100 in. long for Mach numbers less than 1.0. The stagnation pressure may be varied from 0.25 to 2.0 atm. The tunnel test section has been recalibrated to determine the relationship between the free-stream Mach number and the test chamber reference Mach number. The hardware was the same as that of an earlier calibration in 1972 but the pressure measurement instrumentation available for the recalibration was about an order of magnitude more precise. The principal result of the recalibration was a slightly different schedule of reentry flap settings for Mach numbers from 0.80 to 1.05 than that determined during the 1972 calibration. Detailed tunnel contraction geometry, test section geometry, and limited test section wall boundary layer data are presented.

14. SUBJECT TERMS
Langley 8-Foot Transonic Pressure Tunnel; Transonic wind tunnel; Tunnel calibration; Tunnel test capabilities

15. NUMBER OF PAGES
70

16. PRICE CODE
A04

17. SECURITY CLASSIFICATION OF REPORT	18. SECURITY CLASSIFICATION OF THIS PAGE	19. SECURITY CLASSIFICATION OF ABSTRACT	20. LIMITATION OF ABSTRACT
Unclassified	Unclassified	Unclassified	

NSN 7540-01-280-5500

Standard Form 298(Rev. 2-89)
Prescribed by ANSI Std. Z39-18
298-102